

IMPLEMENTATION OF DISTRIBUTED HIERACHICAL CONTROL FOR A STANDALONE  
SINGLE-PHASE MICROGRID

DARITH LENG

A THESIS SUBMITTED IN PARTIAL FULFILLMENT  
OF THE REQUIREMENTS FOR THE DEGREE OF  
DOCTOR OF ENGINEERING IN ELECTRICAL ENGINEERING  
FACULTY OF ENGINEERING  
KING MONGKUT'S INSTITUTE OF TECHNOLOGY LADKRABANG

2020

KMITL-2020-EN-D-018-075

COPYRIGHT 2020

FACULTY OF ENGINEERING

KING MONGKUT'S INSTITUTE OF TECHNOLOGY LADKRABANG



THESIS CERTIFICATION  
FACULTY OF ENGINEERING  
KING MONGKUT'S INSTITUTE OF TECHNOLOGY LADKRABANG

---

**Thesis Title** Implementation of Distributed Hierarchical Control for a Standalone Single-Phase Microgrid

**Student** Mr. Darith Leng

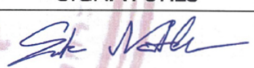




**Student Id.** 59601029

**Degree** Doctor of Engineering

**Program** Electrical Engineering

**Thesis Advisor** Dr. Sompob Polmai

**Thesis Reference Number** KMITL-2020-EN-D-018-075

EXAMINERS		SIGNATURES
Asst. Prof. Dr. Sumate Naetiladdanon		
Assoc. Prof. Dr. Somchat Jiriwibhakorn		
Assoc. Prof. Dr. Supat Kittiratsatcha		
Asst. Prof. Dr. Nirudh Jirasuwankul		
Dr. Sompob Polmai		

**Date** 1<sup>st</sup> July 2020 **Time** 10.00 a.m. -12.00 p.m.

**Place** Video Call

สถาบันเทคโนโลยีพระจอมเกล้าเจ้าคุณทหารลาดกระบัง  
KING MONGKUT'S INSTITUTE OF TECHNOLOGY LADKRABANG



( Assoc. Prof. Dr. Anuwat Jangwanitlert )

Acting Dean of Faculty of Engineering

1<sup>st</sup> July 2020

Thesis Title	Implementation of Distributed Hierarchical Control for a Standalone Single-Phase Microgrid
Student	Darith Leng
Student ID	59601029
Degree	Doctor of Engineering
Program	Electrical Engineering
Year	2020
Thesis Advisor	Dr. Sompob Polmai

## ABSTRACT

The depletion of fossil fuel and the environmental concern leads to the widespread deployment of renewable resources in the form of a microgrid. However, the intermittent of power output from renewable energy resources such as photovoltaic (PV) and wind turbines are subjected to degrade the power quality and stability of the system. This research aims to propose a distributed hierarchical control that could provide a fast response and high reliability to tackle the major issues in a standalone microgrid. The proposed control consists of three levels; namely the primary layer, secondary layer, and tertiary layer. The primary layer functionality is to ensure the power-sharing in parallel operation of the distributed generator with plug-and-play capability. Hence, two communication-less control scheme called modified droop control and virtual synchronous generator are investigated. The secondary layer responds for frequency restoration and elimination the impact of the intermittent nature of the renewable source. Therefore, frequency restoration and PV power fluctuation mitigation are implemented. The role of the top layer, tertiary layer, is to provide a supervisory control as well as to endow the smart and automation feature to the microgrid. In this layer, the multiagent system, Internet of Things, and PV power prediction are implemented. To verify the proposed hierarchical, a MATLAB/Simulink model and a laboratory-scale of a standalone microgrid are implemented. Numerous case studies are carried out. The results prove the effectiveness and correctness of each control layer such as to perform power-sharing, frequency restoration, PV power fluctuation mitigation by attenuating the maximum overshoot of frequency deviation from 50.13Hz to 50.02Hz, and autonomous and intelligent decision-making. Also, through this demonstration, it is clear that the developed hierarchical control is industrially applicable for actual microgrid and future smart grid.

## ACKNOWLEDGEMENTS

First of all, I am really grateful to my family for their unconditional supports especially my parents, who are always so supportive in every step in my life.

I would like to express my sincere gratitude to Dr. Sompob Polmai for his excellent supervision, ideas, and encouragement throughout this research. It was a great honor for me to pursue my higher education under his supervision.

I would like to express my thoughtful gratitude to Prof. Ise Toshifumi (Osaka University, Japan) and Dr. Long Bun (ITC, Cambodia) who are my co-investigating in the AUN/SEED-Net CR programm for their advices.

I wish to express my acknowledgement to ASEAN University Network/Southeast Asia Engineering Education Development Network (AUN/SEED-Net) for awarding me the scholarship with the financial support for Doctoral degree within 3 years. Furthermore, I also extend my sincere appreciation to KMITL for giving me the great opportunity to do research in a warmly and friendly environment.

My gratefully acknowledge goes also to all professors, lecturers and supporting staffs in Department of Electrical Engineering, who always help and give me guidelines and conveniences during the whole period of my dontoral study.

Finally, I would like to recognize all friends, international students and Thai students for the enjoyable and stimulating atmosphere that they provide with their companion and friendship.

Bangkok, July 2020




Darith Leng

# TABLE OF CONTENT

	Page
ABSTRACT . . . . .	i
ACKNOWLEDGEMENT . . . . .	ii
TABLE OF CONTENT . . . . .	iii
LIST OF FIGURES . . . . .	vii
LIST OF TABLES . . . . .	x
LIST OF ABBREVIATIONS . . . . .	xi
CHAPTER 1	
1 INTRODUCTION . . . . .	1
1.1 Background and Motivation . . . . .	1
1.2 Objectives and Scope . . . . .	3
1.3 Contribution of the Dissertation . . . . .	4
1.4 Organization of the Dissertation . . . . .	4
2 MICROGRID: CONCEPT, OPERATION, CHALLENGE AND CONTROL . . . . .	6
2.1 Microgrid Concept and Structure . . . . .	6
2.1.1 Operation Mode . . . . .	7
2.1.1.1 Standalone Mode . . . . .	7
2.1.1.2 Grid Connected Mode . . . . .	8
2.1.2 Challenges and Opportunities . . . . .	8
2.1.2.1 Technical Challenges . . . . .	8
2.1.2.2 Opportunities in Microgrid . . . . .	9
2.1.3 Control Scheme of Inverter-Based Distributed Generators . . . . .	10
2.1.3.1 Control Structure in Grid-connected Mode . . . . .	10
2.1.3.2 Control Structure in Islanded Mode . . . . .	12
3 PRELIMINARIES IN CONTROL AND THEORIES . . . . .	14
3.1 Phase Lock Loop . . . . .	14
3.2 The Current Control Strategies . . . . .	15

3.2.1	Proportional Integral Current Controller in the Synchronous Reference Frame . . . . .	15
3.2.2	Proportional Resonance (PR) Current Controller in Stationary Reference Frame . . . . .	17
3.3	Advance Intelligent Control and Optimization Methods . . . . .	19
3.3.1	Optimization Method . . . . .	19
3.3.1.1	Genetic Algorithm . . . . .	19
3.3.1.2	Particle Swarm Optimization . . . . .	19
3.3.1.3	Backtracking Search Optimize Algorithm . . . . .	20
3.3.2	Multiagent System . . . . .	21
3.3.2.1	The Multiagent System Versus SCADA . . . . .	22
3.3.2.2	Standard for Agent Development . . . . .	23
3.3.2.3	Multiagent System Development Toolkit . . . . .	24
3.3.3	Artificial Neural Network . . . . .	28
3.3.3.1	Neural Network Term . . . . .	29
3.3.3.2	Type of Neural Network . . . . .	29
<b>4</b>	<b>IMPLEMENTATION OF LABORATORY SCALE MICROGRID AND HIERARCHICAL CONTROL . . . . .</b>	<b>32</b>
4.1	Microgrid Components . . . . .	32
4.1.1	Distributed Generator . . . . .	32
4.1.2	Photovoltaic . . . . .	34
4.1.3	Battery Energy Storage System . . . . .	34
4.1.3.1	Bi-directional Inverter . . . . .	35
4.1.4	Loads . . . . .	38
4.1.5	Communication Protocol . . . . .	39
4.2	Distributed Hierarchical Control . . . . .	40
4.2.1	Primary Control . . . . .	41
4.2.1.1	Modified Droop Control . . . . .	41

4.2.1.2	VSG Control . . . . .	43
4.2.1.3	Tuning VSG Parameter Based on BSA . . . . .	44
4.2.2	Secondary Control . . . . .	46
4.2.2.1	Frequency Restoration . . . . .	46
4.2.2.2	Frequency Deviation Miltigation . . . . .	46
4.2.3	Tertiary Control . . . . .	48
4.2.3.1	Multiagent System . . . . .	48
4.2.3.2	Internet of Things . . . . .	49
4.2.3.3	PV Power Prediction . . . . .	50
<b>5</b>	<b>RESULTS AND DISCUSSION . . . . .</b>	<b>54</b>
5.1	Simulation Results . . . . .	54
5.1.1	Primary Control . . . . .	55
5.1.1.1	Power Sharing . . . . .	55
5.1.1.2	Load Transition . . . . .	56
5.1.1.3	Comparison Between Constant and Tuning Parameters of VSG . . . . .	57
5.1.2	Secondary Control . . . . .	59
5.1.2.1	Frequency Restoration . . . . .	59
5.1.2.2	PV Power Fluctuation Miltigation . . . . .	60
5.2	Experimental Results . . . . .	67
5.2.1	Primary Layer . . . . .	69
5.2.2	Secondary Layer . . . . .	70
5.2.2.1	Frequency Restoration . . . . .	70
5.2.2.2	Frequency Deviation Mitigation . . . . .	71
5.2.3	Tertiary Layer . . . . .	72
5.2.3.1	Multiagent System . . . . .	72
5.2.3.2	Internet of Thing . . . . .	74
5.2.3.3	PV Power Prediction Based Artifical Neural Network . . . . .	74
<b>6</b>	<b>CONCLUSION AND FUTURE WORKS . . . . .</b>	<b>77</b>

6.1 Conclusion . . . . .	77
6.2 Future works . . . . .	77
 REFERENCES . . . . .	78
APPENDICES . . . . .	85
 DESIGN OF LCL FILTER . . . . .	85
A.1 Design of the Inverter-Side Inductor . . . . .	85
A.2 Filter Capacitor Design . . . . .	86
A.3 Grid-Side Inductor Design . . . . .	86
 OPERATION PROCEDURE . . . . .	87
B.1 Starting Distributed Generator . . . . .	87
B.2 Starting PV Simulator . . . . .	87
B.3 Starting BESS . . . . .	88
B.4 Multiagent System Execution . . . . .	89
BIOGRAPHY . . . . .	92
LIST OF PUBLICATIONS . . . . .	94

1.1	Centralized, decentralized, and distributed control scheme . . . . .	2
2.1	Basic structure of microgrid . . . . .	6
2.2	Grid-following strategy of a PV generator with avariable DC bus voltage for MPPT.	10
2.3	Grid-following strategy of a PV generator with a generator-side converter for MPPT. . . . .	11
2.4	Power dispatching strategy of a gas micro-turbine for a VSI control. . . . .	11
2.5	Phasor diagram of microsource . . . . .	12
3.1	Schematic diagram of PLL . . . . .	14
3.2	Schematic diagram and model of SRF-PLL . . . . .	15
3.3	Block diagram of SRF control . . . . .	16
3.4	Block diagram of stationary control . . . . .	18
3.5	Flowchart of BSA . . . . .	20
3.6	A simple agent in its environment . . . . .	22
3.7	Overview of FIPA standard . . . . .	23
3.8	FIPA agent management reference model . . . . .	24
3.9	Jade architecture . . . . .	25
3.10	The system architecture of agency in Mobile-C . . . . .	26
3.11	Schematic drawing of biological neurons . . . . .	28
3.12	Single layer of neurons . . . . .	30
3.13	Multi-layer network . . . . .	30
3.14	Reccurent neural network . . . . .	31
4.1	Laboratory scale microgrid . . . . .	32
4.2	Physical of kikusui PCR2000M . . . . .	33
4.3	DG designed control system . . . . .	33
4.4	PV emulator system . . . . .	34
4.5	Control structure of BESS . . . . .	35
4.6	Circuit diagram of bi-directional inverter . . . . .	35
4.7	Charging circuit diagram . . . . .	36
4.8	BESS in charging state . . . . .	37
4.9	Discharging circuit diagram . . . . .	37
4.10	BESS in discharging state. . . . .	38
4.11	Loads Control . . . . .	38
4.12	Communication protocol . . . . .	39
4.13	Opto-isolated CANbus system . . . . .	40



4.14	Configuration of opto-isolated CANbus . . . . .	40
4.15	Concept of proposed hierarchical control . . . . .	41
4.16	Modified droop control block diagram . . . . .	42
4.17	Control block diagram of Virtual synchronous generator . . . . .	44
4.18	BSA-Simulink interfacing . . . . .	45
4.19	Testing BSA turning: System frequency . . . . .	45
4.20	Frequency restoration . . . . .	46
4.21	ESS respond based on proposed smoothing method . . . . .	47
4.22	Proposed PV power smoothing technique based on BESS . . . . .	47
4.23	Single-line diagram . . . . .	48
4.24	GUI of Thingsboard . . . . .	50
4.25	LSTM cell . . . . .	50
4.26	LSTM diagram . . . . .	51
5.1	Single-phase diagram of standalone microgrid . . . . .	55
5.2	Total power demand . . . . .	56
5.3	Power sharing based on modified droop control . . . . .	56
5.4	Power sharing based on VSG . . . . .	56
5.5	Total active power demand. . . . .	57
5.6	Frequency respond: VSG Vs Droop control. . . . .	57
5.7	Parameter adapting based on BSA. . . . .	58
5.8	Total active power demand. . . . .	59
5.9	Frequency response based on load transient: Adaptive VSG Vs Const. Vs Droop control. . . . .	59
5.10	Load transition . . . . .	60
5.11	Frequency restoration . . . . .	60
5.12	Worst PV power fluctuation profile. . . . .	61
5.13	System without energy storage system. . . . .	61
5.14	Energy, SOC and power produce by the smoothing methods . . . . .	62
5.15	Respond of each control method . . . . .	63
5.16	Frequency respond: Without ESS, LPF smoothing and proposed method . . . . .	63
5.17	Smoothing method for HESS . . . . .	64
5.18	Worst PV power fluctuation profile. . . . .	64
5.19	Frequency respond: VSG Vs DQ decoupling control. . . . .	65
5.19	Power & SoC of hybrid energy storage system. . . . .	66
5.20	Frequency response based on PV power fluctuation: Constant Vs Adaptive VSG's parameters . . . . .	67

5.21	Single-line diagram . . . . .	67
5.22	Laboratory scale Microgrid . . . . .	68
5.23	Droop control: (E1) Active and reactive power of demands; (E2) Active power of Gen#1 (Green) and Gen#2 (Orange); (E3) Reactive power of Gen#1 (Ping) and Gen#2 (Blue) . . . . .	69
5.24	Frequency restoration: (E1) Active and reactive power of demands; (E2) Active power of Gen#1(Green) and Gen#2(Orange); (E3) Ping (Frequency) and Cyan (Voltage) . . . . .	70
5.25	Without BESS: (E1:cyan) Power of GEN#1 and Gen#2; (E2) Output power of PV; (E3) Total power demand; (E4) Grid's frequency . . . . .	70
5.26	LPF smoothing technique: (E1:cyan) power of GEN#1 and Gen#2; E2 (green-graph) output power of PV and E2 (orange-graph) output power of BESS; (E3) Total power demand; (E4) system frequency. . . . .	71
5.27	Proposed smoothing technique: (E1:cyan) power of GEN#1 and Gen#2; E2 (green-graph) output power of PV and E2 (orange-graph) output power of BESS; E3 (ping-graph) BESS's voltage and E3 (blue-graph) BESS's current; (E4) system frequency. . . . .	71
5.28	Control reserve generator: (E1) Yellow (Critical load) and Red (Non-critical load); (E2) Power of Gen#1; (E3) Power of Gen#2; (E4) Cyan (PV) and Gray (f-Hz) . . . . .	73
5.29	Load-shedding: (E1) Blue (Critical load) and Red (Non-critical load); (E2) Power of Gen#1; (E3) Power of Gen#2; (E4) Cyan (PV) and Gray (f-Hz) . . . . .	73
5.30	Real-time web remote and monitoring . . . . .	74
5.31	PV power predicted based on LSTM . . . . .	75
5.32	PV power predicted based on MLP . . . . .	76
A.1	Single-phase full-bridge inverter with LCL filter . . . . .	85
B.1	System without energy storage system. . . . .	87
B.2	PV emulator operation guideline . . . . .	88
B.3	BESS operation guideline . . . . .	89
B.4	PV ideal profile . . . . .	89
B.5	SPADE web user interface . . . . .	90
B.6	Web user interface of ThingsBoard . . . . .	90
B.7	Shell command for executing the LSTM algorithm . . . . .	91

3.1	Summary of MAS development platforms . . . . .	25
4.1	AGENTS and Task . . . . .	49
4.2	Correlation Coefficient . . . . .	53
5.1	Microgrid's parameters in simulation . . . . .	54
5.2	Microgrid's parameters . . . . .	68
5.3	LSTM and MLP Parameters . . . . .	75
A.1	Maximum harmonics limits of grid current . . . . .	86
A.2	Inverter's parameters . . . . .	86

## LIST OF ABBREVIATIONS

ACC	Agent Communication Channel
ACL	Agent Communication Language
AID	Agent Identifier
AMS	Agent Management System
AP	Agent Platform
CCM	Current Controlled Mode
CHP	Combined Heat and Power
DER	Distributed Energy Resources
DF	Directory Facilitator
DG	Distributed Generation/Distributed Generator
DSP	Digital Signal Processor
EMS	Energy Management System
ESS	Energy Storage System
FIPA	Foundation for Intelligent Physical Agents
GUI	Graphical User Interface
IEEE	Institute of Electrical and Electronics Engineers
JADE	Java Agent Development Environment
MAS	Multi Agent System
MG	Microgrid
MQTT	MQ Telemetry Transport
MTP	Message Transport Protocol
MTS	Message Transport Service
OS	Operating Systems
P2P	Peer-to-Peer
PCC	Point of Common Coupling
PI	Proportional Integral
PLL	Phase-Locked Loop
PR	Proportional Resonant
PWM	Pulse Width Modulation
PV	Photovoltaic
RES	Renewable Energy Sources
SCADA	Supervisory Control and Data Acquisition
TCP/IP	Transmission Control Protocol / Internet Protocol
VCM	Voltage Controlled Mode
XMPP	Extensible Messaging and Presence Protocol



## INTRODUCTION

In the face of energy challenges, the application of renewable energy sources (RES) in the form of the microgrid can be considered as a sustainable solution. However, to bring microgrid to light, the control and stability issue should be properly solved. In this chapter, we first present the background, motivation, and objectives of the research. Afterward, some literature reviews on microgrid as well as its state-of-art control strategies are addressed. Finally, the major contributions and organization of this book are summarized.

### 1.1 Background and Motivation

Electrical energy plays a major role in our life and it is a key driver of industrialized societies. The significant increase of power consumption, the extinction of conventional energy resources such as coal, oil and gas, and the environmental pollution which is impacted by the energy production, are the main challenge for the electric utility. To handle these issues, the application of renewable energy is the best alternative resources. Moreover, the aging of power system structure as well as high-power quality required by user emerge that building a new sustainable energy system is inevitable. Building a new sustainable energy system with the integration of the renewable source is expected to play a major role in the transformation of the conventional energy supply to a future energy system. Through this concept, a new form of the power grid is emerging, so-called microgrid. A microgrid is a new paradigm of electrical grid with the high integration of renewable energy. It could be considerate as a promising technology to handle the increase of energy demand, environmental concern and a key toward a future smart grid.

However, the application of distributed generators based on renewable energy sources can cause as many problems as it may solve. The inherently intermittent and fluctuating power of the renewable sources such as photovoltaic (PV) and wind turbines as well as the variation of power demand are the key factors of system stability degradation, especially when the microgrid is operated in islanded mode. Hence, a sophistication microgrid's control is a must.

In conventional power system, the operation, control, and monitoring accomplished by using centralize techniques like SCADA/EMS. The structure of the centralized control is demonstated in Fig. 1.1(a). In this control architecture, the necessary information from the various subsystem such as voltage, current, generator, load status ., etc. is transmitted to the single point known as the central controller before it commands back the control signal. This scheme of control could improve the accuracy of the control and drives the

operation into an optimal region by considering many variables in the system, but the total reliance on high bandwidth communication links and powerful computers (central controller). The highly rely high bandwidth communication and one central controller are not only requires the additional cost of implementation and maintenance, but also reduce the system's reliability [1], flexibility and efficiency [2], and makes the whole system collapse possible by communication system failure [3, 4].

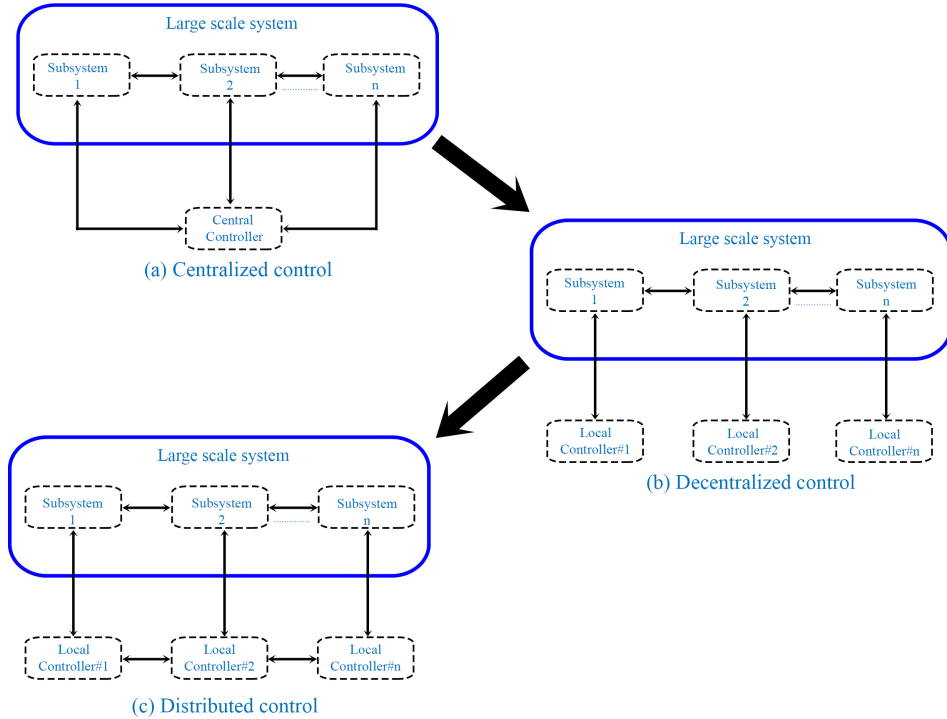


Fig. 1.1: Centralized, decentralized, and distributed control scheme

Moreover, the enormous penetration of renewable energy resources in power systems could lead the system event more complex. Hence, the traditional control techniques based on centralized employed in the conventional power system seems not suitable for the system. As a result, it needs different and special techniques to ensure system stability and reliability, and enhanced power quality. These issues could be solved by introducing the decentralized control, Fig. 1.1(b), which equipped the local controller to each subsystem. For the sake of simplicity, each local controller is usually designed and implemented by ignoring the interactions from other subsystems and only using its locally available information [5]. This is essentially equivalent to imposing structural constraints on the centralized controller. Thus controllability is restricted by the decentralized approach and system control performances are deteriorated. One typical example of the consequences of the drawbacks of such control strategy is the widespread blackout of August 2003 in North America [6]. In that accident, each subsystem only focused on maintaining its own subsystem stability and transferred the extra load to other

subsystems, which made the overload more severe and eventually caused a cascading corruption [7].

The advancement and reliability of communication techniques have paved the way to implement the control strategy that could work in a distributed scheme. As a result, the distributed control has been widely studied and implemented successfully in various fields such as process control [8], traffic control [9], and so on. In distributed control, the local controller is equipped with a designed communication network topology that allows them to exchange information among each other. The control structure of the distributed control scheme is illustrated in Fig. 1.1(c).

## 1.2 Objectives and Scope

For the sake of smart grid development, the application of control automation, the integration of renewable energy, energy storage system, converter, two-way flow of information and electricity are essential. This results in a flexible, reliable and efficient electrical grid. In this context, the microgrid can be considered as a promising system and a cornerstone for future smart grid development. Among the existing control strategies for a microgrid, hierarchical control seems to be a good solution especially when it comes to standardization. It classifies the control methods into layers such as primary, secondary and tertiary; based on the control functionality and the control speed. The functionality of the primary layer is to realize the load sharing between the different converters. In its standard form, the secondary layer response to the voltage and frequency restoration which caused by deviation on the primary layer and the intermittent of the renewable source. The highest level is defined as the tertiary layer. It performs energy management.

Regarding the potential of distributed and hierarchical control, this research aims to implement a distributed control scheme for the laboratory scale microgrid by bringing together the different control methods to work in a hierarchy, called distributed hierarchical control.

Due to the time constraint and the shortage of equipment, there is a minor difference between the simulation and experiment, and this study has limited scope as follow:

- Primary layer: In the simulation, there is a comparison of two control methods (droop Vs VSG) for better power-sharing of parallel operation of two inverter-based generators. But, in hardware experiments only droop control is implemented.
- Secondary layer: In the simulation, the PV power fluctuation mitigation is implemented based on hybrid supercapacitor/battery energy storage. Meanwhile, only battery energy storage is implemented in hardware experiment for the PV power

fluctuation mitigation purpose.

- Third layer: As most controls in this layer relate to hardware, hence, no simulation studies were conducted in this layer.

### 1.3 Contribution of the Dissertation

This paper is aimed to implement a distributed hierarchical control scheme for the laboratory scale microgrid by bringing together the different control methods to work in a hierarchy. This hierarchical control consists of three levels and its mains contributed are described below:

- In primary control, the performance comparison of two well-known control is investigated.
- Proposed and implemented the PV power fluctuation mitigation and compared it with the commonly used method.
- Developing a low-cost supervisory control system based on embedded MAS and integrated the IoT technology to the microgrid. Comparing to previous research [10], this work results in cost reduction for MAS implementation and it is applicable to the field control.

### 1.4 Organization of the Dissertation

This thesis is organized into six chapters and separated into two experiments such as simulation and hardware experiments. For the simulation experiment, the microgrid model was implemented using MATLAB/Simulink. Meanwhile, in the hardware experiment, a laboratory scale microgrid is implemented. The system consists of two distributed generators, a PV simulator, a battery energy storage system and a group of loads. Following the introductory chapter, the rest of the disseration is outlined as follows.

- Chapter 2: Microgrids: Concept, Operation, Challenge and Control.  
In this chapter, the Microgrids' structure is firstly presented. Then, the duties of the MG in different operation modes, namely grid-connected and islanded, are described. Finally, a brief description of the existing control strategies is given, explaining why hierarchical control seems to be one of the most promising.
- Chapter 3: Preliminaries in Control and Theories.  
This chapter addressed the relevance control theory which is the most important for designing the control system. The chapter is divided into three main sections.



The primary section and secondary section are related to inverter synchronized scheme and inverter control strategies. Tertiary section, some basic knowledge as well as the theory are provided regarding advanced intelligent methods such as optimization, multiagent system, and artificial neural network.

- Chapter 4: Implementation of Laboratory Scale Microgrid and Hierarchical Control. This chapter presented the implementation of laboratory scale microgrid and the design of the proposed control system.
- Chapter 5: Results and Discussion. The results which obtain from both simulation and hardware experiment are illustrated in this chapter. As the tertiary layer are mainly about hardware experiment, the result only regarding to primary and secondary control layer are presented in simulation. Whereas, the experimental section which verified to simulation are discussed cover the results obtaining from those three layers.
- Chapter 6: Conclusion and Future Work. A summary regarding the results of the simulation, experiment and remark on the future work that can be done is presented in this chapter.



## MICROGRID: CONCEPT, OPERATION, CHALLENGE AND CONTROL

The integration of renewable energy resources in terms of the microgrid is expected to solve the vast increase of global energy consumption, environmental concern as well as to improve the reliability of the system. However, the strong dependence on the meteorological of renewable sources like PV and wind turbines pose a great challenge to the system operation, system's stability and quality. Hence, to exploit the benefit of those inverter-based generators, it is required to well acknowledge its behavior as well as its impact. Therefore, the introduction of an AC microgrid is presented in this chapter. Starting from the description of its physical structure, continuing with an analysis of the peculiarities and the issues related to the microgrid's operation modes, namely standalone and grid-connected. Then, the challenge, opportunity, and control in the microgrid are demonstrated.

### 2.1 Microgrid Concept and Structure

A microgrid is a small scale power system that has the designed objective to supply to the small community such as an island, university, military base ., etc. A general structure of the microgrid is demonstrated in Fig. 2.1. It forms by the interconnection of dispersed energy resources, such as wind turbines, PV, fuel cells, micro-gas turbines, energy storage systems such as flywheels, supercapacitors, and batteries, and controllable loads. The implementation of the microgrid system is expected to gain several benefits as described below.

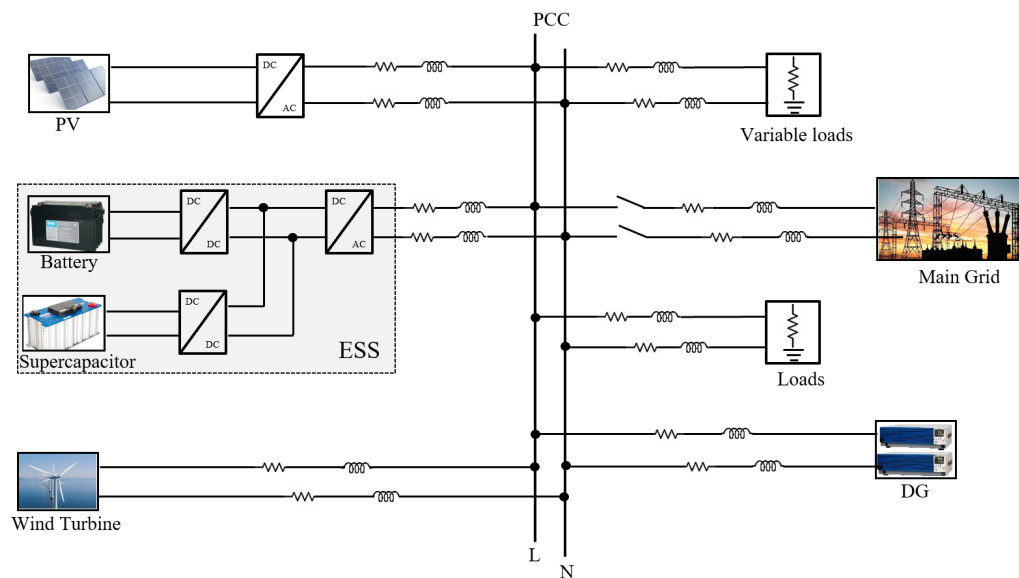


Fig. 2.1: Basic structure of microgrid

**From a grid point of view**, the main advantage of a microgrid is that it is treated as a controlled entity within the power system. It can reduce the power flow on transmission and distribution lines; as the result, the power losses and the costs for additional power are reduced. Moreover, It can deduce the load on the network by eliminating the impasse in meeting electricity needs and help repair network in case of errors [11].

**From the customers' point of view**, microgrids are beneficial for locally meeting their electrical/heat requirements. They can supply uninterruptible power, improve local reliability as well as network quality, reduce feeder losses and provide local voltage support and can reduce the cost to be incurred by the user.

**From environmental point of view**, microgrids are a promising solution to handle environmental pollution and global warming through utilization the renewable energy resources.

### 2.1.1 Operation Mode

Microgrid development has done by many countries such as India, Malaysia, and Haiti [12] since it offers many advantages such as better power quality and more environmentally friendly. Moreover, the economic potential that may still be used from this system is the opportunity to utilize the waste heat from the engine generator using a combined heat and power (CHP). However, to achieve a stable and secure operation, a number of technical, regulatory and economic issues have to be resolved before microgrids can become commonplace. Some problem areas that would require due attention are the intermittent and climate-dependent nature of generation of the distributed energy resource (DER), low energy content of the fuels and lack of standards and regulations for operating the microgrids in synchronism with the power utility. The study of such issues would require extensive real-time and off line research, which can be taken up by the leading engineering and research institutes across the globe.

Microgrid can be operated either grid-connected or standalone system. Thanks to the possibility of using the voltage source inverter (VSI) in the so called Voltage Controlled Mode (VCM) and Current Controlled Mode (CCM). When operating in VCM, the power output of the VSI is controlled by adjusting the voltage amplitude and frequency. Meanwhile, in the CCM, the output current is regulated to the desired value. Furthermore the transition from one operational mode to the other can be done seamlessly. In the following section, the features of both operating modes are described.

#### 2.1.1.1 Standalone Mode

As mentioned earlier, the microgrid can be operating in standalone or islanded mode and grid-connected mode. In the islanded mode, the microgrid is separated from the main grid by opening the main switch at the point of common coupling (PCC). The

microgrid switch to the islanded mode when the upstream system (main grid) faces some inconvenient condition like upstream fault or maintenance purpose. In this operation mode, the total power demand is fully supplied by the DGs of the microgrid. During the supply-demand unbalancing, some low priority loads (non-critical load) could be disconnected from the system to secure the system from collapse as the power supply shortage. Moreover, the system voltage and frequency are not fixed which are dynamic accordingly the active and reactive power requirement. The all about problems can be solved by developing some control techniques, which conducted by other researchers to regulate voltage and frequency as well as perform load-shedding.

#### 2.1.1.2 Grid Connected Mode

Another operation mode of the microgrid is grid-connected. This mode of operation, the voltage, and frequency of microgrid are followed to utility's voltage and frequency. The power flow from microgrid to the main grid when the power demand is less than the total rated power of the DGs and flow from the main grid to microgrid in case of over demand. The control system is responsible to issue the proper power command for the system. The commanded power is computed based on the various criteria such as the economic and optimal operation of the microgrid, microgrid condition as well as requirements, and the main grid conditions and requirements. For example, the control system may decide to charge the BESS when the electricity's price of the main grid is cheap or discharge the BESS when the electricity's price is high. At the same time, the control system may control the DER to absorb the reactive power from the main grid to prevent the overvoltage on the grid side. On the other hand, it is worth mentioning that in the system which consists of motor load, a slight transient in voltage causes large power swing. So the voltage at PCC should not deviate from its normal value and the VSCs must quickly supply to power demand.

### 2.1.2 Challenges and Opportunities

#### 2.1.2.1 Technical Challenges

- **Operation** Due to the un-dispatchable of microgrid's energy resource, the system is often experiencing a large power mismatch during islanded operation mode. This matter leads to voltage and frequency control problem [13, 14].
- **Components and Compatibility:** As mention earlier, the microgrid is a promising technology for future smart grid development. It forms by a combination of various components such as renewable source, diesel generator, microturbine, fuel cell, energy storage system, inverters, communication system, and control software. The divers characteristic of these components such as power generation, startup/shutdown time, operation cost and efficiency, energy storage charging/disch-

arging rate, control and communication introduce more constraint of integration, operation, and control [13, 15].

- **Integration of Renewable Generation:** The intermittent nature of renewable sources is the main factor of system stability degradation [16--18]. Normally, a renewable source like PV strongly dependence on the grid-tie inverter to integrate into the main grid. The grid-tie inverter with traditional control confronts some problems such as lacking the grid-forming ability as well as inertia support.
- **Protection:** Designing the system protection for the microgrid is the most challenging issue as it must handle both microgrid and the main grid fault. The different operation mode provides the different fault current magnitude [19]. Unlike the conventional power system that the system protection is designed based on unidirectional fault current flow in the radial distribution system, the integration of DG into the power grid allows the fault current flow in bi-direction. As a result, designing system protection has become even more complex. Numerous protection schemes [20, 21] are presented to address the microgrid protection.
- **Policy or Regulation:** To enable widespread microgrid application, regulation plays a major role to provide the guideline covering the DER integration, DER penetration rate, and main grid connection. It ensures the standardize of DG integration as well as microgrid-main grid interconnection without disturbing the functionality and safety of the main grid [13]. However, the most complained challenge to interconnect microgrids with the main grid is the high connectivity costs because of high connection fee policies [22].

#### 2.1.2.2 Opportunities in Microgrid

Regarding microgrid challenge, several possible solutions are discussed below.

- The impact stochastic nature of renewable energy resources could be solved with energy storage system [23], and the penetration rate can be increased by revising the conventional control method of the grid-tie inverter to virtual synchronous generator [24]. Additionally, the harmonics which are caused by power electronic (switching) can be mitigated by proper filters designed [18]. The stability classifications and analysis methods for microgrid have been investigated in [25].
- To ensure the safety and reliability operation, various protection schemes have been presented. In [26] present a microprocessor-based overcurrent relays and directional elements. Adaptive protection system presented in [27], symmetrical component theory provided in [28] and differential protection discussed in [29].

### 2.1.3 Control Scheme of Inverter-Based Distributed Generators

Due to more and more integration of renewable energy resources, power electronics becomes a significant contribution to enable grid interfacing. The DG based on renewable source like PV usually needs the back-to-back converter to supply the AC power to the main grid. The back-to-back converter consists of a generator-side converter (PV) and a grid-side converter (main grid). The grid-side converter commonly adopts the maximum power point tracking to ensure the maximum power output from PV. While the control system for the grid-side converter (inverter) can be distinguished according to the microgrid operating mode that will describe below.

### 2.1.3.1 Control Structure in Grid-connected Mode

In grid-connected mode or grid-following strategy, the voltage and frequency are maintained by the main grid. Hence, the inverter is usually controlled to inject the available power. The control method can be dispersed based on DG, and it will present below.

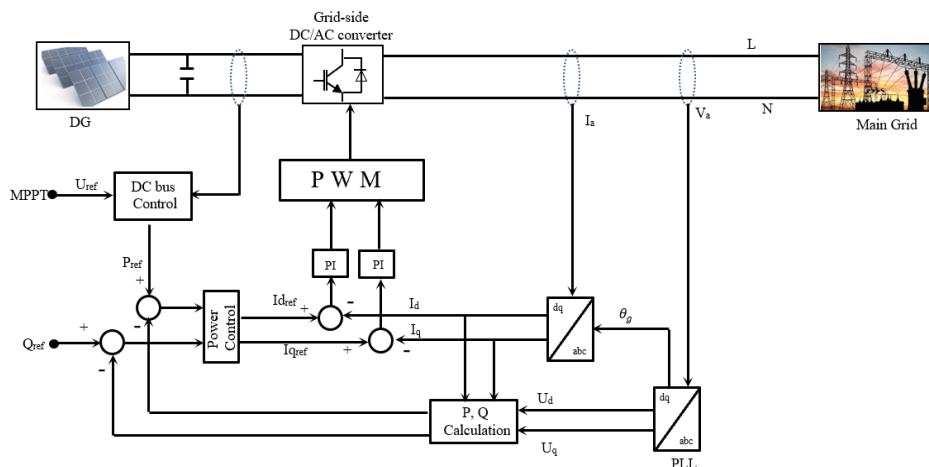


Fig. 2.2: Grid-following strategy of a PV generator with variable DC bus voltage for MPPT.

## † Non-dispatchable Distributed Generators

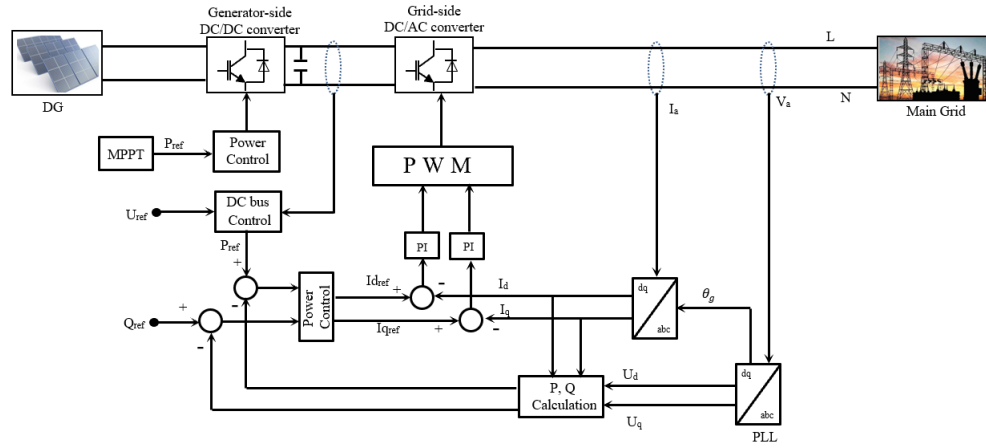


Fig. 2.3: Grid-following strategy of a PV generator with a generator-side converter for MPPT.

Renewable energy resources like PV and wind turbine can be classified as non-dispatchable distributed generator. The maximum power point tracking is commonly implemented to realize the maximum power output, and the DC link voltage can be controlled by the grid-side converter (inverter) as shown in Fig 2.2 to inject the desired reactive power.

The alternative control method can be implemented as presented in Fig 2.3. The DC link voltage can be controlled by adjusting the power reference ( $P_{ref}$ ). The reactive power is controlled by regulating the magnitude of the inverter's reactive current.

### † Dispatchable Distributed Generators

For dispatchable generators such as gas microturbine and fuel cell, the generated power can be varied. Hence, the DC link voltage can be maintained constant. The control scheme for these DGs is demonstrated in Fig 2.4. The grid-side inverter can control the active and reactive power.

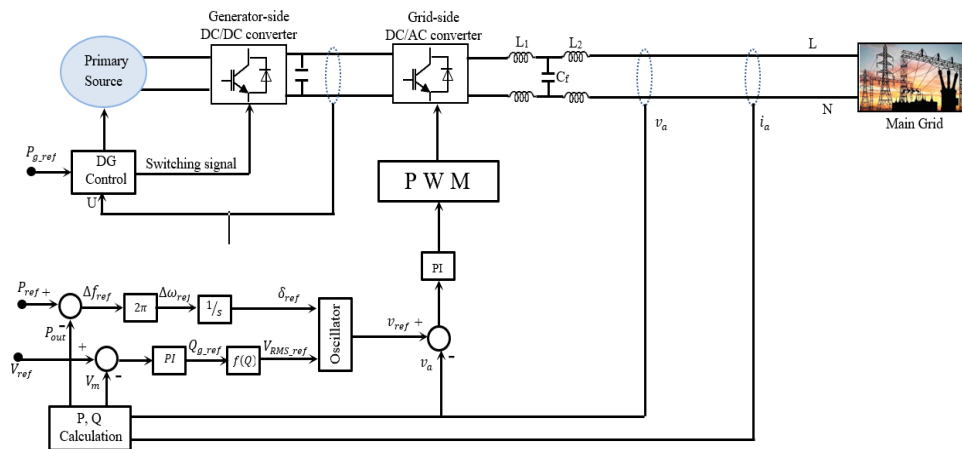


Fig. 2.4: Power dispatching strategy of a gas micro-turbine for a VSI control.

### 2.1.3.2 Control Structure in Islanded Mode

In islanded mode, it is necessary to establish the common bus voltage and at the same time provide the demanded active and reactive powers. Based on this strategy, a DG unit should attempt to balance the power demand while regulating the voltage and stabilizing the frequency of the autonomous microgrid.

To understand this control structure, a simplified of the DG supply to the system is shown in Figure 2.5(a). All vectors and their associated reference direction can be seen in it. Figure 2.5(b) is the vector diagram of the micro source.

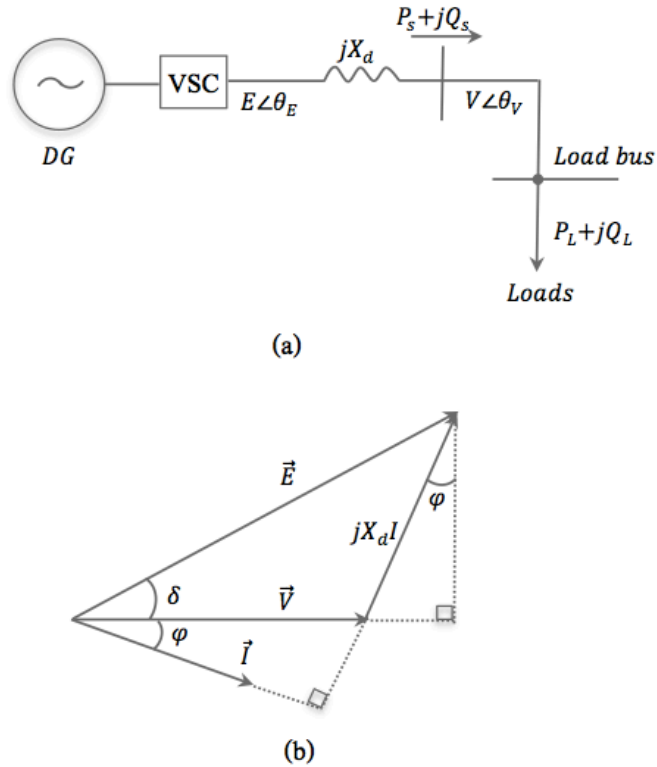


Fig. 2.5: Phasor diagram of microsource

The power inject from the DG can be described as follow:

$$S = P_s + Q_s \quad (2.1)$$

$$P_s = VI \cos \varphi \quad (2.2)$$

$$Q_s = VI \sin \varphi \quad (2.3)$$

Notice that  $\cos \varphi$  is the power factor,  $\varphi = \angle \theta_V - \angle \theta_I$ ;  $\delta = \angle \theta_E - \angle \theta_V$ . By apply geometry knowledge to Figure 2.5(b), Eq. (4.10) and Eq. (2.5) can be got:

$$X_d I \cos \varphi = E \sin \delta \quad (2.4)$$



$$X_d I \sin \varphi + V = E \cos \delta \quad (2.5)$$

Simplified Eq. (ref4) and Eq. (2.5), Eq. (2.6) and Eq. (2.7) can be got:

$$I \cos \varphi = \frac{1}{X_d} \sin \delta \quad (2.6)$$

$$I \sin \varphi = \frac{1}{X_d} (E \cos \delta - V) \quad (2.7)$$

With Eq. (2.6) and Eq. (2.7), Eq. (4.11) and Eq. (4.9) are rewritten as:

$$P_s = \frac{EV \sin \delta}{X_d} \quad (2.8)$$

$$Q_s = \frac{EV \cos \delta - V^2}{X_d} \quad (2.9)$$

Considering that the power angle  $\delta$  is small (less than 0.1 rad), we can assume  $\sin \delta = \delta$  and  $\cos \delta = 1$ , then the equation Eq. (2.8) and Eq. (2.9) can be simplified as:

$$P_s = \frac{EV}{X_d} (\theta_E - \theta_V) \quad (2.10)$$

$$Q_s = \frac{V}{X_d} (E - V) \quad (2.11)$$

From equation Eq. (4.8) and Eq. (2.11), it's clear that the active power from DG depends on converter output voltage phase angle  $\theta_E$  and the reactive power rely on converter output voltage amplitude  $E$ . So the active power is controlled by control  $\theta_E$  and the reactive power is controlled by control  $E$ . This control structure is known as droop control.



## PRELIMINARIES IN CONTROL AND THEORIES

As stated in section 1.2, the objective of this research is to solve the major issues of the microgrid by designing the decentralized hierarchical control. To realize this, a comprehensive knowledge related to the control theories is a must. This chapter covers the theory behind the grid-tie synchronize method, inverter control, and advance and intelligent control strategies.

### 3.1 Phase Lock Loop

To possible integration of renewable energy resource into the AC grid, the RES with DC nature highly relies on inverter that its inverter must be synchronized with the grid through verification of grid's voltage, phase angle and frequency as specified in IEEE standard 1547-2003. Due to alter behavior of the grid, the grid voltage may fluctuate. To ensure a high-quality power injection to the grid, a phase-locked loop (PLL) is need. The PLL extracts the information from the grid such as voltage amplitude, phase angle and frequency. Through this information, the synchronized between the inverter and the grid is achieved and maintained. There are two well-known PLL techniques, namely zero crossing PLL (ZC-PLL) [35] and synchronous reference frame PLL (SRF-PLL) [36, 37]. According to the author [38], the SRF-PLL is found to have better attenuate the grid voltage harmonic compare to the ZC-PLL. Hence, the SRF-PLL is adopted in this dissertation. The SRF-PLL used the real-time sampling of the instantaneous value of the grid voltage and its principle operation is shown in Fig. 3.1 .

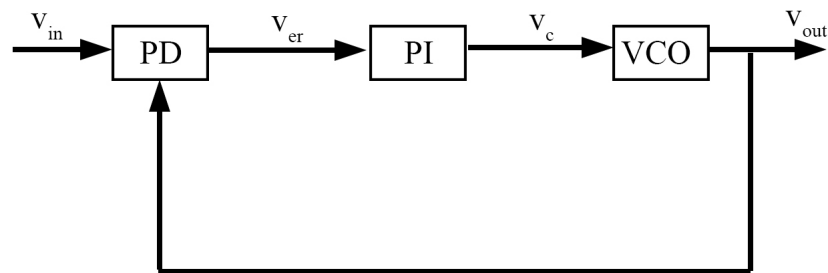


Fig. 3.1: Schematic diagram of PLL

The SRF-PLL has three main function blocks such as phase detector (PD), propotional integrator (PI), and voltage-controlled oscillator (VCO). The PD block compares the phase of grid and the inverter to generate the error quantity ( $V_{er}$ ). The PI block processes the  $V_{er}$  and sends it to the VCO function block. The VOD regulates the frequency to ensure that PLL is tracked the grid's information correctly via the close loop process.

Figure 3.2 shows the principle of SRF-PLL for single-phase grid-connected inverter,

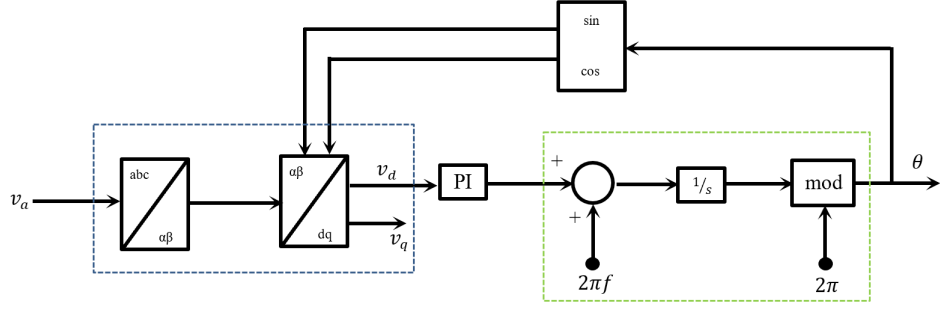


Fig. 3.2: Schematic diagram and model of SRF-PLL

where PD is depicted in the blue dash-line frame, VCO is depicted in the green dash-line. The single-phase transformation from natural frame ( $abc$ ) to the stationary frame ( $\alpha\beta$ ) is provided in Eq. 3.1 that  $V_\alpha$  is in phase with  $V_a$  and  $V_\beta$  is obtained by shifted  $V_a$  in  $-90^\circ$  (lagging), and the stationary frame to the synchronous frame is expressed in Eq. 3.2.

$$\begin{bmatrix} v_\alpha \\ v_\beta \end{bmatrix} = \begin{bmatrix} v_a \\ v_a(\omega t - \pi/2) \end{bmatrix} \quad (3.1)$$

$$\begin{bmatrix} v_d \\ v_q \end{bmatrix} = \begin{bmatrix} \cos(\theta) & \sin(\theta) \\ -\sin(\theta) & \cos(\theta) \end{bmatrix} \begin{bmatrix} v_\alpha \\ v_\beta \end{bmatrix} \quad (3.2)$$

### 3.2 The Current Control Strategies

In grid-connected inverter, current control is a high-status issue, which needs to be dealt with. The main function of current control is to ensure that the measured output value is followed by the desired value. The current control can be implemented in several ways such as natural reference frame ( $abc$ ), the synchronous rotating reference frame ( $dq$  decoupling), and the stationary reference frame ( $\alpha\beta$ ). The below section will describe in detail about each control framework.

#### 3.2.1 Proportional Integral Current Controller in the Synchronous Reference Frame

Proportional-Integral (PI) controller gains a great popularity in many fields which relate to system control. The transfer function of a PI controller is defined by Eq. 3.2 [39]:

$$G_{pi}(s) = k_p + \frac{k_i}{s} \quad (3.3)$$

where  $k_p$ ,  $k_i$  are the proportional and the integral gain of the PI controller.

In grid-connected inverter, the PI controller has been deployed in synchronous

reference frame (SRF) to track the reference current so that the desired current can be injected into the grid. The SRF control block diagram is demonstrated in Fig. 3.3

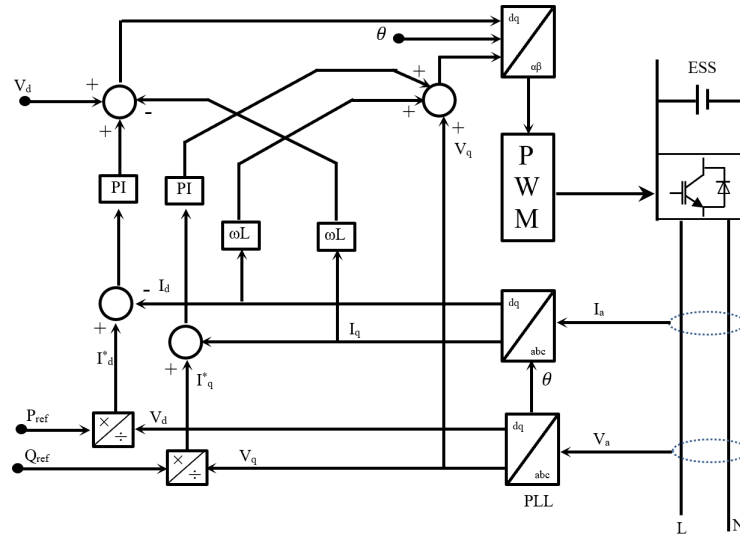


Fig. 3.3: Block diagram of SRF control

To perform the SRF or  $dq$  decoupling control, the measured inverter's output voltage and current, which is in the natural frame ( $abc$ ) need to transform to synchronous reference frame ( $dq$ ) first. The single-phase transformation from natural frame ( $abc$ ) to stationary frame ( $\alpha\beta$ ) is provided in Eq. 3.1 that  $V_\alpha$  is in phase with  $V_a$  and  $V_\beta$  is obtained by shifted  $V_a$  in  $-90^\circ$  (lagging). Then, the stationary frame to the synchronous frame is expressed in Eq. 3.2. The inner current control loop controls the current supplied by the converter to match its desired value by comparing the desired current value ( $I^* = \frac{P}{V}$ ) with the measured current  $I_d$ . The modulating signal ( $m_d$  and  $m_q$ ), which uses to control the switching time ( $IGBT$ ) can be obtained via the Eq. 3.4.

$$\begin{aligned} m_d &= V_d - I_q \omega L + k_p(I_d^* - I_d) + k_i \int (I_d^* - I_d) \\ m_q &= V_q + I_d \omega L + k_p(i_q^* - I_q) + k_i \int (I_d^* - I_q) \end{aligned} \quad (3.4)$$

Although the PI controllers are so far the most widely applied controllers in industry, it still has some drawbacks as listed below:

- In the stationary reference frame, the PI controller cannot eliminate the steady-state error [40, 41].
- PI controller has poor performance due to cross-coupling between d and q coordinators. Consequently, the functioning of the PI controller can be enriched by

presenting a decoupling term between the d and q coordinators and the voltage feedforward [42].

- The PI controller cannot ride through the low order harmonic issues. Hence, there is a concern when apply to grid-connected inverter [43].
- Required more transformation from three to two phases. As a result, more space is needed in a low-cost fixed-point DSP [44].

### 3.2.2 Proportional Resonance (PR) Current Controller in Stationary Reference Frame

Seeing the shortcomings of the PI controller, an alternative current controller scheme has been introduced, so called the proportional resonant controller (PR). The PR controller is formed by two terms such as proportional and resonant. The PR controller can be defined by the transfer function express in Eq. 3.5

$$G_{PR}(s) = K_p + K_i \frac{s}{s^2 + \omega_f^2} \quad (3.5)$$

Where,  $K_p$  and  $K_i$  are proportional and integral gain of the controller,  $\omega_f$  ( $\omega_f = 2 * \pi * f$ ) is the fundamental frequency. In order to solve the stability issues which cause by infinite gain, a non-ideal PR controller is introduced. The transfer function of non-ideal PR controller is expressed in Eq. 3.6.

$$G_{PR}(s) = K_p + K_i \frac{2\omega_c s}{(s^2 + 2\omega_c s + \omega_f^2)} \quad (3.6)$$

where,  $K_p$  and  $K_i$  are the proportional and integral gain of the controller, respectively.  $\omega_f$  is the fundamental frequency, and  $\omega_c$  is the cut off frequency.

Furthermore, to eliminate the low order harmonics ( $3^{rd}, 5^{th}, 7^{th}$ ) in grid-connected inverter, the Harmonic Compensator (HC) term is commonly added in parallel with the PR controller.

The transfer function of ideal harmonic compensator is provided in Eq. 3.7 :

$$G_H(s) = \sum_{h=3,5,7,..} K_{ih} \frac{s}{s^2 + (h\omega_f)^2} \quad (3.7)$$

where,  $K_{ih}$  is the Resonant term at the particular harmonic and  $h\omega_f$  is the resonant frequency of the particular harmonic. The harmonic compensator for each harmonic frequency is added to the fundamental frequency PR controller to form the complete current controller.

The ideal harmonic compensator as expressed in Eq. 3.7 rise the same problem to the fundamental PR controller that it can give stability problems due to the infinite gain. To solve this issue, the harmonic compensator equation can be made non-ideal by representing it using 3.8.

$$G_H(s) = \sum_{h=3,5,7,..} K_{ih} \frac{2\omega_c s}{(s^2 + 2\omega_c s + (h\omega_f)^2)} \quad (3.8)$$

where,  $\omega_c$  is the bandwidth around the particular harmonic frequency of  $h\omega_f$ . Comparing to the ideal HC in Eq.3.7, the gain of modified HC, Eq. 3.8, is finite. But it is large enough to provide compensation.

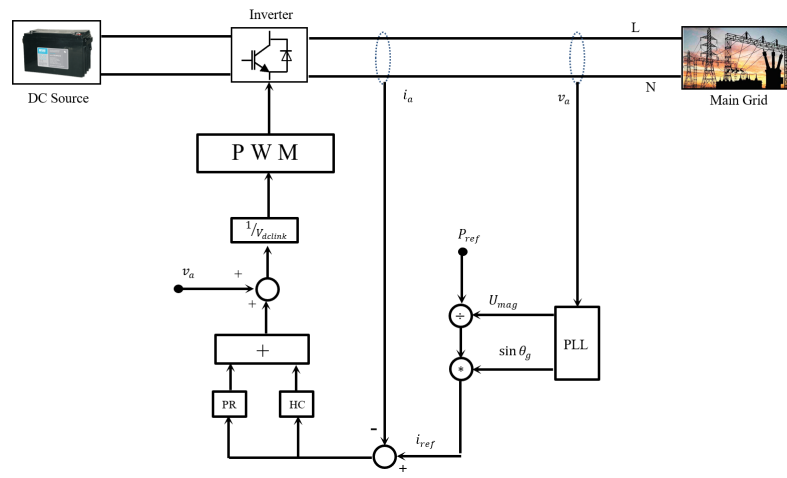


Fig. 3.4: Block diagram of stationary control

The application of PR controller can be found in stationary reference frame ( $\alpha\beta$ ) method [43, 45]. The control block diagram of PR plus harmonic compensation based current control in  $\alpha\beta$  is illustrated in Fig. 3.4.

Compare to the PI controller, PR controller found to be superior as describe below follows:

- The PR controller can eliminate the steady-state error by offering sufficiently large gain at the specific resonant frequency [46].
- The PR controller can supplement with harmonic compensator to eradicate the low-order harmonic frequency. As a result, a high-quality injected current is accomplished [47].
- No cross-coupled and Park's transformation required in PR control. Hence, reduce the error and the computation burden.

### 3.3 Advance Intelligent Control and Optimization Methods

#### 3.3.1 Optimization Method

Besides the conventional control method, numerous advanced control techniques such as optimization-based control, the multiagent system as well as the artificial neural network have been successfully applied in various purposes. For instance, the application of an advanced optimization algorithm to adjust the parameter of the controller to address the different operation both normal and abnormal or the transition among them, and it is proved the improvement of the controller performance.

For this reason, to enhance the robustness and to increase the performance of the traditional parameter-tuning techniques, some nature-inspired metaheuristic approaches that widely use in this aspect are given in the following sub-sections.

##### 3.3.1.1 Genetic Algorithm

Genetic Algorithms is a well-known optimization technique based on evolutionary algorithm. It was developed in 1975 by Holland and his collaborator [48]. GA solves the optimization problem through natural evolution mechanisms such as crossover, mutation, and selection. The procedure to search for the solution of GA describes below:

- Step1: Encoding of the optimization function.
- Step2 : Definition of a fitness function or selection criterion
- Step3 : Initializing a population.
- Step4 : Evaluation the fitness of all the individual in the population
- Step5 : Creation of a new population by performing crossover, mutation, and selection.
- Step6 : Update of the old population by the new one.

Steps 4, 5, and 6 are then repeated until certain stopping criteria are met. In the end, the best chromosome is decoded to obtain a solution to the problem.

##### 3.3.1.2 Particle Swarm Optimization

Particle Swarm Optimization (PSO) is a metaheuristic optimization which inspired from natural behavior of swarm such as fish and bird schooling. It first introduced in 1995 by Kennerdy and Eberthart [49]. PSO searches the space of an objective function by adjusting the trajectories of individual particles. Each particle traces a piecewise path that it can be modeled as a time-dependent positional vector. The movement of a swarming particle consists of two major components: a stochastic component and a

deterministic component. Each particle moves toward the location of the current global best and its own best-known position in memory. After a particle detects a location that is better than any previously found locations, it updates this location as the new current best for particle  $i$ . There is a current best for all  $N$  particles at any time  $t$  at each iteration. The aim is to find the global best among all the current best solutions until the objective no longer improves or after a certain number of iterations.

### 3.3.1.3 Backtracking Search Optimize Algorithm

Backtracking search optimization algorithm (BSA) [50] is one of the new population-based evolutionary algorithms. It bases on an iterative process which tries to minimize the objective function. Five evolutionary mechanisms such as initialization, selection-I, mutation, crossover, and selection-II are employed in BSA. The complete process of BSA provides in Fig. 3.5.

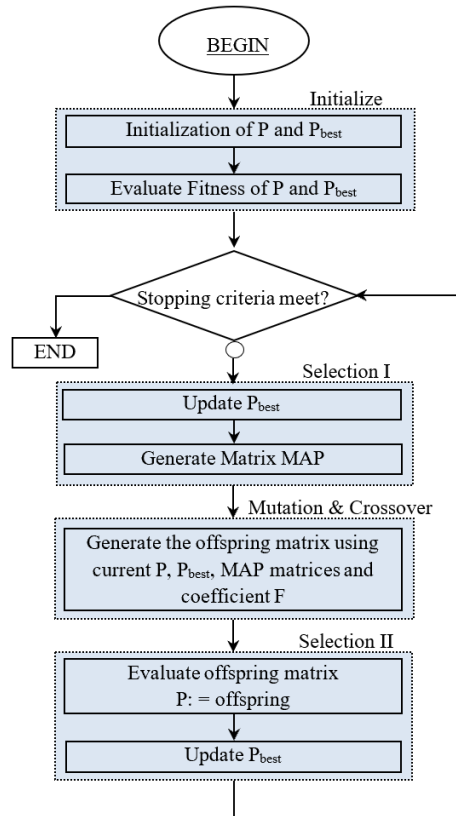


Fig. 3.5: Flowchart of BSA

- Initialization: The population  $P = (P_{i,j})_{(N,M)}$  and  $oldP_{i,j}$  is initialized via a uniform stochastic selection of particle values within the solution space, as shown by expression 3.9. The fitness function is first evaluated by using the initialized value of the population.



$$\begin{aligned}
P_{ij} &= P_{jmin} + rnd(P_{jmax} - P_{jmin}); && \text{Initialization of population, } P. \\
oldP_{i,j} &= P_{jmin} + rnd(P_{jmax} - P_{jmin}); && \text{Initialization of } oldP. \\
fitnessP_{i,j} &= objFun(P_i); && \text{Initial fitness value } P.
\end{aligned} \tag{3.9}$$

Where  $(i) \in \{1, \dots, N\}$ ,  $(j) \in \{1, \dots, M\}$ .  $N$  is the number of population and  $M$  is the number of dimensions. The dimensions are referred to the number of variables that need to define ( $J$  and  $D$ ).

- *Selection – I* : There are three things done in *Selection – I* such as update  $P_{best}$  matrix, memorize the previous experience ( $oldP$ ) and random order based on Equation 3.10, and generate binary integer-valued matrix ( $map$ ).

$$oldP_{ij} = permuting(oldP). \tag{3.10}$$

- *Mutation* : The trial population Mutant is initialized in the Mutation step by following the Equation 3.11.

$$\begin{aligned}
mutant_{ij} &= P_{ij} + F(P_{bestij} - P_{ij}) \\
(i) &\in \{1, \dots, N\}; (j) \in \{1, \dots, M\}
\end{aligned} \tag{3.11}$$

Where  $F$  is a real number to control the step size of search path or direction.

- *Crossover* : Generates the final form of the trial population (offspring).  
- *Selection – II* checks whether fitness offsprings give better fitness value than that obtained so far using the initial population or not. If fitness offsprings give better results, then update offsprings by fitness offsprings via  $P_{best}$  matrix; otherwise, keep the previous one. Keeping doing this same process until the termination criterion is met.

### 3.3.2 Multiagent System

An agent is a software or hardware-based computer system that is situated in some environment. It is capable to perform autonomous action in the environment in order to meet its design objectives [51]. Agents take sensory input from their environment, produce output actions accordingly as shown in Fig. 3.6.

Agents can be described with several properties:

- **Autonomy**: Agents are capable of operating without any intervention from human supervision.
- **Social ability**: Agents are able to communicate with each other as well as human operators using a common language.

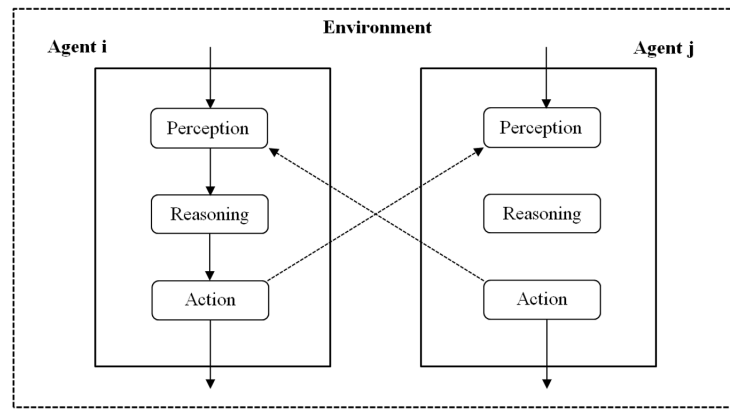


Fig. 3.6: A simple agent in its environment

- **Reactivity:** Agents can identify the change in their environment and respond quickly to changes that may occur.
- **Pro-activity:** Agents can exhibit goal-directed behavior by taking the initiative.

### 3.3.2.1 The Multiagent System Versus SCADA

Most conventional power systems rely on Supervisory Control and Data Acquisition (SCADA) for systems control and communications. SCADA works like a centralized control system. It collects a large data from the system before it does some control tasks. Therefore, SCADA may provide slowly response when the system is highly dynamic. In terms of a microgrid, the aim is to allow for flexible integration of a multitude of different distributed energy resources and non-conventional renewable energy sources (NCRES) that those resources are intermittent nature. As a result, the system is more complex and dynamic. In this context, SCADA is not suitable for microgrid control. In contrary to SCADA, MAS works like a decentralized control system. It allows for a complex task to be broken down into several smaller tasks and assigned to a group of agents through information sharing. This allows for easier handling of a larger problem. The use of multiagent system (MAS) to provide distributed control capabilities to the microgrid applications offer various advantages over conventional SCADA systems as describe below:

- Most of MAS development platforms are Free and Open-Sources applications and available in various languages such as Python, Java, C# and  $C/C^{++}$ , etc. This makes them paltform independent.
- MAS can also be combined with external programming to interface with different external hardware and software systems. These advantages make MAS more suited for microgrid control.

- MAS are inherently flexible and extensible.
- Local loads and sources will have different specifications and systems. Therefore, an intelligent distributed control system like MAS is the best solution.
- In some cases, the microgrid will have to take rapid autonomous decisions regarding the seamless transition to the islanded mode from grid-connected mode and protecting critical loads by load shedding. This can be done quickly by MAS.

### 3.3.2.2 Standard for Agent Development

#### † Foundation for Intelligent Physical Agents Standards

Foundation for Intelligent Physical Agents (FIPA) was originally proposed in 1996. It is an international organization that is dedicated to promoting the industry of the intelligent agents by openly developing specifications supporting inter-operability among agents and agent-based application [52]. FIPA has been widely recognized as the major standards in the area of agents-based computing. Many standard specifications have been developed, such as Agent Communication Language (ACL) and Interaction Protocols (IPs), etc. Figure 3.7 shows the overview of the FIPA standards. Here, only one main FIPA standard specification; agent management system standard, is presented.

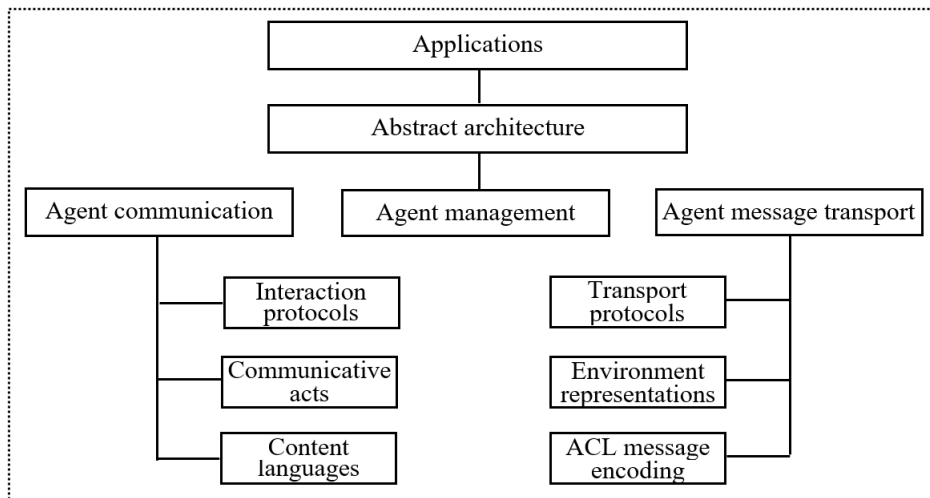


Fig. 3.7: Overview of FIPA standard

#### † FIPA Agent Management System Standard

The FIPA Agent Management System Standard Specification (SC00023K) denoted as agent management reference model of the runtime environment that FIPA agents inhabit. The logical reference is established for agent creation, registration, communication, location, migration and retirement. The referent model includes a set of logical-based entities, such as:

- an agent runtime environment for defining the notion of agent used in FIPA and lifecycle;
- an agent platform (AP) for deploying agent in a physical infrastructure;
- a Directory Facilitator (DF) which provides a yellow page's service for the agents registered on the platform;
- an Agent Management System (AMS) acting as a white pages service for supervisory control over access to the agent platform;
- a Message Transport Service (MTS) for communication between the agent registered on different platform.

Figure 3.8 gives the FIPA agent management reference model constitution.

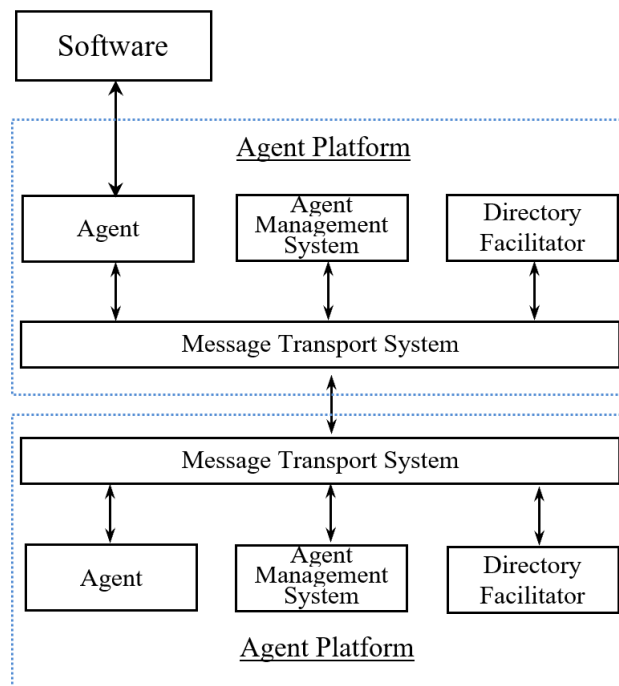


Fig. 3.8: FIPA agent management reference model

### 3.3.2.3 Multiagent System Development Toolkit

A complete description of a conceptual design process for creating MAS is to follow the generic four stages development process:

- Analysis : Modeling agent roles and behaviors. Identifying the application domain and problem.
- Design : Defining solution architectures for problems identified in the Analysis step

- Development : Programming agent goals, ontology and functionality
- Deployment : Launching generated MAS, run-time agent management, message passing and data processing.

Building a MAS requires an agent development environment that supports at least some stages of the MAS conceptual design process. The most often used platforms by researchers for developing MAS for microgrid control applications is summarized in Table 3.1 and discussed as below:

Table 3.1: Summary of MAS development platforms

	JADE	Mobile-C	SPADE	VOLTTRON
Free and Open Source	Yes	No	Yes	Yes
FIPA Compliant	Yes	Yes	Yes	No
Editor	Gui	command line	wui	command line
Platform support	Active	Active	Active	Active
Programming	Java	C/C++	Python	Independent
leal application	Scalable Microgrid	Automation	Automation	Building Energy Management

#### † JADE

JADE was originally developed under TILab, formerly CSELT, in Italy (Bellifemine et al. 2005) to address the lack of support available for building agent systems. As its name suggests, this framework offers an environment in which to create agents written in Java. It provides a runtime environment, which the agents require in order to operate, an extensive library of classes with methods built around the FIPA specification of agent characteristics, and graphical interfaces for monitoring active agents. As shown in Fig. 3.9, Jade is composed of four main components such as:

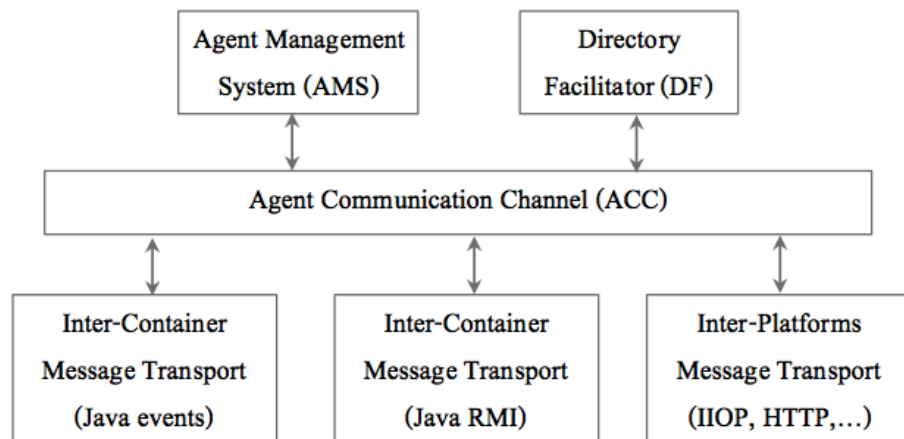


Fig. 3.9: Jade architecture

- **Agent management system:** The AMS ensures that each agent has a unique name and can be used for creating and removing agents from the platform.
- **Directory facilitator:** It implements like the yellow page service. From DF, an agent can register their service or get from other agent in the system.
- **Agent communication channel:** It works as gate or route for agent to exchange information by using an agent communication language (ACL).
- **Message transport:** It uses to transfer data from agent to agent.

Each instance of a runtime environment is called a container; several of these make up a platform. The first container to be created needs to be designated as the main container; subsequent containers then registers with this as they join the platform. Containers can be spread across several networked computers. The main container hosts an agent management service (AMS) and a Directory Facilitator (DF).

#### † Mobile-C

Mobile-C [53] is a mobile agent building toolkit, which develops based on C/C++ language and compliant to IEEE FIPA (Foundation for Intelligent Physical Agents). Mobile-C has been developed for deploying in real-time applications like the embedded system and network intelligent mechatronics.

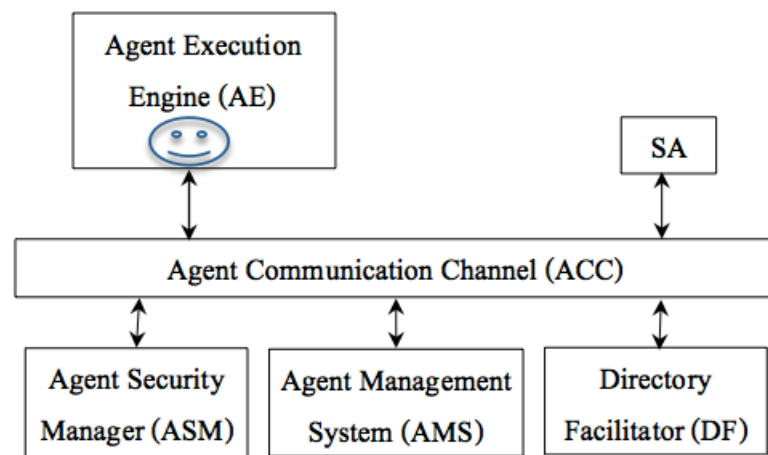


Fig. 3.10: The system architecture of agency in Mobile-C

The architecture of Mobile-C is shown in Fig. 3.10. Unlike Jade, Mobile-C composes of two elements such as Agency and Agent. Agency resides in each node of a network and works as a container or environment for mobile agents execution. The interaction from one agency to other agency in order to exchange information is possible by migrating agent in XML format. The core elements of agency are listed below:

- Agent Communication Channel (ACC): It works as gate or route for agent to exchange information by using an agent communication language (ACL).
- Agent Management system (AMS): It works like the system supervisor. It controls all agent functions and life cycle of agents as well. All agents need to register with AMS in order to get an AID.
- Agent Security Manager (ASM): The ASM is responsible for maintaining security policies for platform and infrastructure.
- Directory Facilitator: It implements like the yellow page service. From DF, an agent can register their service or get from other agent in the system.
- Agent Execution Engine (AEE): It works like container or environment where the agent executes or invokes with Ch runtime.

#### † **Smart Python multi-Agent Development Environment (SPADE)**

SPADE [54] is an agent building platform written in Python programming language and based on XMPP/Jabber. It is FIPA compliant platform and the FIPA-Acl message is embedded in XMPP message.

The most noticeable feature of SPADE are listed as below:

- Develops using Python.
- Covers the FIPA standard.
- Implements four message transport protocol such as XMPP, P2P, HTTP and SIMBA.
- Supports two content languages: FIPA-SL and RDF.
- SPADE agents do reach their goals by running deliberative and reactive tasks.
- Has a web interface to manage the platform.
- Allows its execution in several platforms and operating systems.
- Presences notification allows the system to determine the current state of the agents in real-time.
- Multi-user conference allows agents to create organizations and groups of agents.

#### † **VOLTTRON**

VOLTTRON [55] is a distributed agent execution framework designed by Pacific Northwest National Laboratory (PNNL) specifically for use in electrical power systems.

The open-source and modular platform are intended to support transactions between networked entities over the grid. Communication is established through a central ‘MessageBus’ in the form of topics and subtopics (for example, ‘topic/subtopic/subtopic/’ = ‘weather/location/Temperature/’). The control architecture is modeled as a three-level hierarchy of agent classes:

- Cloud Agent : Publishing data to and from a remote platform
- Control Agent : Interact with devices
- Passive Agent : Interact with sensors and record data

A combination of agent classes can be employed to derive a variety of agents, and the VOLTTRON development page on Github provides clear examples. While a prototype implementation of VOLTTRON is available in Python, the platform is programming-language agnostic. VOLTTRON also provides driver support for most Modbus and BACnet devices.

### 3.3.3 Artificial Neural Network

In order to understand what artificial neural network and how it works, it is worth to study about the human brain first. The human brain is a decision system in the human being. It makes up of millions of neurons in complicated connection. Every neuron consists of three main components such as dendrites, cell body and axon as illustrated in Fig. 3.11. Dendrites which locates in branches of cell, carry the signals from other neuron to cell body which act as input neural. Cell body process the information receives from dendrites. The axon can be considered as neuron output which transmit signal to other neuron.

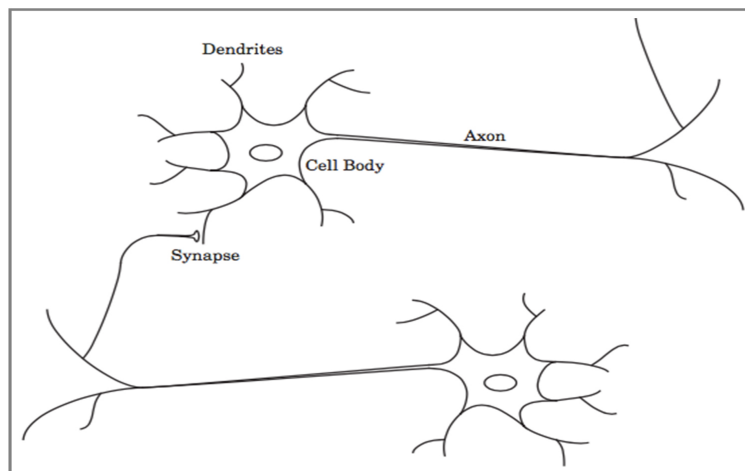


Fig. 3.11: Schematic drawing of biological neurons



The brain could solve various complex problems such as mathematical calculations, posture, motion, etc. through memorizing and learning from previous cases with the wonderful speed. Inspired from the ability of human brain, a new mimicked approach called artificial neural network (ANN) is emerged. The ANN can be considered as an intelligent mathematical algorithm which is successfully applied to predict many practical problems.

### 3.3.3.1 Neural Network Term

**Neuron:** It is the basic unit of a neural network. It gets a certain number of inputs and a bias value.

**Activation Function:** Activation functions are used to introduce non-linearity to neural networks modeling. It squashes the values in a smaller range. A specification activation function is chosen to satisfy the problem that the neuron attempts to solve. The most commonly used activation functions are Sigmoid, Tanh and ReLU.

**Input layer:** The input layer consists of the system's inputs. The "input layer" is simply a vector of the inputs.

**Hidden layer(s):** This layer, performs the mathematical calculations to provide the proper outputs.

**Output layer:** This layer is the last layer in the network and receives input from the last hidden layer. With this layer, we can get the desired number of values and in the desired range.

**Weights:** A weight represents the strength of the connection between units. If the weight from node 1 to node 2 has greater magnitude, it means that neuron 1 has greater influence over neuron 2.

**Batch Size:** The number of training examples in one forward/backward pass. The higher the batch size, the more memory space you will need.

**Training Epochs:** It is the number of times that the model is exposed to the training dataset.

**Normalization:** Data normalization is the process of rescaling one or more attributes to the range [0, 1]. Normalization is a good technique which could speed up the learning process.

### 3.3.3.2 Type of Neural Network

The different types of neural networks utilize different principles in determining their own rules. There are numerous types of artificial neural networks, each with their unique strengths. Here are some of the most important types of neural networks:

### † Single Layer Feed-forward Neural Networks

The single layer feed-forward network consists of a single layer, where the inputs are directly connected to the outputs, via a series of weights. It is the simplest type of feedforward network and can only classify separable cases with a binary target. Figure 3.12 shows the structure of single layer neural network.

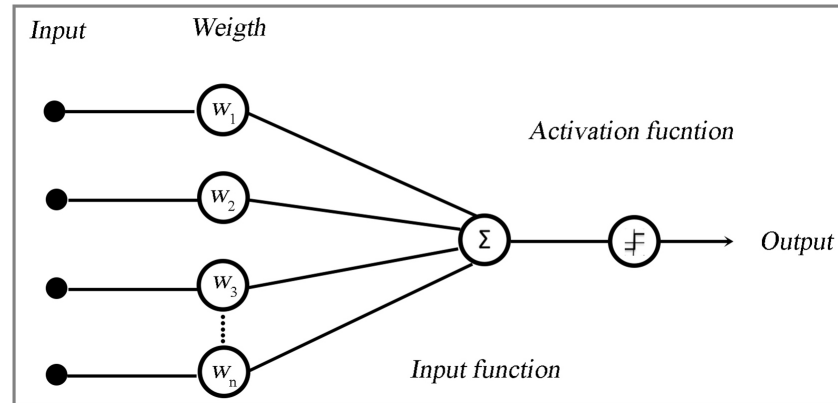


Fig. 3.12: Single layer of neurons

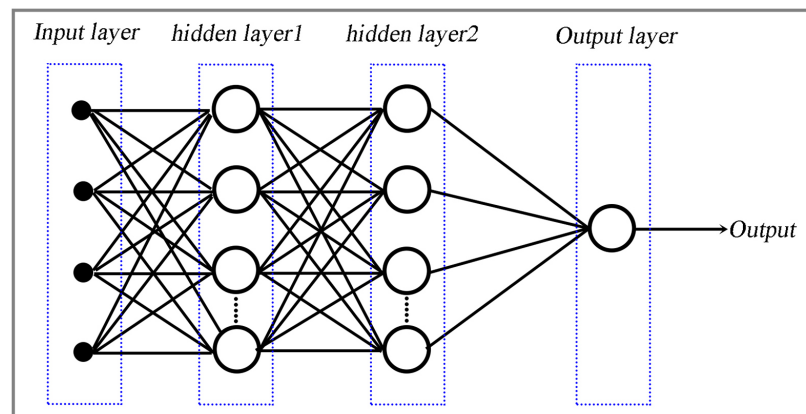


Fig. 3.13: Multi-layer network

### † Multi Layer Feed-forward Neural Networks

A multilayer feed-forward neural network has the same structure of a single layer network with one or more hidden layers. Network data and calculations flow in a single direction, from the input data to outputs. The hidden layers sit in between the input and output layers. Figure 3.13 demonstrates the structure of multiple layers of neural network.

† **Recurrent Neural Network** In these networks, the outputs of the neurons are used as feedback inputs for other neurons. The feedback feature qualifies these networks for dynamic information processing, meaning that they can be employed on time-variant

systems, such as time series prediction, system identification and optimization, process control, and so forth.

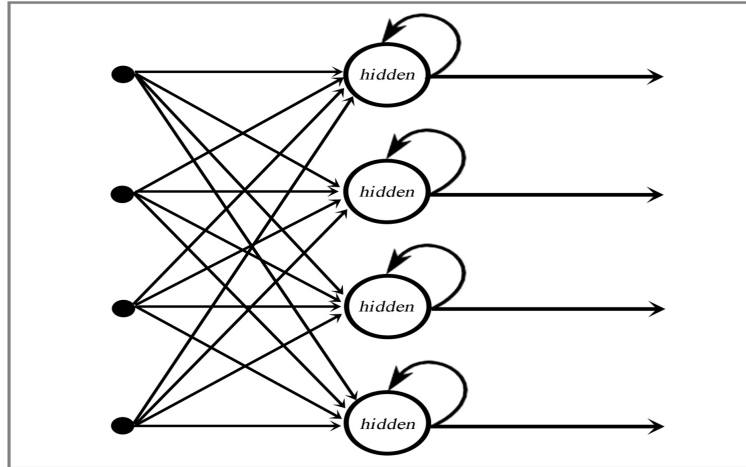


Fig. 3.14: Recurrent neural network

Unlike the traditional neural network, RNN has the ability to pass information from one time step to the next step and allow information to persist during the learning stage. In other words, RNNs connect previous information to the present task. Indeed, using previous sequence samples may help in the understanding of the present sample. A graphical representation of a basic RNN is given in Fig. 3.14. This figure shows that the hidden neurons receive input values from both the input neurons and the hidden neurons. The output of a particular layer is saved and fed back to the input. This helps predict the outcome of the layer.



## IMPLEMENTATION OF LABORATORY SCALE MICROGRID AND HIERARCHICAL CONTROL

The ultimate validation of the control performance could prove through the tests carried on a hardware level. In this chapter, the main component of laboratory-scale microgrid and its configuration is introduced. The steady-state and dynamic analysis can give many insights on the performance of the control, but it is only after realizing a scaled-down version of a microgrid that it is possible to assess the actual quality of the design. The details of the hardware setup that implements the proof-of-concept for the microgrid will be given in this chapter.

### 4.1 Microgrid Components

Figure 4.1 shows a laboratory-scale microgrid that is implemented to test the operation and the controller performance. It composes of two DGs, a PV simulator, battery energy storage system and loads. The detail of the major components is described in the following subsection.

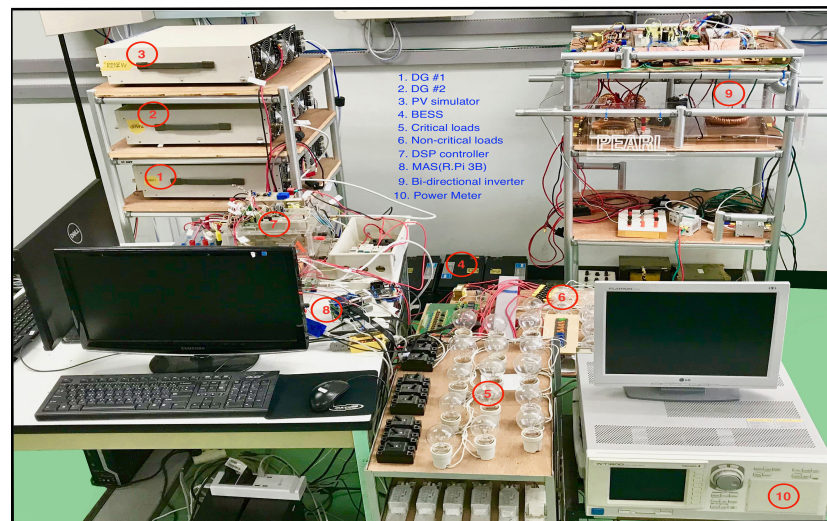


Fig. 4.1: Laboratory scale microgrid

#### 4.1.1 Distributed Generator

The Kikusui PCR2000M is a compact controllable AC/DC power supply that inherits the high quality and high performance. It has a wide operation range of output voltage and frequency. It comes with three options for interfacing as listed below.

- GPIB interface board (IB21): This is an interface board used to control the PCR-M with the GPIB.

- USB interface board (US21): This is an interface board used to control the PCR-M with the USB.
- Analog interface board (EX04-PCR-M): This interface board is used to control the output with external analog signals. The following functions are expanded.
  - The voltage of the output AC waveform (sine wave) is varied according to the input DC signal (EXT-AC mode).
  - The input waveform is simplify amplified and output (EXT-DC mode).

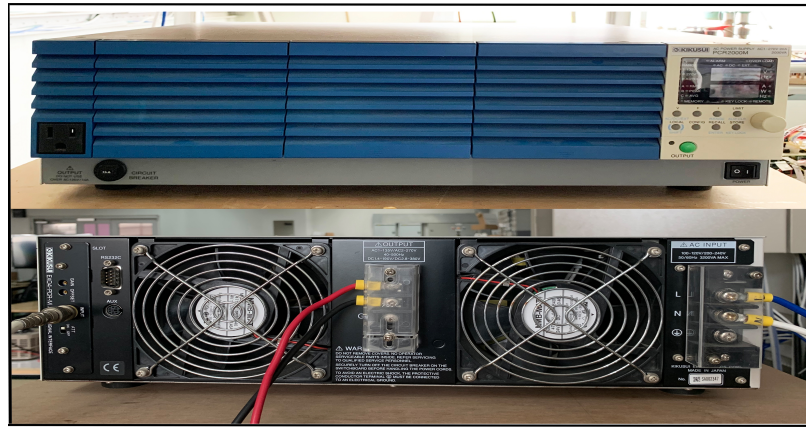


Fig. 4.2: Physical of kikusui PCR2000M

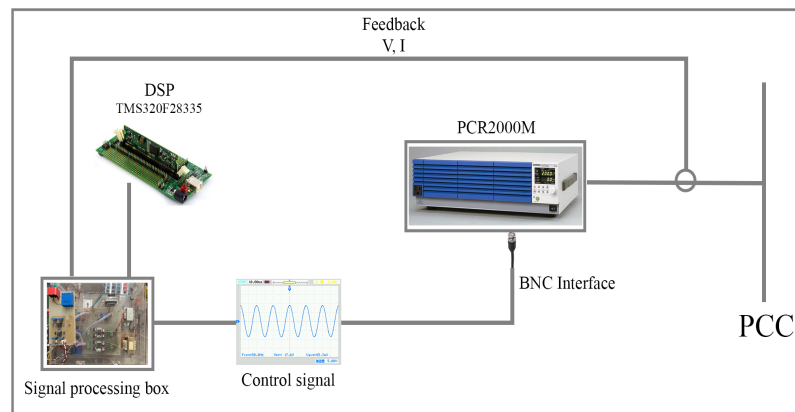


Fig. 4.3: DG designed control system

In this research, the PCR2000M has been used to emulate the inverter-based generator. Its physical is demonstrated in Fig. 4.2. The analog interface board is adopted as an interface method between the DSP controller and PCR2000M. Figure 4.3 shows the diagram of the designed control system. The control algorithm is executed in the DSP controller. Then, the control signal is converted from digital to analog through signal processing box, and command to the PCR2000M.

#### 4.1.2 Photovoltaic

Photovoltaic (PV) is a promising renewable energy resource with inexhaustible, clean, and easily accessible. However, its intermittent nature will bring new unavoidably challenges when it is integrated with the microgrid. Hence, study the impact of PV is important. To incorporate the behavior of PV, a PCR2000M programmable power supply is implemented to emulate the intermittent nature of the PV. Figure 4.4 shows the PV emulator system. It consists of a desktop computer (PC), DSP controller, signal processing box and PCR2000M. A graphic user interface (GUI) based on C# Microsoft Visual Studio is implemented and ran on the PC. It reads the PV power profile and sends it to the DSP controller via USB-Serial232. In DSP, a computation is performed and generated the control signal to command the output power from PCR2000M through the signal processing box as interfacing.

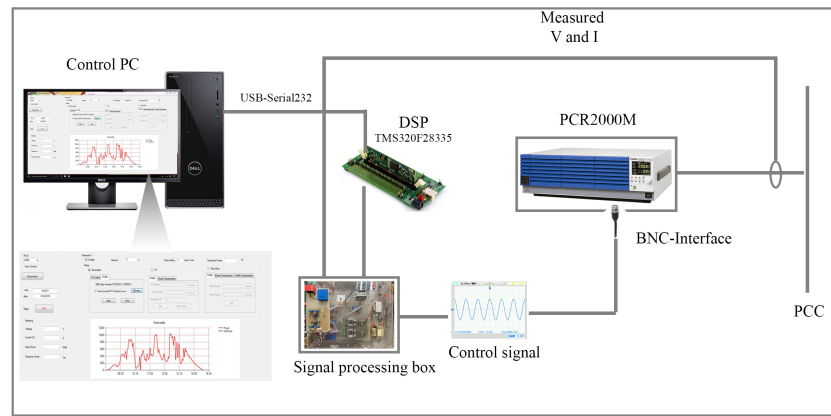


Fig. 4.4: PV emulator system

#### 4.1.3 Battery Energy Storage System

Energy storage systems are an essential part of the renewable power generation system. Renewable power sources like solar, and wind are fluctuating resources that the power output is varied with solar irradiation and wind speed. To supply smooth output power to the power grid, these stochastic energy resources strongly need the energy storage systems to compensate for their fluctuation nature. There are various types of energy storage, such as electric double-layer capacitor (EDLC), BESS, superconducting magnetic energy storage (SMES), flywheel (FW), etc.

In this study, eight pieces of 12V, 65Ah battery are connected in series to form the battery energy storage system (BESS). Figure 4.5 shows the control structure of the BESS. It composes of a laptop computer, desktop computer, DSP controller, BESS and power converter. The laptop is used to debug and start the control algorithm for BESS. A GUI is implemented and ran on the desktop. It reads the ideal PV power profile and sends

it to the DSP controller via CANbus. In DSP, a computation is performed and generated the control signal for the power converter. Through the control command, the power converter is controlled such that BESS is charged/discharged accordingly. As the power converter is an evitable component; hence, the below section will be introduced the principle operation of the bi-directional inverter.

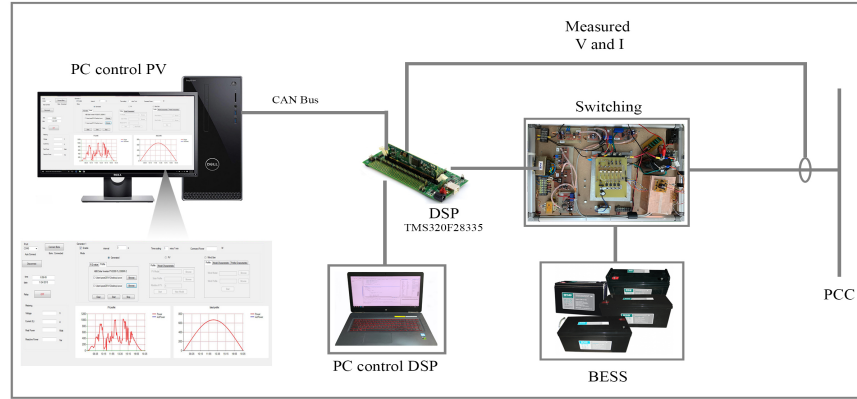


Fig. 4.5: Control structure of BESS

#### 4.1.3.1 Bi-directional Inverter

Figure 4.6 illustrates the topology of the single-phase bi-directional inverter. It composes of a buck-boost converter and a full-bridge inverter. At the output side of the DC source, a DC-link capacitor,  $C_{dc}$ , is utilized to reduce the voltage ripple as well as to ensure the stable voltage supply to the inverter side. At the output stage, it consists of an inverter and a LCL filter. The inverter converts the DC input voltage to the AC output voltage, and the filter is designed to eliminate the switching noise and harmonics.

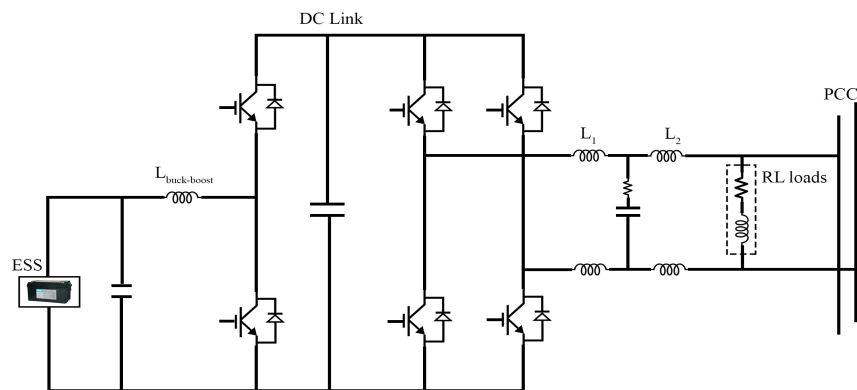


Fig. 4.6: Circuit diagram of bi-directional inverter

The bi-directional AC-DC converter can turn alternating current into direct current during the battery charging mode and convert direct current into alternating current in

battery charging mode. So, total function of this bi-directional converter can be divided into two modes: charging mode and discharging mode.

#### ★ BESS Charging State

In charging operation, the power will flow from the grid to BESS as shown in Fig. 4.7. The full-bridge will work as a rectifier. It converts the grid current from sinusoidal waveform to the direct current. Meanwhile, the chopper will work as the buck converter to step down the voltage to a value which is lower than the DC link voltage to allow the current flow in the BESS. Figure 4.8 (a)(b) demonstrates the operation of the inverter while the BESS is in charging state.

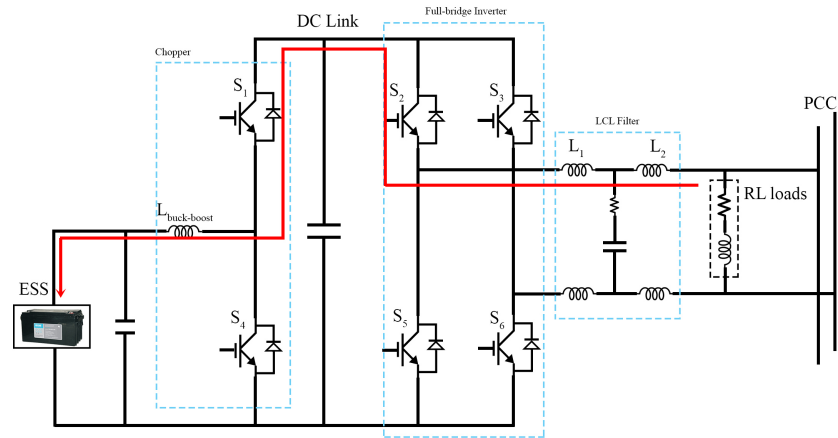


Fig. 4.7: Charging circuit diagram

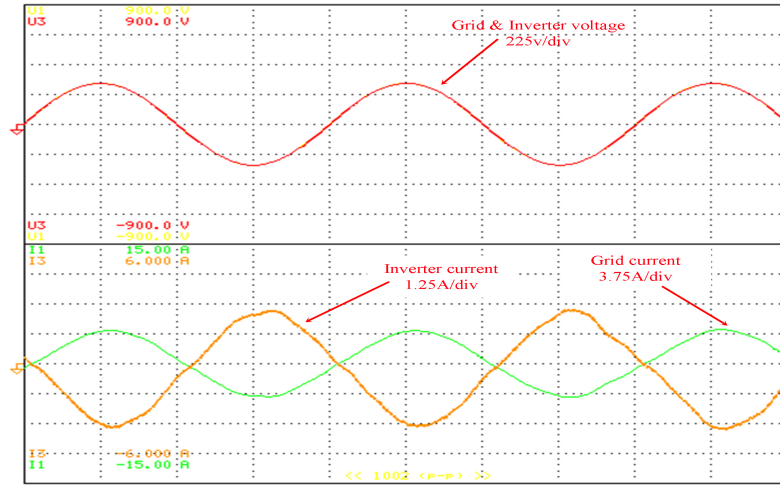
Store:Stop	1	Uover : Iover :	Spd : Trq :	U1 : I1 :	300V 50mV
Irms1	2.8737	A	Q1	0.1175	kvar
Urms2	218.21	V	P2	-0.002	kW
Irms2	0.00	A	Q2	0.000	kvar
Urms3	217.72	V	P3	-0.415	kW
Irms3	1.99	A	Q3	0.127	kvar
Uac4	0.00	V	P4	0.0000	kW
Iac4	0.0000	A	fU1	50.000	Hz
P1	0.6155	kW	λ3	-0.9562	Power Factor/

(a) Numerical value of inverter's power output

#### ★ BESS Discharging State

In this state, the BESS transfers the power to the system as illustrated in Fig. 4.9. The chopper operates as a boost converter to step up the voltage, and the full-bridge works as an inverter to convert the current from DC to AC. Figure 4.10 shows the operation of the bi-directional inverter while the BESS switches to the discharging state.





(b) Wave form of inveter's power output

Fig. 4.8: BESS in charging state

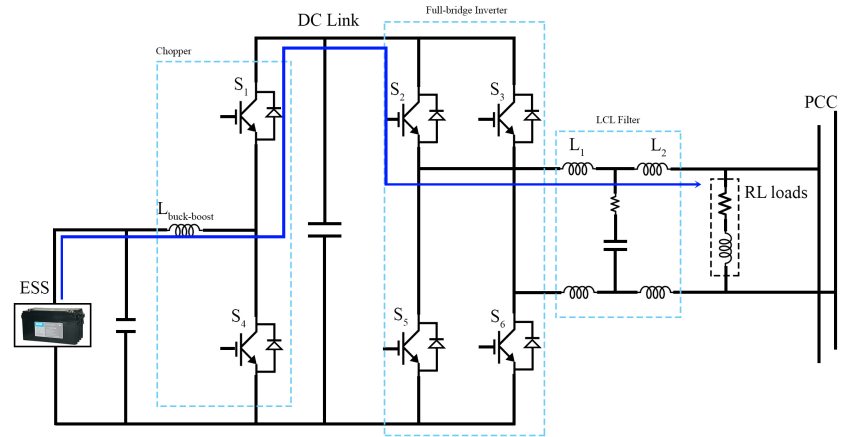
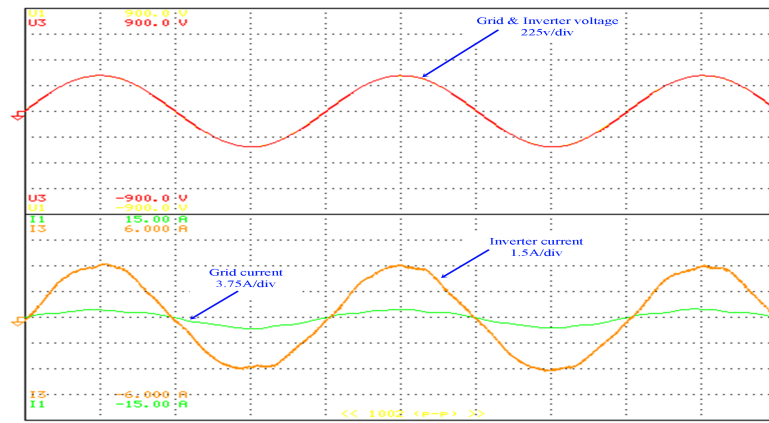


Fig. 4.9: Discharging circuit diagram

Store:Stop	Uover: 300V	Spd: 50Hz	U1: 300V	300V
Cnt. 1	Iover: 50A	Trq: 50Nm	I1: 50A	50A
<u>I<sub>grid</sub></u>	<u>I<sub>rms1</sub></u>	0.8955 A	Q1	0.0482 kvar
	<u>U<sub>rms2</sub></u>	220.12 V	P2	-0.000 kW
	<u>I<sub>rms2</sub></u>	0.00 A	Q2	0.000 kvar
	<u>U<sub>rms3</sub></u>	220.73 V	P3	0.488 kW <u>P<sub>inverter</sub></u>
<u>I<sub>inv</sub></u>	<u>I<sub>rms3</sub></u>	2.22 A	Q3	0.044 kvar
	<u>U<sub>ac4</sub></u>	0.00 V	P4	0.0000 kW
	<u>I<sub>ac4</sub></u>	0.0000 A	fU1	50.001 Hz
<u>P<sub>grid</sub></u>	<u>P1</u>	0.1910 kW	λ3	0.9960 <u>Power Factor</u>

(a) Numerical value of inveter power output



(b) Wave form of inveter power output

Fig. 4.10: BESS in discharging state.

#### 4.1.4 Loads

Power demand is a crucial component in power system. The households and commercial users that attache to the grid do not have ideal constant or periodic needs. A significant amount of devices are switched on and off at an arbitrary time over the day which could result in electric fluctuation in the system. To study the system performance, the RL loads connect with controllable relay is implemented as shown in Fig 4.11 to mimic the real power demand behavior. A graphic user interface is implemented using C#, Microsoft Visual Studio. This GUI communicates with the Arduino controller via CANbus. The On/Off command send from GUI which runs in the host computer, to Arduino. Then, the Arduino translates the control command to pull GPIO high or low to command On/Off load through connecting relay board. As a result, the load levels in a microgrid could be changed to any level as desired. This implementation could enhance the microgrid concept in hardware more realistic and achievable as well as to stress the microgrid system to its fullest potential to evaluate the proposed control performance.

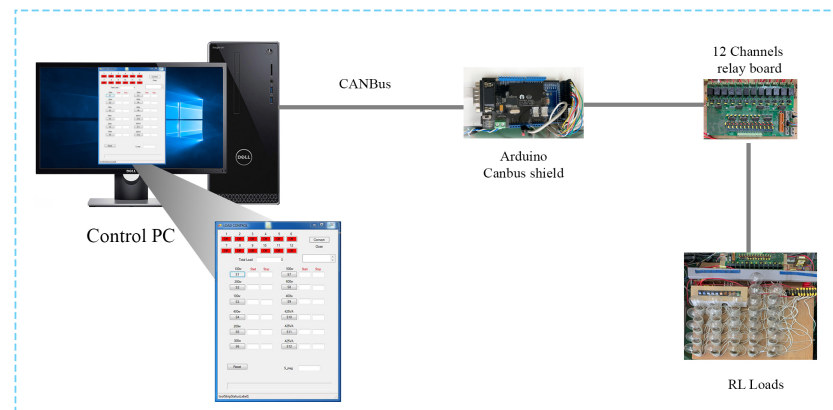


Fig. 4.11: Loads Control

#### 4.1.5 Communication Protocol

The data distributed plays a major role in distributed control. In this research, two standard communication protocols are used to realize local-and-inter information exchange as demonstrated in Fig. 4.12. The CAN-bus protocol is used for exchanging information between the agent and DSP local controller and local controller-to-local controller. Figure 4.12 (Left-side) is the CAN-bus sniffer which used to monitor the data flow in CAN-bus. The TCP/IP protocol is used for exchanging the data among the agents based on FIPA-ACL standard and agent-to-cloud. Figure 4.12 (Right-side) is the agent-sniffer which is used to keep track of MAS.

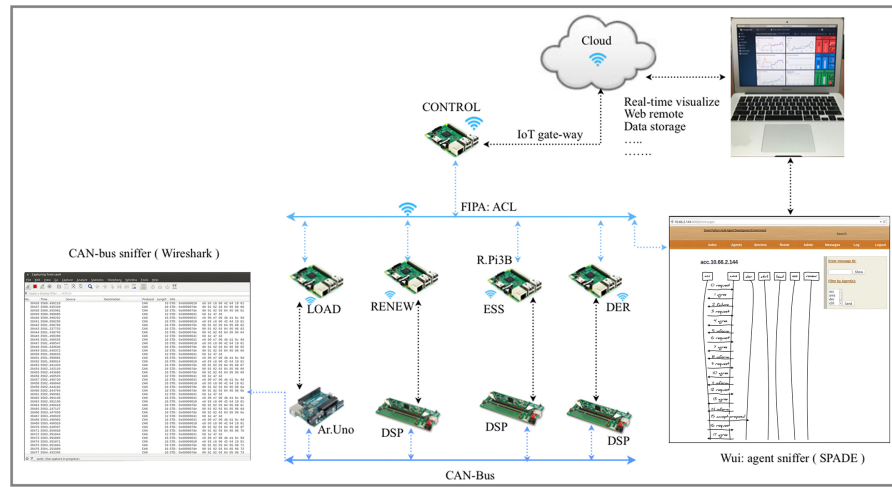


Fig. 4.12: Communication protocol

The grid-connected inverter is a vital component in a microgrid. It provides the DC nature renewable source or BESS the ability to integrate with the AC system. The power inverter normally produces the common mode voltage and common mode current which causes a high-frequency electromagnetic interface (EMI) noise. The CANbus composes of three major components such as host controller, CAN controller, and CAN transceiver. The transceiver transmits the data from the CANbus to the CAN controller to convert the data, and then to the host controller. The EMI has a major impact on the CANBus data transmission. The affected signal cause the CAN controller to misjudge the received as a correct signal and thus causing a node error. The error may result in stopping data transmission in the node.

To improve and protect the CANbus system, an optocoupler isolator is employed as shown in Fig. 4.13, and its implementation is demonstrated in Fig. 4.14. The optocoupler places at the front-end of the CAN controller so that it will protect all data flow on the bus. The optocoupler (6N137) can directly receive, filter out the noise, and isolate the bus signal with EMI. As a result, the transmission error and bit error is eliminated.

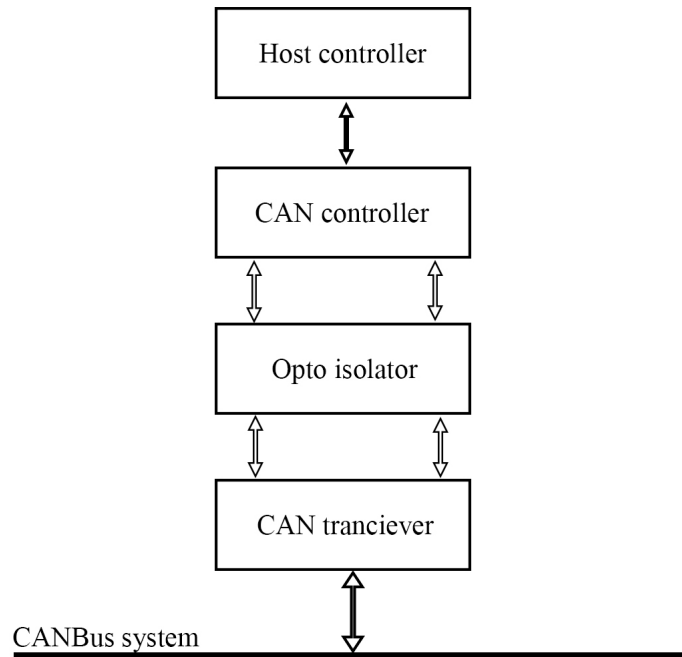


Fig. 4.13: Opto-isolated CANbus system

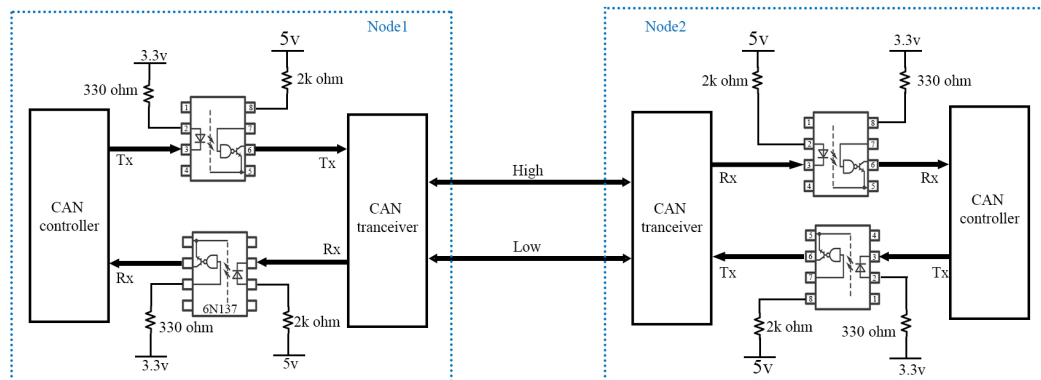


Fig. 4.14: Configuration of opto-isolated CANbus

## 4.2 Distributed Hierarchical Control

Conventional electric power systems are facing continuous and rapid changes to alleviate environmental concerns, address governmental incentives, and respond to the consumer demands. The notion of the smart grid has recently emerged to introduce an intelligent electric network. Improved reliability and sustainability are among desired characteristics of smart grid affecting the distribution level. These attributes are mainly realized through microgrids which facilitate the effective integration of distributed generators (DG) [56]. Proper control of microgrid is a prerequisite for stable and economically efficient operation [57]. The principal roles of the microgrid control structure are [58].

- Voltage and frequency regulation for both operating modes.
- Proper load sharing and DG coordination.
- Microgrid resynchronization with the main grid.
- Eliminate the impact of RES's intermittent nature.
- Power flow control and optimizing.

These requirements are of different significances and time scales, thus requiring a hierarchical control structure [57] to address each requirement at a different control hierarchy.

Inspired by the hierarchical control in conventional power systems [59] and IEC 62264 standard, a hierarchical control structure that consists of three levels has been defined for a standalone microgrid as demonstrated in Fig. 4.15. The control hierarchy is from the upper to the lower layer and the control response from the lower layer to the upper layer.

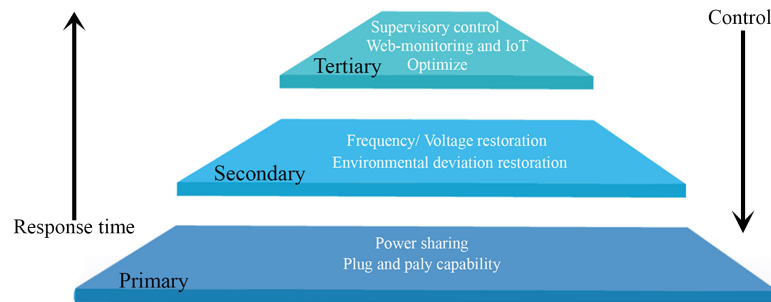


Fig. 4.15: Concept of proposed hierarchical control

Moreover, the smartgrid vision compels microgrid to adopt distributed cooperative methods as a result of the highly dynamic behavior of microgrids. Hence, the distributed and decentralized control technique is used in this proposed hierarchical control. The detail of each control level is described below:

#### 4.2.1 Primary Control

##### 4.2.1.1 Modified Droop Control

Droop control is a well-known decentralized technique that has been used to realize the power-sharing in parallel operation of the inverter. With this control strategy, the frequency and voltage could be controlled by regulating the active power and reactive power, respectively. The modified droop control is express in Eq. 4.1. To improve the transient response of the system, the power deviation term is included in the droop control [60] as expressed in Eq. 4.2.

$$\begin{aligned}\omega &= \omega_{ref} - k_f * (P_{fb} - P_{ref}) \\ E &= E_{ref} - k_v * (Q_{fb} - Q_{ref})\end{aligned}\quad (4.1)$$

$$\begin{aligned}\omega &= \omega_{ref} - k_f * (P_{fb} - P_{ref}) + k_p \frac{dP_{fb}}{dt} \\ E &= E_{ref} - k_v * (Q_{fb} - Q_{ref}) + k_q \frac{dQ_{fb}}{dt}\end{aligned}\quad (4.2)$$

Where

- $\omega$  and  $E$  are the operating frequency and voltage,
- $\omega_{ref}$  and  $E_{ref}$  are the reference frequency and voltage amplitude.
- $k_f$  ( $k_f = \frac{\Delta\omega}{P_{max}}$ ) and  $k_v$  ( $k_v = \frac{\Delta E}{Q_{max}}$ ) are the  $P - \omega$  and  $Q - v$  droop coefficient.
- $P_{fb}$  and  $Q_{fb}$  are the output active power and reactive power.
- $k_p$  and  $k_q$  are the power deviation constant. These parameter could be adjusted to improve the transient response.

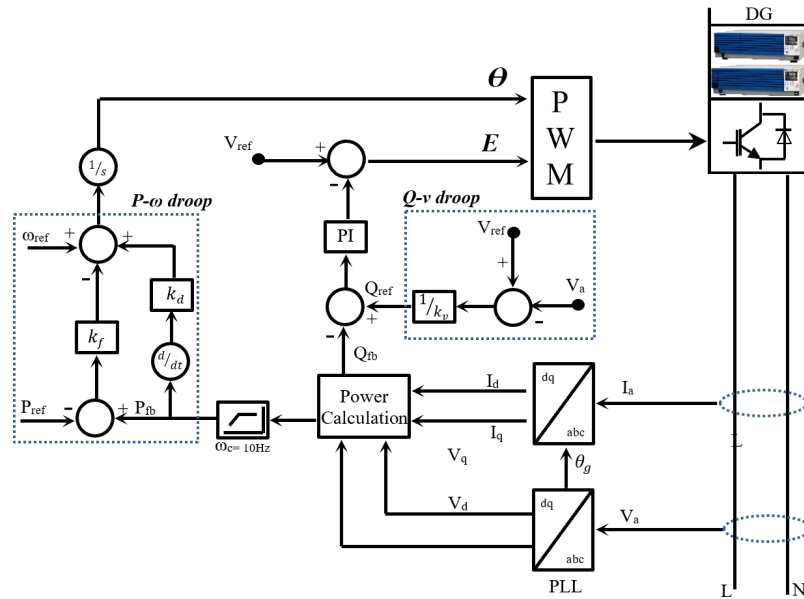


Fig. 4.16: Modified droop control block diagram

Figure 4.16 is the control block diagram of the modified droop control. The current and voltage at the output side of the inverter is measured, transformed to dq-frame and injected to the power calculation block. In the power calculation block, the output active power ( $P_{fb}$ ) and reactive power ( $Q_{fb}$ ) are computed based on Eq.4.3. A low-pass filter with cut-off frequency  $\omega_c=10$  Hz is used to diminish the measuring output power ripple.

The output from the  $P - \omega$  and  $Q - v$  droop control block is the desired frequency and voltage signals for control inverter's switching.

$$\begin{aligned} P_{fb} &= \frac{1}{2} \left( \frac{1}{\tau_s + 1} \right) (V_d I_d + V_q I_q) \\ Q_{fb} &= \frac{1}{2} \left( \frac{1}{\tau_s + 1} \right) (V_q I_d - V_d I_q) \end{aligned} \quad (4.3)$$

#### 4.2.1.2 VSG Control

The VSG is a relatively new decentralized control scheme which is proposed to mimic the synchronous generator characteristic. The swing equation of a synchronous generator is the core of implementing VSG, and it is given in Eq. 4.4.

$$J\omega_m \frac{d\omega_m}{dt} = P_{in} - P_{fb} - D(\omega_m - \omega_{pcc}) \quad (4.4)$$

Where  $P_{in}$  is the input power to VSG and  $P_{fb}$  is the measured output power.  $\omega_m$  is VSG's angular frequency, and  $\omega_{pcc}$  is the angular frequency at the point of common coupling. J and D are the virtual inertia and virtual damping factor, respectively. Designing the VSG's parameter such as J and D is a challenging task. For the sake of simplicity, the parameter (J, D) could be calculated based on Eq. 4.5 [61], which follows the synchronous generator.

$$\begin{aligned} J &= \frac{2HS}{\omega^2} \\ D &= \frac{\Delta S}{\omega \Delta \omega} \end{aligned} \quad (4.5)$$

Where H is the inertia constant, which is in the range  $[2s - 10s]$ .  $S_n$  is the base power of the generator,  $\omega$  is the angular frequency which equals to  $2\pi f$  and  $\Delta\omega$  ( $\Delta\omega = \omega_m - \omega_{pcc}$ ) is the allowable deviation frequency which equals to  $2\pi$ . To understand the effect of virtual inertia and damping factor on the system's frequency, the Eq. 4.4 is derived as.

$$\frac{d\omega_m}{dt} = \frac{\frac{P_{in}}{\omega_m} - \frac{P_{out}}{\omega_m} - \frac{D(\omega_m - \omega_{pcc})}{\omega_m}}{J} \quad (4.6)$$

$$\Delta\omega = \frac{P_{in} - P_{out} - J\omega_m \frac{d\omega_m}{dt}}{D} \quad (4.7)$$

In Equation (4.6), assuming that  $(\frac{P_{in}}{\omega_m} - \frac{P_{out}}{\omega_m} - \frac{D(\omega_m - \omega_{pcc})}{\omega_m})$  is constant. If the value of J is increased, the  $\frac{d\omega_m}{dt}$  will be decreased. Similarly; in Equation (4.7), assuming that  $(P_{in} - P_{out} - J\omega_m \frac{d\omega_m}{dt})$  is constant. If the parameter D gets bigger,  $\Delta\omega$  will become smaller. Hence, the large value of J and D result in a small frequency deviation; at the same time, they maximize the power, generated or absorbed by the energy storage system. However, there is a side-effect for larger value selection of parameters J and

D such as causing overload the inverter, increasing the settling time, requiring the high accuracy of PLL. Therefore, the optimum value selection of J and D could significantly ensure system stability.

The overall control block of the VSG control is provided in Fig. 4.17. The power calculation block computes the VSG's output active power and reactive power based on Eq. 4.3. The output from the VSG control block is the virtual angular frequency,  $\omega_m$ . By applying the integrator to  $\omega_m$ , the reference phase angle  $\theta_m$  is obtained. The reference voltage amplitude, E, is realized through the  $Q-v$  droop control block. The voltage magnitude references (E) and the phase angle reference ( $\theta_m$ ) create the sinusoidal duty-cycle in the form of  $E \cdot \sin(\theta_m)$  to control the switching time of IGBT.

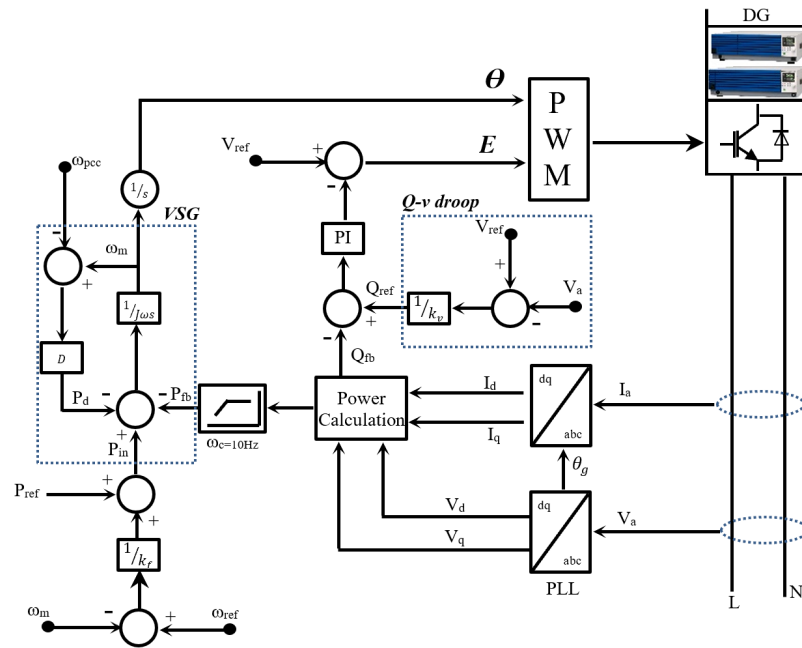


Fig. 4.17: Control block diagram of Virtual synchronous generator

#### 4.2.1.3 Tuning VSG Parameter Based on BSA

An optimization is a powerful tool which is used by the researchers in various application over the past few decades. It aims to extract maximum benefits from the system by finding the best values of system parameters through the maximization or minimization of the objective function.

As discussed in previous section, the VSG emulates the SG's dynamic characteristic by representing the SG fundamental swing equation to create the virtual inertia and damping factor. Unlike a real synchronous machine, the VSG's can be tuned to improve the dynamic response of the system. In this research, a new evolution optimizes called BSA is used to online turning the parameter of VSG such as J and D.



The objective function:

$$ISE = \int_{T_{start}}^{T_{stop}} (\omega_{ref} - \omega_m)^2 \quad (4.8)$$

Designed problem can formulate by minimizing ISE to determine the values J and D.

Figure 4.18 demonstrates the interface between the simulation model with the optimization algorithm (BSA). The BSA embeds in the Simulink environment using the Level-2 S-function. The parameter J and D are set as the turnable parameter. Figure 4.19 is a testing case result to observe whether the parameter is properly online turned or not. At the time of the simulation start, the value of J and D are intentionally wrong initialized. As shown in Fig. 4.19, at time 0.5s, the large loads are connected, and the system is unstable as the virtual inertia and damping constant is wrong initialized. To update the VSG parameter which generates by BSA, it requires to enable update mode from Simulation menu in Simulink (Simulation → Update Diagram). One the update diagram is clicked, the VSG parameter is kept updating based on BSA as seen in Fig. 4.19 from 3s to the end of the simulation.

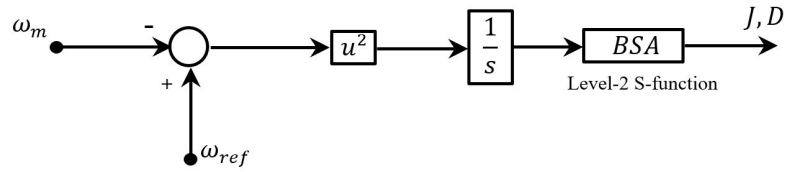


Fig. 4.18: BSA-Simulink interfacing

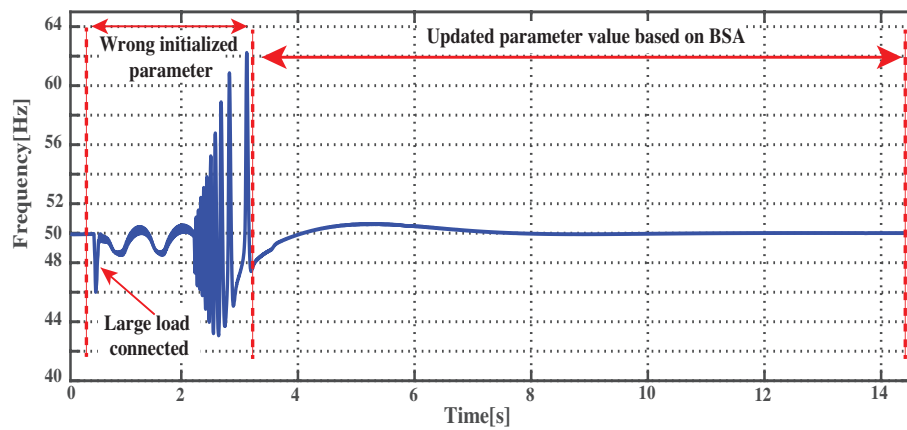


Fig. 4.19: Testing BSA turning: System frequency

## 4.2.2 Secondary Control

### 4.2.2.1 Frequency Restoration

The functionality of the secondary control is to compensate for the voltage and frequency deviations caused by the operation of the primary controls, the intermittent output power of renewable sources and the sudden change of large loads. Although the droop control is a well-known technique with significant advantages such as communication-less and plug-and-play ability, it has a remarkable drawback as it could result in frequency deviation from the acceptable range [62]. As a result, the frequency restoration is implemented to keep the operating frequency close to the desired frequency ( $\omega \simeq \omega_{ref}$ ). The frequency restoration is described in Eq. 4.9 and expressed in a dash-line area of Fig. 4.20 to restore the frequency back to standard range.

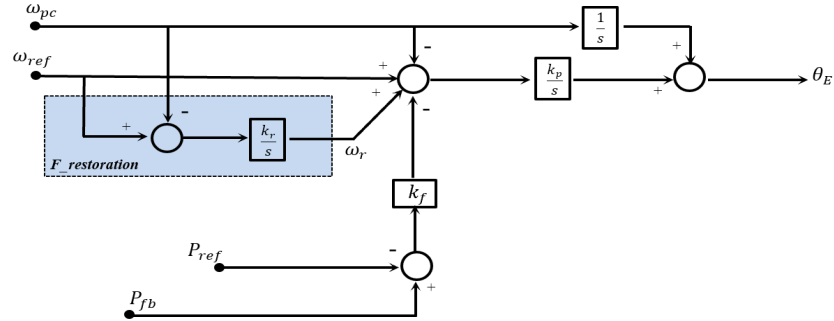


Fig. 4.20: Frequency restoration

$$\omega_r = K_r \int (\omega_s - \omega_v) \quad (4.9)$$

Where  $K_r$  is a controller gain which is proportional to generator's angle droop coefficient. The restoration frequency ( $\omega_r$ ) is added with Eq. 4.1 to correct the local droop controller. Therefore, Eq. 4.1 can be rewritten as below:

$$\omega = \omega_{ref} - k_f * (P_{fb} - P_n) + \omega_r \quad (4.10)$$

### 4.2.2.2 Frequency Deviation Miltigation

The high penetration of renewable energy systems with its intermittent power output results in high-frequency variation. Therefore, to address these issues, the standalone microgrid highly relies on the energy storage system (ESS) to mitigate the frequency deviation.

Inspired by [63], instead of using ramp rate and step moving average, an Ideal PV power profile is used. The ideal PV power is obtained by comparing the daily PV output power during one year and select the one with low variation. The idea behind this method

is to inject the smooth power to the system with aiding of ESS. Hence, the impact of PV's intermittent is diminished. As shown in Fig. 4.21, the ESS is used to compensate the deviation power of PV. When the power from PV is greater than ideal power, the ESS will absorb otherwise the ESS will release the power to compensate. Therefore, the power supply from the PV plus energy storage system is like an ideal power.

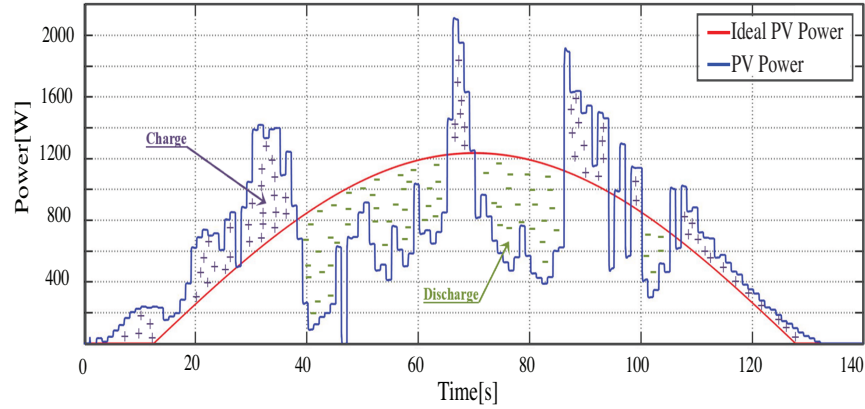


Fig. 4.21: ESS respond based on proposed smoothing method

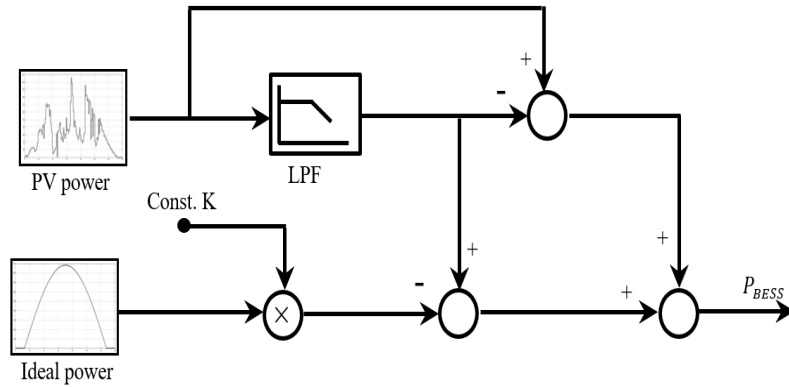


Fig. 4.22: Proposed PV power smoothing technique based on BESS

The block diagram of proposed PV power smoothing method is shown in Fig. 4.22. Here, a low-pass filter ( $f_c=0.5$  Hz) and an ideal power are used to generate the power reference for battery, and it is expressed in Eq. 4.11.

$$P_{high} = P_{pv} - P_{pv} * \frac{1}{\tau_1 s + 1}$$

$$P_{BESS} = P_{pv} * \frac{1}{\tau_1 s + 1} - K * P_{ideal} + P_{high} \quad (4.11)$$

Where  $P_{pv}$  is the measured PV output power.  $\tau_1$  is time constant of the low-pass filter.  $P_{ideal}$  is the ideal PV output power. K is a constant to determine the amplitude of

ideal PV power which is in a range [0, 1]. In case the PV power prediction is included, the constant K is obtained by dividing the average of prediction power by the average ideal power ( $K = \frac{\bar{P}_{predic}}{\bar{P}_{ideal}}$ ). The PV power prediction and the method to determine the value of constant K will be detailed in the next research work. In this study, the constant K is pre-selected to K=0.5.

However, the usage of battery in the above application could seriously shorten the battery lifespan. To improve the lifespan of the battery by reducing the battery stress, the Battery\Supercapacitor Hybrid Energy Storage System (HESS) is introduced and discussed in Section 5.1.2.2. The supercapacitor is responsible for the high-frequency power variation while the battery corresponds to the low-frequency power variation.

### 4.2.3 Tertiary Control

Since the microgrid is a promising technology for the future smartgrid; therefore, the autonomous decision-making, real-time monitoring, and web-remote are implemented at the tertiary level to conform to the smartgrid criteria.

#### 4.2.3.1 Multiagent System

In the conventional power system, the control could be done by using SCADA. However, the increased system complexity on the modern power distribution, using a conventional approach like centralized control (SCADA) is no longer sufficient. Therefore, the multiagent system (MAS) is employed. MAS can be considered as hardware or software-based computer system which aims to solve the complex task in distributed technique. By comparing to SCADA, the MAS offers various advantages in terms of implementing an intelligent microgrid such as flexible, reliable, usable at field control, and implementing cost reduction.

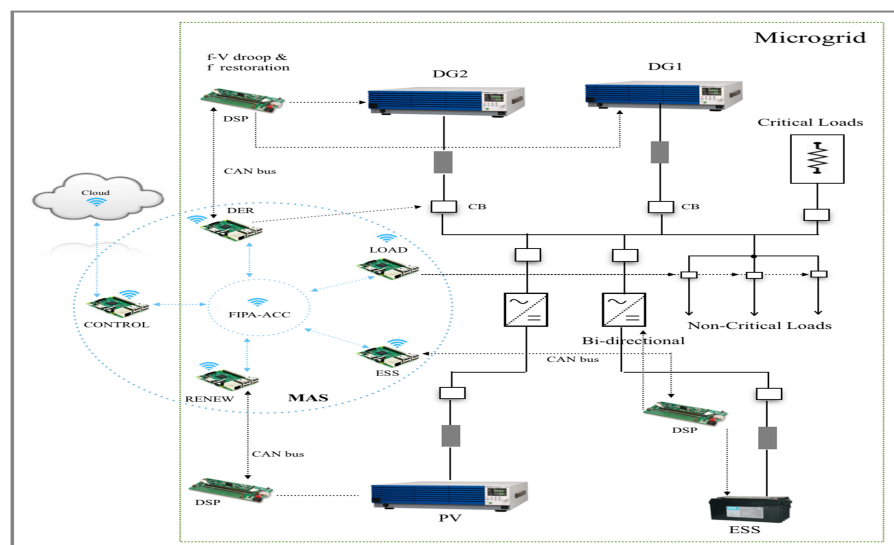


Fig. 4.23: Single-line diagram

Figure 4.23 (dash-line area) is the group of agents assigned to each component of the microgrid. Those agents are executed in Raspberry Pi3. Each agent has a different responsibility as described in Table 4.1. The MAS is implemented using an open-source agent building toolkit, called SPADE [54].

Table 4.1: AGENTS and Task

AGENT	TASKs
DG agent	It contains the information of DGs such as DG's capacity, actual power, status (On/Off) .., etc.
	It controls the reserve generator either autonomous or manual through <b>web user interface</b>
LOAD agent	It performs Demand Respond Management such as load-shedding and demand shift.
	It receives the command from <b>wui</b> for control the demand in manual.
PV agent	It manages the information of PV such as actual power.
ESS agent	It keeps tracks the storage level (SOC).
	It makes the decision whether the ESS need to charge or discharge.
CONTROL agent	It works as a backup agent in case of any agent is down.
	It gathers the data from various agents and feed to the IoT platform for data storage and monitoring.

#### 4.2.3.2 Internet of Things

The vast evolution of embedded device and Ethernet-based communication system allows the internet to penetrate the real-world physical object. The combination of sensors and actuators with the internet is defined as the Internet of Think or IoT for short. Through this integration, the embedded devices will be harnessed in a broad range of applications such as building and industrial automation, smart metering, remoting and monitoring, etc.

In this layer, to enable the online remoting and monitoring, the IoT feature has been embedded in MAS. The Open-Source IoT platform called ThingsBoard has been used as the IoT cloud platform. It can run on a server computer as a server system. Figure 4.24 is the graphic user interface of the ThingsBoard platform. It provides the build-in function of the MQTT broker and MQTT client to listen to and to handle MQTT messages received from devices.

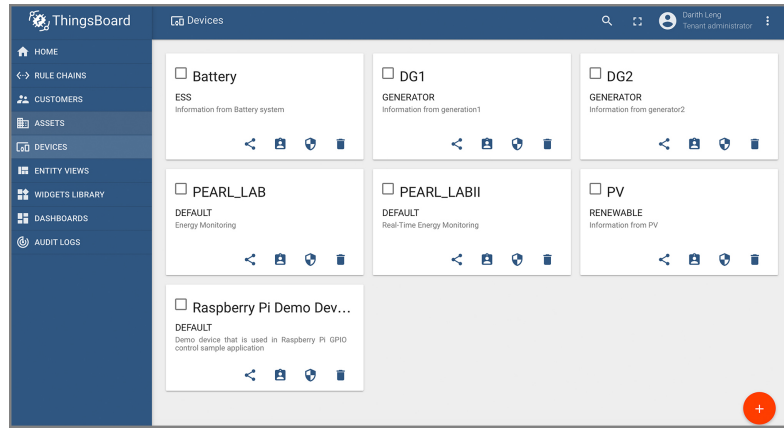


Fig. 4.24: GUI of Thingsboard

#### 4.2.3.3 PV Power Prediction

The integration of renewable energy sources with intermittent behavior poses numerous problems to the electricity grid operator. These problems can be partially solved by introducing energy storage and improving production forecasting methods. The PV power fluctuation mitigation based on BESS has been discussed in section 4.2.2.2. The below section will discuss the PV power prediction based on long-short term memory recurrent neural network.

##### † Long-Short Term Memory Recurrent Neural Network (LSTM-RNN)

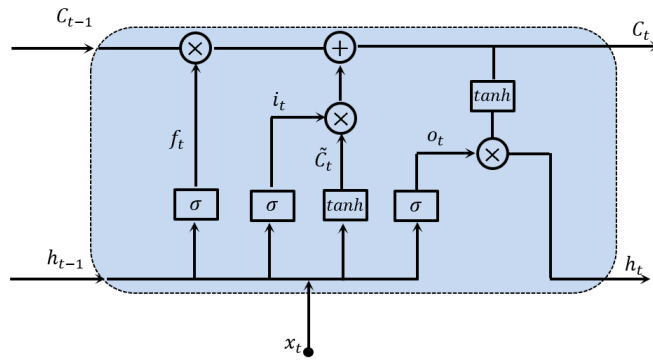


Fig. 4.25: LSTM cell

LSTMs is a special kind of RNNs, capable of learning short-term dependencies. Unlike RNNs, LSTMs were designed to avoid the long-term dependency problem. LSTM network is trained using backpropagation through time, and it overcomes the vanishing gradient problem. Comparing to the traditional neural networks, LSTM networks have memory blocks that are connected through successive layers. The LSTM unit is shown in Fig 4.25, there are 4 layers and three gates. The task of each gate can be summarized as follows:

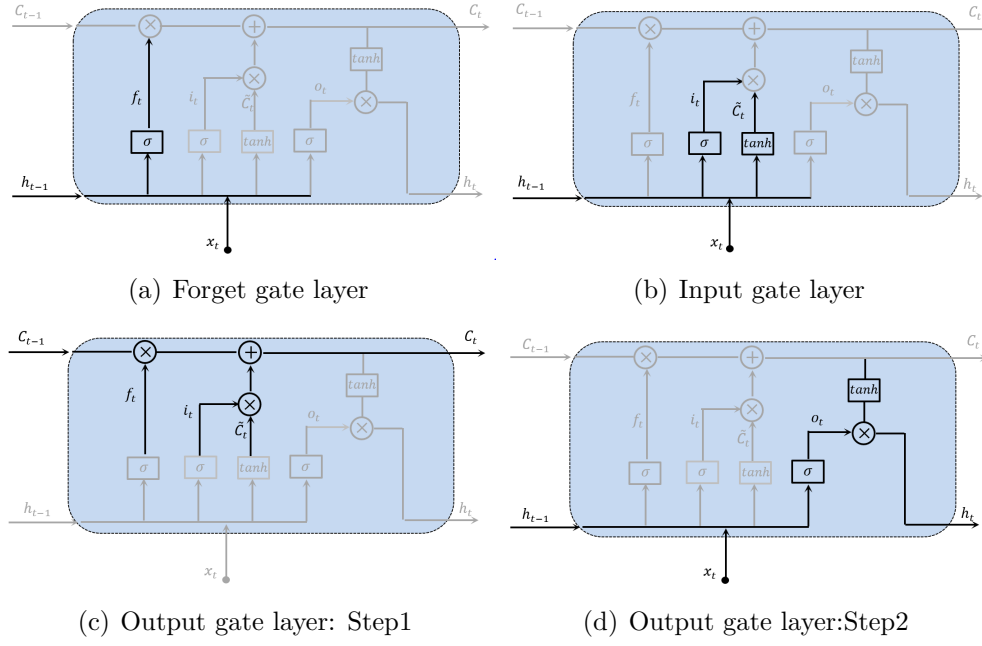


Fig. 4.26: LSTM diagram

- **Forget gate:** It decides what information to throw away from the cell state. It looks at the  $h_{t-1}$  and  $x_t$ , and outputs number 0 for completely get rid and 1 for completely keep. The process of the forget gate is shown in Fig 4.26 (a) and expressed in Eq. 4.12.

$$f_t = \sigma(W_f \cdot [h_{t-1}, x_t] + b_f) \quad (4.12)$$

- **Input gate:** In this gate, there are two layers as shown in Fig. 4.26 (b). The *sigmoid* layer decides which value to update, and the *tanh* layer creates a vector of candidate values,  $\tilde{C}_t$ . By multiplying these two layers as demonstrated in Eq. 4.13, an update state is created.

$$\begin{aligned} i_t &= \sigma(W_i \cdot [h_{t-1}, x_t] + b_i) \\ \tilde{C}_t &= \tanh(W_c \cdot [h_{t-1}, x_t] + b_c) \end{aligned} \quad (4.13)$$

- **Output gate:** There are two things to be done in this gate. First, it updates the old state ( $\tilde{C}_{t-1}$ ) to the new state  $C_t$  by multiplying the forget gate with the old cell state, then sums with  $i_t \times \tilde{C}_t$  as shown in Fig. 4.26 (c). Second, the output gate decides what output should be based on the computation based of the Eq. 4.14. In Fig 4.26 (d), the sigmoid layer decides which part of the cell state to be the output, and tanh layer with the cell state ( $C_t$ ) as the input generates the output between  $[-1, 1]$ . By multiplying the output of these two layers, the desired output

$(h_t)$  is obtained.

$$\begin{aligned} C_t &= f_t \times C_{t-1} + i_t \times \tilde{C}_t \\ o_t &= \sigma(W_o \cdot [h_{t-1}, x_t] + b_o) \\ h_t &= o_t \times \tanh(C_t) \end{aligned} \quad (4.14)$$

The main advantage of using the LSTM unit, unlike traditional neurons used in RNN, is that its cell state accumulates activities over time. Since derivatives distribute over sums, the derivatives of the error do not vanish quickly as they are sent back into time. In this way, LSTM can carry out tasks over long sequences and discover long range features.

#### † Measures of Prediction Accuracy

To evaluate the model's performance, it is necessary to choose a metric to measure the prediction accuracy. Root mean square error (RMSE) is a widely used metric. The equations for calculating RMSE is expressed in Eq. 4.15

$$RMSE = \sqrt{\frac{\sum_{i=1}^N (y_i - y_-)^2}{N}} \quad (4.15)$$

where  $y_i$  is the predicted outputs,  $y_-$  is the measured data, and  $N$  is the number of observations. Smaller values of RMSE indicate that the forecast is a closer approximation of measure value.

#### † Data Selection

Meteorological data were downloaded from <https://www.meteoblue.com> which collected from the Survanaphumbi International Airport. As the data is not recorded at the solar farm, it is obvious to convert to the PV power based on the real installation capacity of the solar farm. The power output from PV based on the maximum power point tracking can be calculated via Eq. 4.16.

$$P_{pv} = \eta SI(1 - 0.005(t_0 - 25)) \quad (4.16)$$

where  $P_{pv}$  is the power output of the PV;  $\eta$  [%] is the conversion efficiency of the solar cell array;  $S$  [ $m^2$ ] is the array area;  $I$  [ $w/m^2$ ] is the solar radiation and  $t$  [ $^{\circ}C$ ] is the outside air temperature.

Regarding the weather parameters measured at the location, it worths investigating the relevance of each variable and selected only variables that are important to the model to deduce the computation burden. The correlation of each variable is obtained through Eq. 4.17.



$$\rho_{X,Y} = \frac{\sum_{i=1}^N (X_i - \bar{X})(Y_i - \bar{Y})}{\sqrt{\sum_{i=1}^N (X_i - \bar{X})^2 (Y_i - \bar{Y})^2}} \quad (4.17)$$

The correlation coefficient is defined in the range  $0 \leq \rho \leq 1$  as:

- if  $\rho = -1$ , then there is a perfect negative linear relationship between  $X$  and  $Y$ .
- If  $\rho = 1$ , there is a perfect positive linear relationship between  $X$  and  $Y$ .
- If  $\rho = 0$ , there is no linear relationship between  $X$  and  $Y$ .

Table 4.2 is the correlation coefficient between each variable.

Table 4.2: Correlation Coefficient

	Radiation	Temperature	Humidity	Total-cloud	Sun-duration	Wind-speed
Radiation	1.0000	0.8980	-0.8533	-0.1349	0.6844	-0.0120
Temperature	0.8980	1.0000	-0.9705	0.0028	0.6456	0.0026
Humidity	-0.8533	-0.9705	1.0000	-0.0089	-0.6120	0.0363
Total-cloud	-0.1349	0.0028	-0.0089	1.0000	-0.5225	-0.2404
Sun-duration	0.6844	0.6456	-0.6120	-0.5225	1.0000	0.0694
Wind-speed	-0.0120	0.0026	0.0363	-0.2404	0.0694	1.0000



## RESULTS AND DISCUSSION

This chapter presents the most relevant results obtained through simulation and experimental regarding hierarchical control strategies which discussed in Chapter 4. Considering the objectives of the control strategies that were proposed, the analysis and discussion of the results are divided into two sections which refer to simulation and experimental results.

### 5.1 Simulation Results

To investigate the performance of each control method, a standalone microgrid is implemented in MATLAB/Simulink platform as shown in Fig. 5.1. The equipment such as power supply, battery energy storage system, PV simulator, etc., are modeled based on the real equipment which is available in the laboratory for later experimental purpose. The important parameters are provided in Table 5.1. Several case studies are carried out and discussed below.

Table 5.1: Microgrid's parameters in simulation

DGs	
Model	Kikusui PCR2000M
Power Rating	220V, 50Hz, 2kVA
P-Angle Droop Coefficient (m)	$2\pi(0.000185)$
Q-V Droop Coefficient (n)	$1/0.002592725$
Xd	4mH
Load	
Variable Load	Based on Load profile from MEA (Pmax = 1.5 kW)
PV Simulator	
Model	Kikusui PCR2000M
Simulate	Based PV profile (Max: 2.1 kW)
Battery storage system	
SOLAR 12-65	8 * (12V 65Ah)
Supercapacitor storage system	
Maxwell BMOD0165	3 * (165F, 48V, 53Wh)
VSG-Constant	
J	0.4863
D	382
VSG-BSA	
Population	25
Epoch	5
J	0.51
D	597

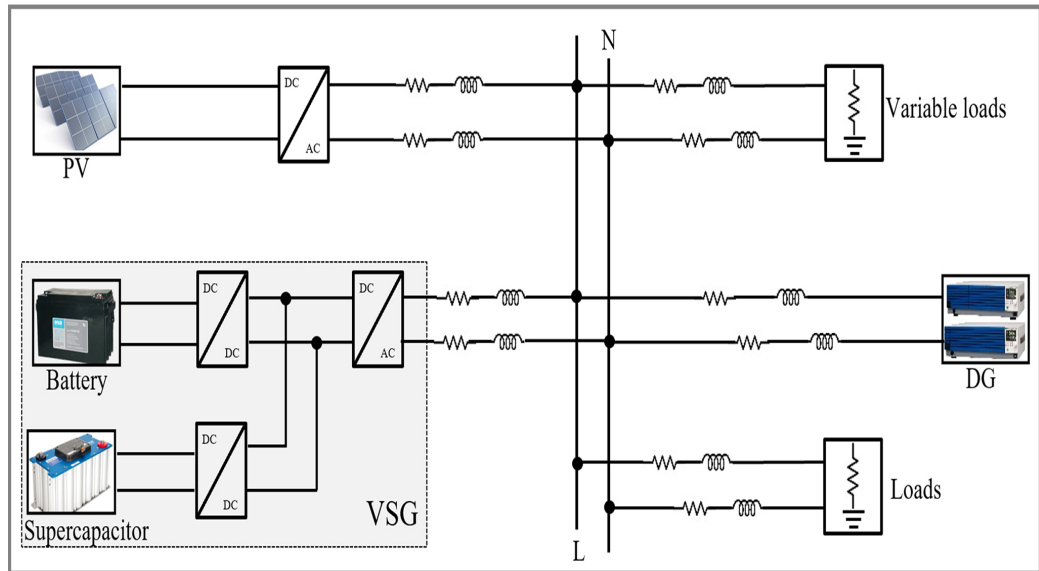


Fig. 5.1: Single-phase diagram of standalone microgrid

### 5.1.1 Primary Control

In this section, dynamic characteristics of modified droop control and VSG control are compared in order to understand the difference in the mentioned control methods which caused by the presence of the swing equation. This comparison aims to find out the proper control for DG by investigating the strength and weaknesses of each control. Two case studies are carried as discussed below:

#### 5.1.1.1 Power Sharing

In this case, the performance of both control schemes will evaluate based on the accuracy of power-sharing among DG. The variable power consumption is applied as shown in Fig. 5.2 to observe the dynamic load sharing of the modified droop control and VSG. Initialize power consumption is  $1000W$ . The power demand increase to  $2500W$  at the time  $t = 1s$  and increases around 50 percent at the time  $t = 10s$ . At the beginning of the simulation, only DG#1 supplies to the loads. Then, the DG#2 is connected to the system at the time  $t = 0.5s$ . Figure 5.3 and Figure 5.4 show the active power-sharing among DG#1 and DG#2 based on modified droop control and VSG control, respectively. These figures demonstrate that both controls could provide the same accuracy for power-sharing accordingly to the power demand change. As the DG#1 and DG#2 have the same rate; hence, both DG could share the power equally for both control methods.

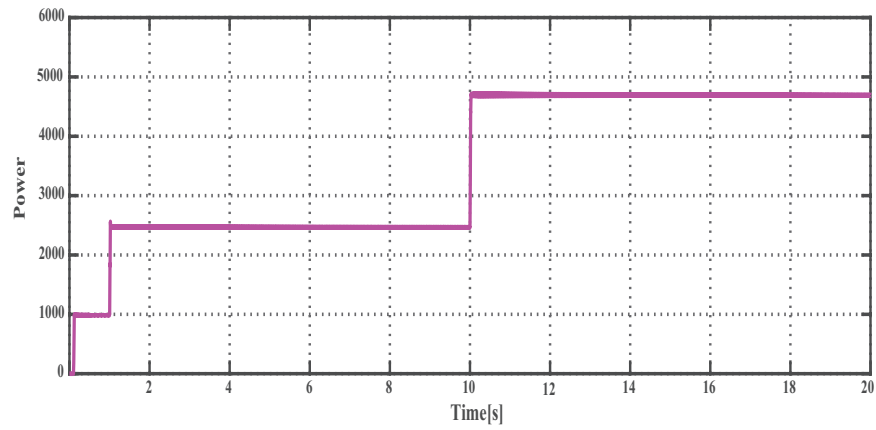


Fig. 5.2: Total power demand

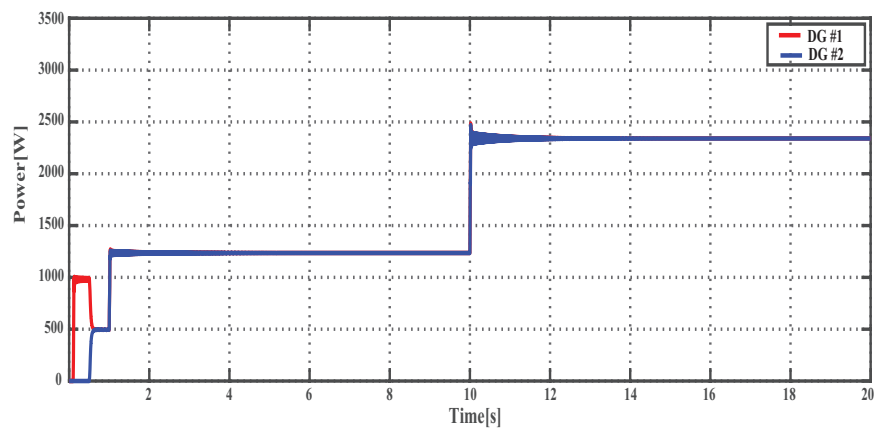


Fig. 5.3: Power sharing based on modified droop control

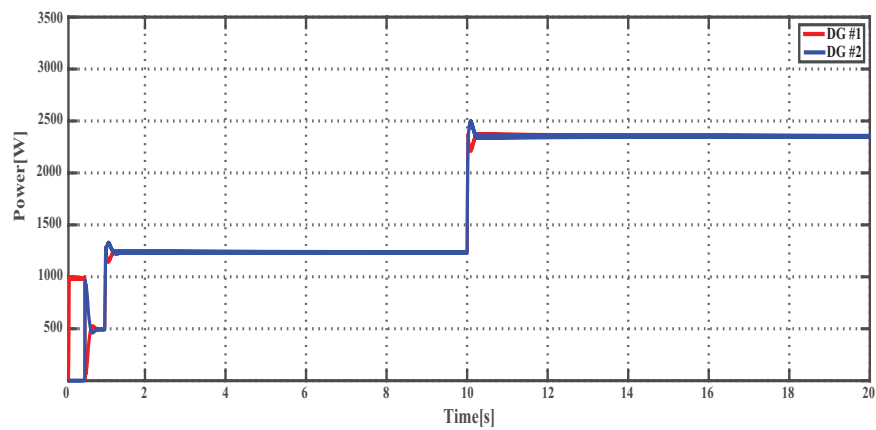


Fig. 5.4: Power sharing based on VSG

### 5.1.1.2 Load Transition

To observe the performance of each control scheme during the load transition, a group of load with the power consumption, 1.5 kW (25%), is connected into the system

at the time  $t = 3$  s with the initial consumption 4.2 kW and disconnected around 45% at the time  $t = 10$  s as shown in Fig. 5.5. In Figure 5.6, the *red – graph* is the frequency response of the VSG, and the *cyan – graph* is the frequency response of the modified droop control. It is clearly seen that the VSG which emulates the synchronous generator dynamic characteristic could provide the inertia and damping support to the system, as a result, it has smaller frequency overshoot/undershoot compare to the modified droop control when there is a sudden increase in power demand.

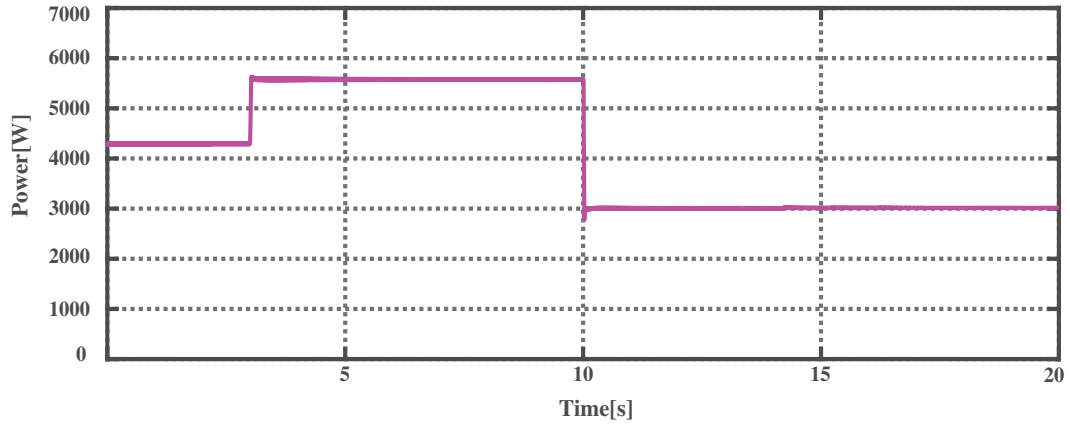


Fig. 5.5: Total active power demand.

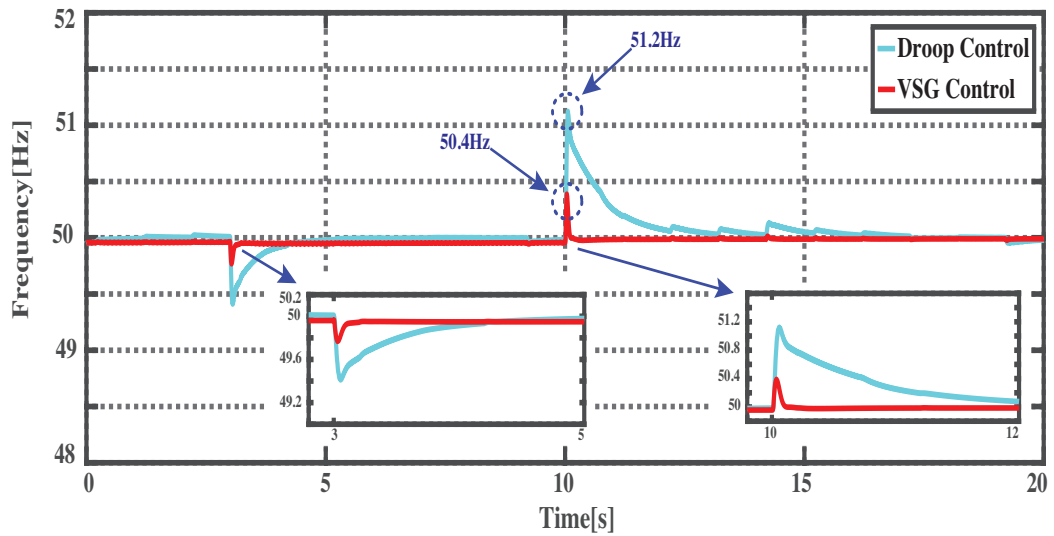
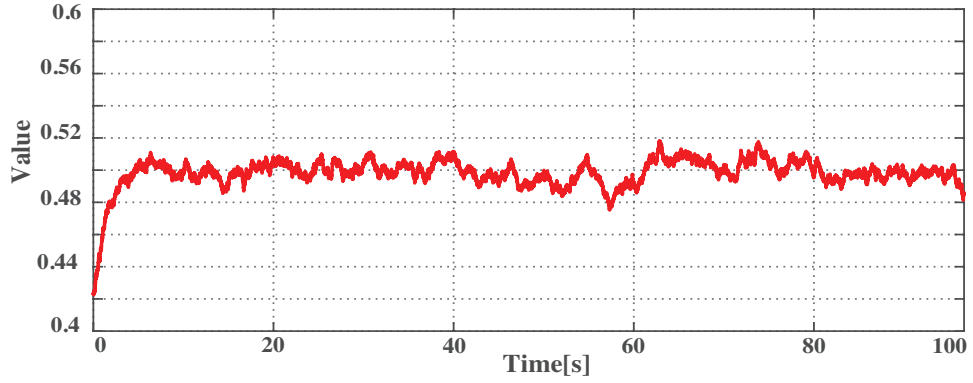


Fig. 5.6: Frequency response: VSG Vs Droop control.

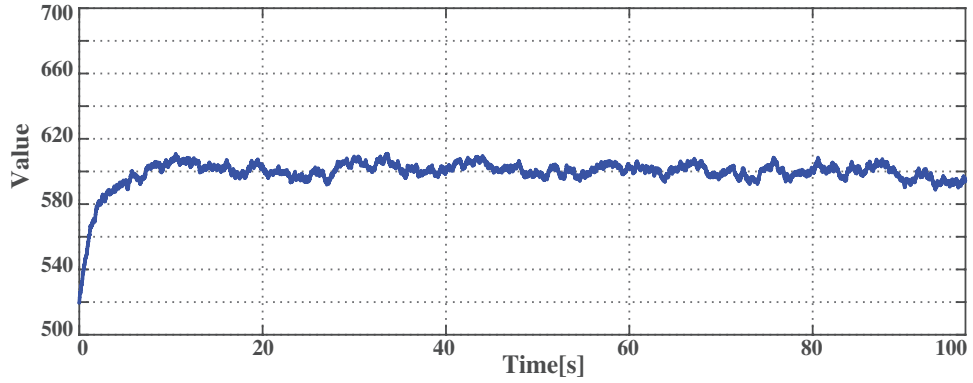
#### 5.1.1.3 Comparison Between Constant and Tuning Parameters of VSG

As mentioned in Section 4.2.1.3, adapting the parameters ( $J$ ,  $D$ ) of VSG is the key superior to the conventional synchronous generator to enhance the dynamical response of the system. Therefore, an online parameter adaptive based on BSA is investigated in this section. It is worth mentioning that the increase in the number of population and

epoch could provide better results by reducing the overshoot and settling time; at the same time, it increases the computation burden and simulation time. The parameter of BSA such as population size and epoch is set to 25 and 5, respectively, by considering the trade-off between computation burden and performance. The virtual inertia ( $J$ ) and damping factor ( $D$ ) which are computed by BSA is shown in Fig. 5.7.



(a) Value  $J$  generate by BSA



(b) Value  $D$  generate by BSA

Fig. 5.7: Parameter adapting based on BSA.

In this case, the load transient is applied to the system supplementary with the high PV power fluctuation. The power demand waveform is shown in Fig. 5.8. To create the load transient event, 45 percent of total power demand is connected and disconnected at time  $t = 5$  s and  $t = 12$  s, respectively. Three control schemes such as modified droop control, constant VSG parameter and adapted VSG parameter are compared. The frequency response of the system demonstrates in Fig. 5.9. By observing at the time  $t = 5$  s and  $t = 12$  s, the system operates in an unacceptable frequency range when the system is equipped with the modified droop control (*cyan – graph*). In case the constant VSG parameter is applied, the system has a relatively large deviation. But, it is still in acceptable frequency range  $\pm 0.5$  Hz (*red – graph*). While the adaptive parameter (*blue – graph*) is adopted, the frequency deviation overshoot is efficiently suppressed which is in range  $\pm 0.2$  Hz. This witness that the online tuning method could reduce the

frequency deviation more effectively compared to the other two control schemes.

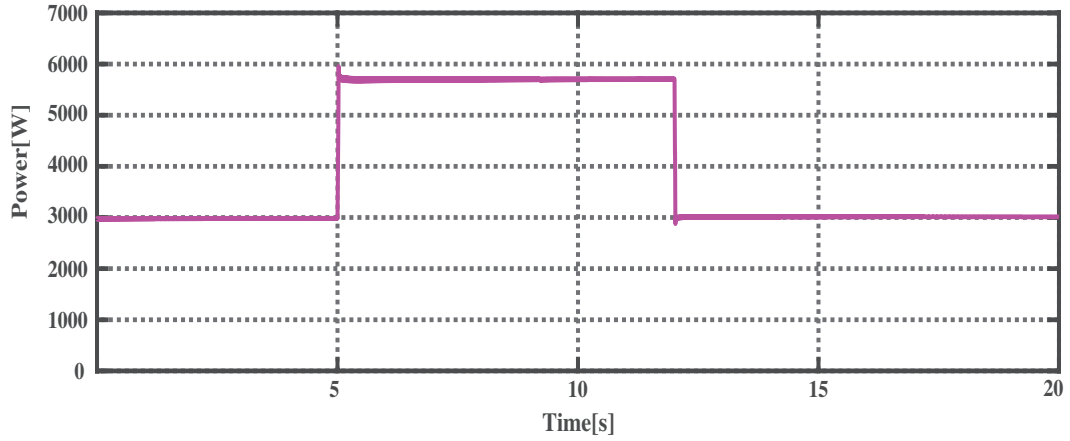


Fig. 5.8: Total active power demand.

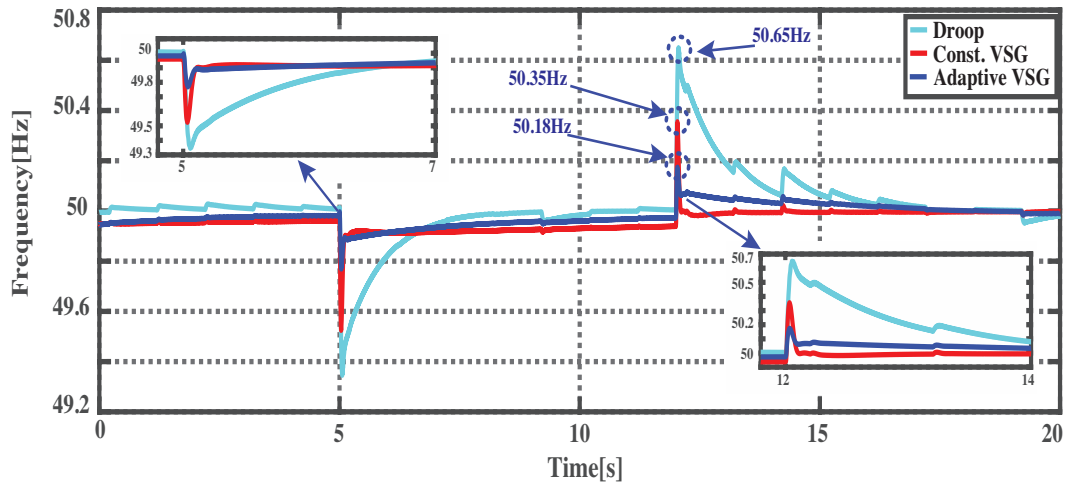


Fig. 5.9: Frequency response based on load transient: Adaptive VSG Vs Const. Vs Droop control.

### 5.1.2 Secondary Control

The main purpose of the secondary control is to handle the voltage and frequency deviation in the system, which results from the primary level and the system's condition. Here, two control method is discussed such as frequency restoration and frequency fluctuation mitigation.

#### 5.1.2.1 Frequency Restoration

Droop based autonomous control offers several advantages such as communication independence, plug-n-play capability, and enhanced reliability of the system. However, with droop control, the system frequency may vary to an unacceptable value while there is a load transaction. This issue is stated as a major drawback of this control technique [62]. To address this issue, the frequency restoration is implemented to keep the operating frequency close to the desired frequency ( $\omega_E \simeq \omega_{Eref}$ ).

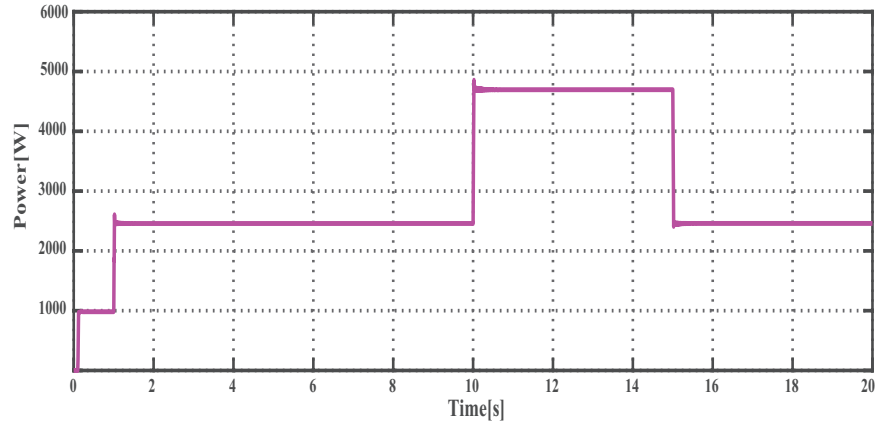


Fig. 5.10: Load transition

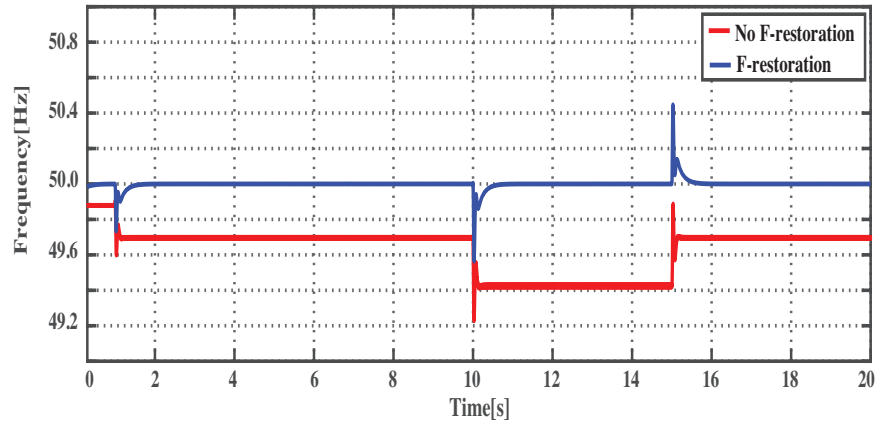


Fig. 5.11: Frequency restoration

To evaluate the performance of frequency restoration, the load transition is applied as shown in Fig 5.10. Then, the frequency response of the system both with/without the frequency restoration is compared. Figure 5.11 illustrates the system's frequency when the load transition is applied. It is clear that the frequency restoration control could maintain the system frequency close to the reference value, *blue – graph*. While, without frequency restoration, the system operates at another frequency value which is in an unacceptable range as depicted in the *red – graph*.

#### 5.1.2.2 PV Power Fluctuation Miltigation

To investigate the impact of the PV integration on the system, a worth case PV profile which is recorded on 24 January 2015 from laboratory Rooftop-PV ( $P \approx 2.1$  kW) is used as illustrated in Fig. 5.12. In this study, five minutes of data in real-time is scaled to 1 s in the simulation environment via Rate-Transition Simulink Block.

Figure 5.13 is demonstrated the system behavior while operates without the energy storage system. It shows that the system has a large frequency variation and the power from DGs has oscillated follows the variation of PV power.



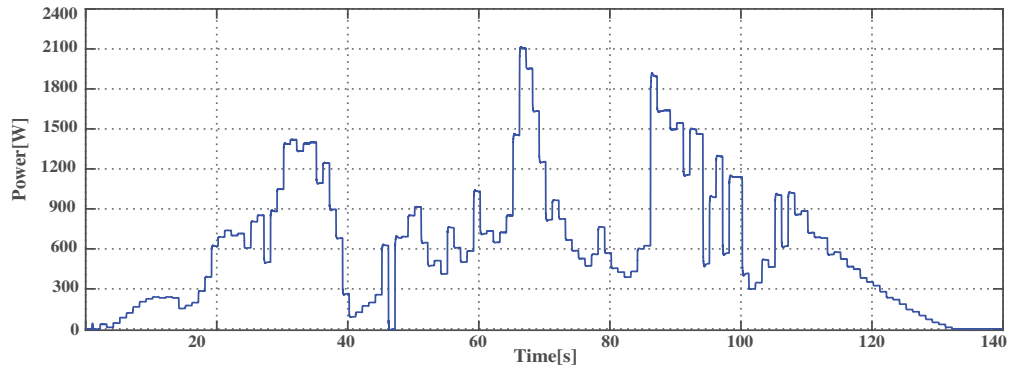


Fig. 5.12: Worst PV power fluctuation profile.

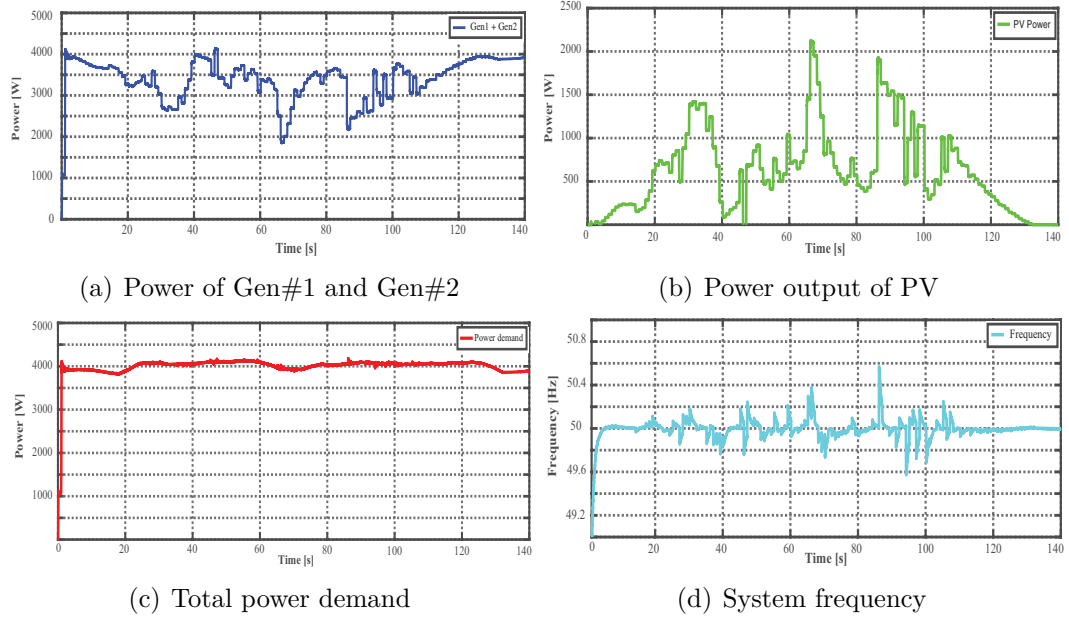


Fig. 5.13: System without energy storage system.

To eliminate the affect of PV power fluctuation, the system is highly rely on ESS. To get the maximum performance of ESS, the PV smoothing method and inverter control algorithm are important. In this section, two case studied are conducted. First, the comparison of smoothing method based on battery energy storage system is investigated. Through this comparison, a proper smothing method is obtained. Then, based on the selected smoothing method, the VSG control algorithm is compared with dq-decoupling control for controlling the grid-connected inverter.

#### † Comparison on PV Power Smoothing Method

In this part, a PV power smoothing method based on LPF is compared with the proposed smoothing scheme. To make a fair comparison, the criteria listed below will be followed:

- The total amount of energy usage.

- How is the battery utilized and what is its state at the end of the day.
- The frequency variation and overshoot suppression ability.

Figure 5.14 is the result obtained from each method, which conforms to the mentioned criteria such as equal energy usage, SoC level and power; at the end of the operation. The time constant of LPF is set to  $\tau = 5s$ , and the constant  $K$  of the proposed method set to 0.656.

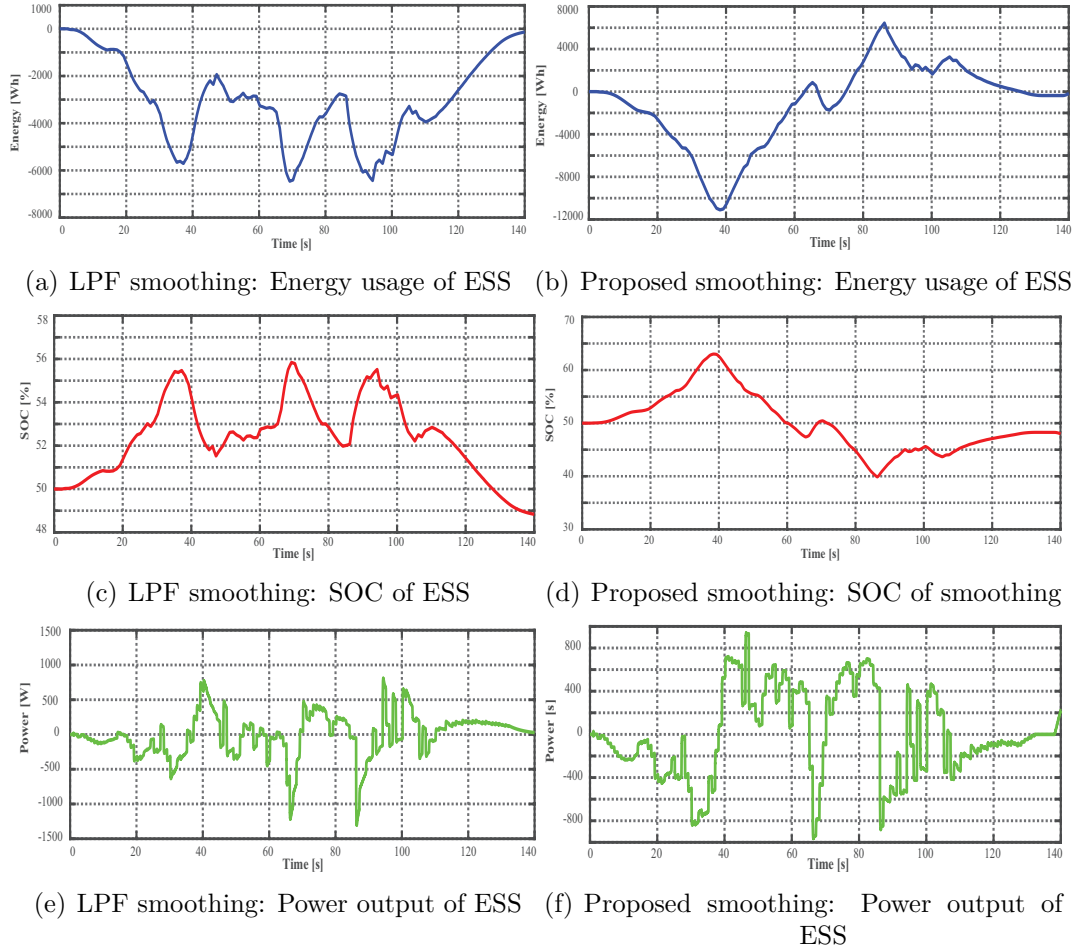


Fig. 5.14: Energy, SOC and power produce by the smoothing methods

The result of each smoothing method is shown in Fig. 5.15. The three subfigures on the left are the power of DGs, power consumption, and the system frequency based on the LPF smoothing method. Meanwhile, the three subfigures on the right are the power of DGs, power consumption and frequency based on the proposed method. The power consumption has the same amount of both methods as can be seen in Fig. 5.15(c) and Fig. 5.15d. By observing the power of DGs and system frequency, it is obvious that the PV power fluctuation mitigation based on LPF has large oscillation compare to the proposed method.

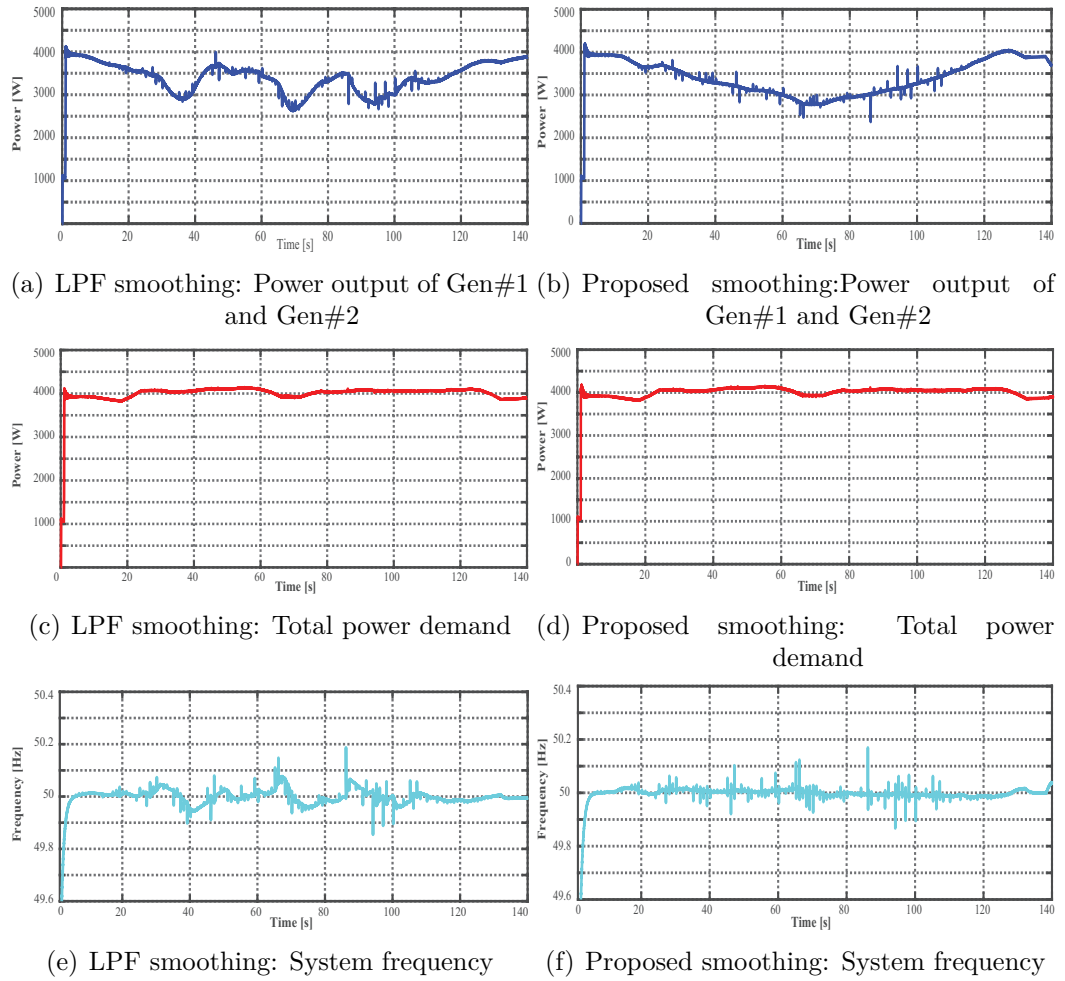


Fig. 5.15: Respond of each control method

Figure 5.16 is the frequency response based on each smoothing method. There are three waveforms in this figure. The *cyan* – *graph* represents the frequency of the system without any energy storage system. The *red* – *graph* and the *blue* – *graph* are the frequency response based on the LPF and the proposed method, respectively.

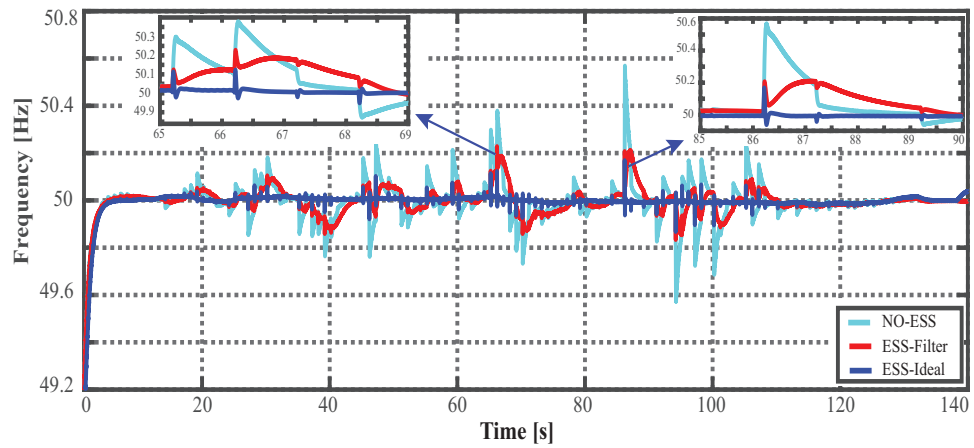


Fig. 5.16: Frequency respond: Without ESS, LPF smoothing and proposed method

According to Fig. 5.16 during the time  $t = 66$  s to  $t = 69$  s and  $t = 85$  s to  $t = 90$  s, it is clear that the frequency deviation mitigation based on LPF has higher variation overshoot and slow respond compare to its counterpart proposed smoothing method.

#### † Comparison Between dq-decoupling Control and VSG Control

This section aims to investigate the performance of VSG control algorithm when it is applied for inverter control of the energy storage system. Thus, a comparison has been made between VSG and dq-decoupling control algorithms. On the other hand, due to large variation of PV power as shown in Fig. 5.18, the usage of battery in this application could seriously shorten the battery lifespan. Hence, to improve the lifespan of the battery by reducing the battery's stress, the supercapacitor/battery hybrid energy storage system (HESS) is introduced in this part. The supercapacitor is responsible for the high-frequency variation power while the battery corresponds to the low-frequency variation power. The proposed smoothing method in **Section 4.2.2.2** has been modified for a hybrid energy storage system as illustrated in Fig. 5.17.

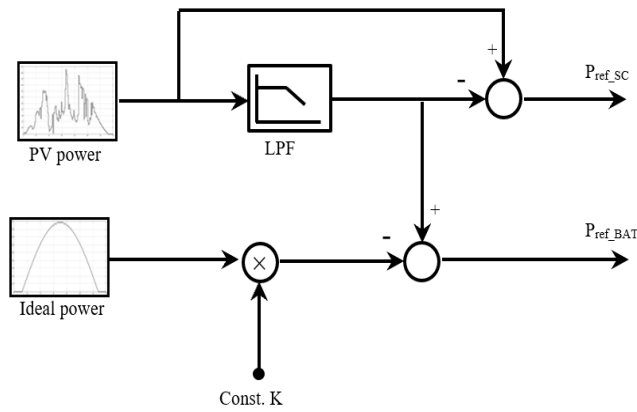


Fig. 5.17: Smoothing method for HESS

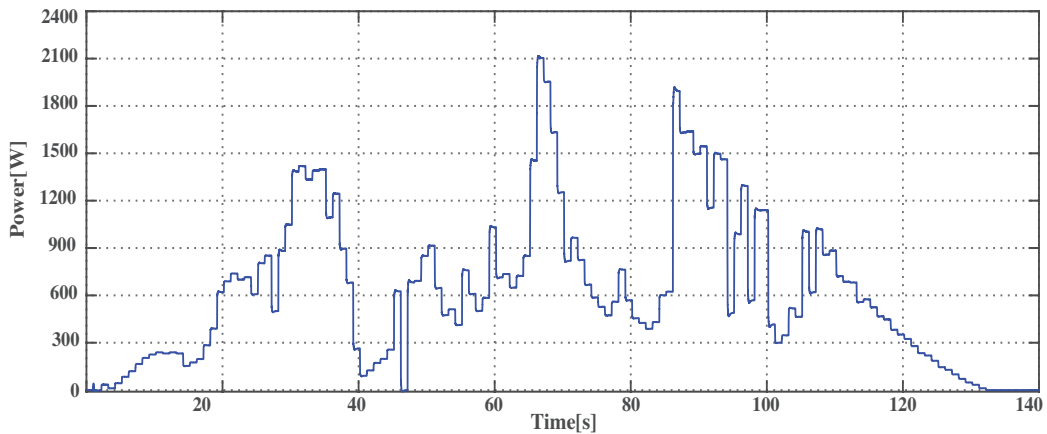


Fig. 5.18: Worst PV power fluctuation profile.

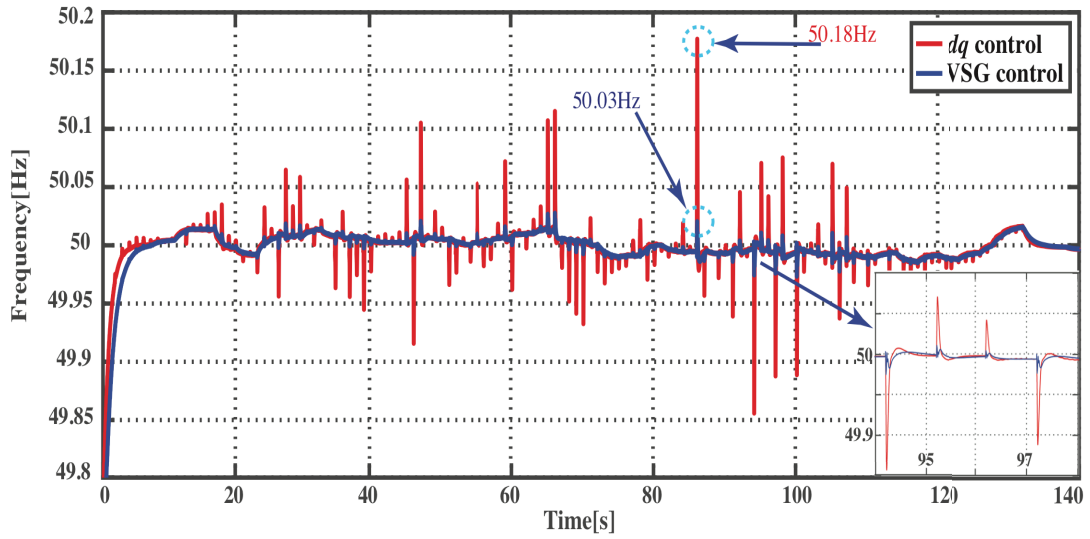
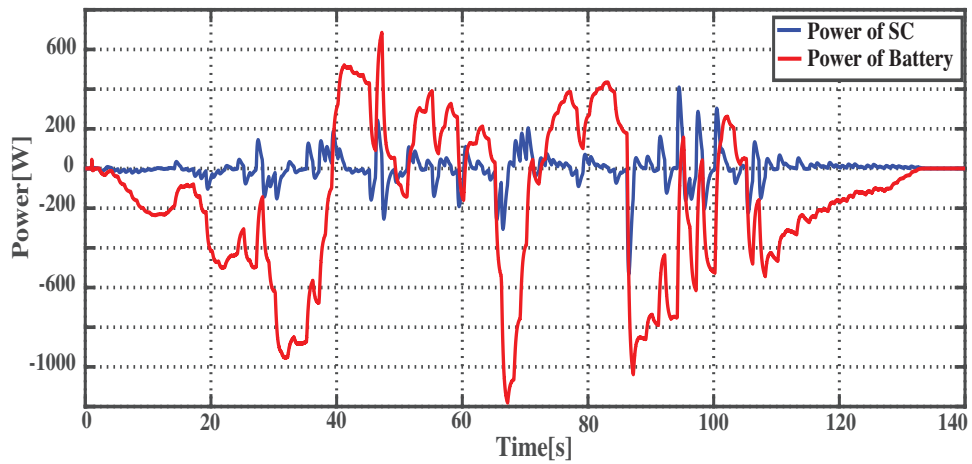
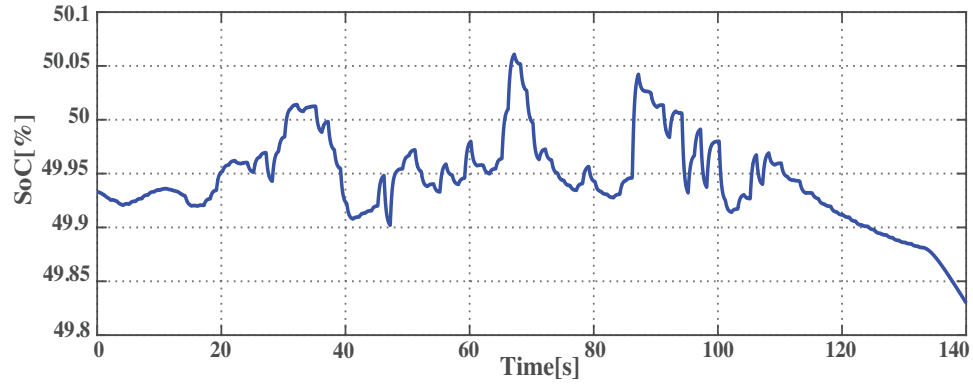


Fig. 5.19: Frequency response: VSG Vs DQ decoupling control.

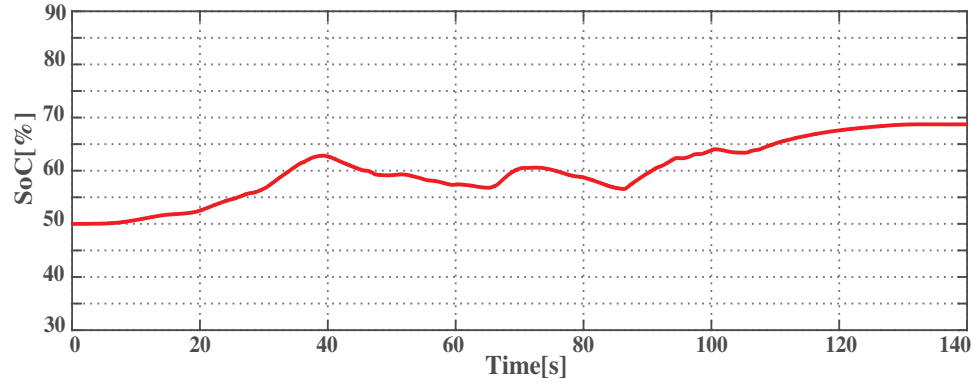
Figure 5.19 presents the frequency response of the VSG control and the current  $dq$  – decoupling. This result is obtained when it takes into account the strong variation of PV output power as shown in Fig. 5.18. According to this waveform, it is obvious that the VSG (*blue – graph*) could suppress the oscillation frequency far effectively than the normal  $dq$  – decoupling control (*red – graph*) by using the same amount of power from HESS. The power and  $SoC$  of the HESS are provided in Fig. 5.19. In Figure 5.19a, the *blue – graph* represents the power of supercapacitor and *red – graph* is the power of battery. Since the supercapacitor is responsible for high power variation, its power and  $SoC$  (Figure 5.19b) are strongly fluctuated. Meanwhile, the battery's power and  $SoC$  (Figure 5.19c) are smoothly changed. As a result, the battery lifespan is expected to be improved due to low stress.



(a) Power of Battery and Supercapacitor



(b) SoC of Supercapacitor



(c) SoC of Battery

Fig. 5.19: Power &amp; SoC of hybrid energy storage system.

#### † Comparing Between Constant and Adaptive VSG's Parameter

As mentioned in **Section 4.2.1.3**, adapting the parameters ( $J$ ,  $D$ ) of VSG is the key superior to the conventional synchronous generator to enhance the system dynamical response. Therefore, an online parameter adapting based on BSA is investigated in this section. It is worth mentioning that the increase in number of population and epoch could provide better results by reducing the overshoot and settling time; at the same time, it increases the computation burden and simulation time. The parameter of BSA such as population size and epoch are set to 25 and 5, respectively, by considering the trade-off between computation burden and performance. The virtual inertia ( $J$ ) and damping factor ( $D$ ) which are computed by BSA shown in Fig. 5.7.

The PV power in Fig. 5.18 is used to realize the high PV power variation. The result of the frequency response with the online updating parameter is compared to the VSG constant parameters. Figure 5.20 is the system frequency response of the adaptive parameter by BSA and the constant parameter. It shows that with the tuning parameter, the system has smaller frequency overshoot compared to the constant parameter. Although the improvement is small, it proves the promising performance of the adaptive parameter.





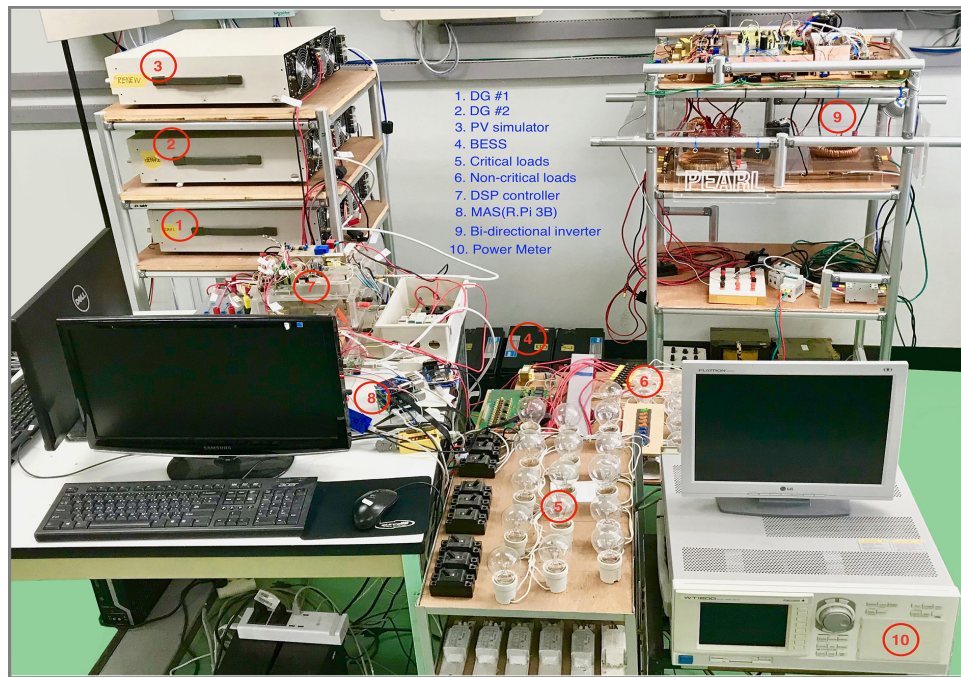


Fig. 5.22: Laboratory scale Microgrid

Table 5.2: Microgrid's parameters

Microsource 1 and 2 (Gen 1, Gen 2)	
Model	Kikusui PCR2000M
Power Rating	220V, 50Hz, 2kVA
P-Angle Droop Coefficient (m)	$2\pi(0.000185)$
Q-V Droop Coefficient (n)	$1/0.002592725$
Digital Controller (DSPF28335)	Sampling Rate: 12.78kHz
Xd	4mH
Load	
Critical Load	1500W, 1275VA
Non-critical load	1300W
PV Simulator	
Model	Kikusui PCR2000M
Simulate	Based PV profile (Max: 1247W)
Energy storage system	
SOLAR 12-65	8 * (12V, 65AH)
Multiagent system	
SPADE	Python (FIPA compliant)
Agent execution	Raspberry Pi 3B (Ubuntu Mate 16.04)



This section presents the most relevant results obtained from the experiment. Section 5.2.1 demonstrates the results regarding the primary layer functionalities in performing load-sharing. The experimental results regarding the secondary layer in frequency restoration and PV power fluctuation mitigation are presented in Section 5.2.2. Finally, the validation of the emergency control strategies such enable/disable reserve generator and load-shedding, power monitoring based on IoT platform, PV power prediction are discussed in section 5.2.3 as tertiary layer.

### 5.2.1 Primary Layer

In this case study, in order to investigate the power transient response of modified droop control, the time scale and sample rate of power meter have been set to  $2s/div$  and  $200ms$ , respectively.

In Figure 5.23, element 1 (E1) represents the power consumption that cyan-graph and red-graph are the total active power and reactive power, respectively. The green-graph (E2) is the active power of generator#1 (Gen#1), the orange-graph (E2) is the active power of generator#2 (Gen#2), the ping-graph (E3) is the reactive power of Gen#1 and the blue-graph (E3) is the reactive power of Gen#2. At the time  $t = 4s$ , the demands are increasing over Gen#1 capacity then the Gen#2 is connected. After 1 second ( $t = 5s$ ), the Gen#2 shares the power with Gen#1 smoothly. It is clearly observed that from the time  $t = 5s$  to  $t = 17s$ , the active power output of Gen#1 (E2: Green) and Gen#2 (E2: Orange) and reactive power output of Gen#1 (E3: Ping) and Gen#2 (E3: Blue) are nearly equal. At the  $t = 18$ , all power smoothly transfer to Gen#1 as the demand drops below Gen#1 capacity. This result proves the effectiveness of modified droop control with better power transient response.

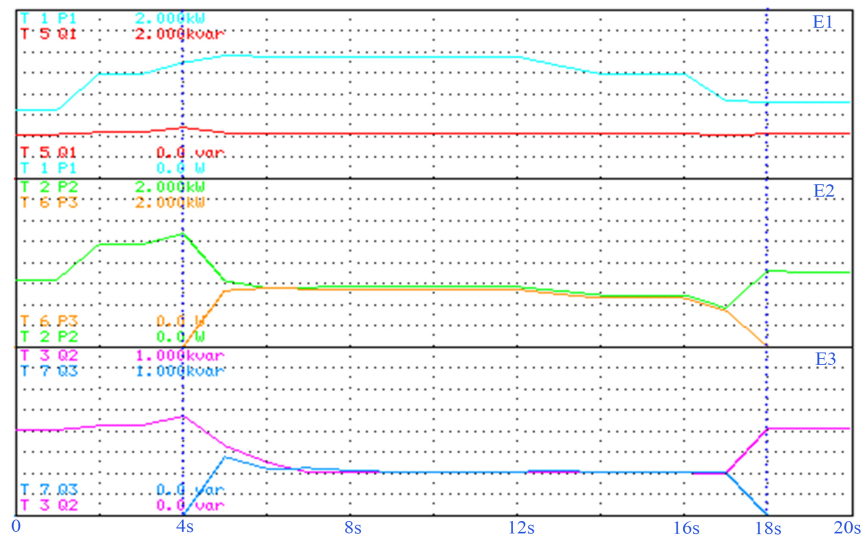


Fig. 5.23: Droop control: (E1) Active and reactive power of demands; (E2) Active power of Gen#1 (Green) and Gen#2 (Orange); (E3) Reactive power of Gen#1 (Ping) and Gen#2 (Blue)

## 5.2.2 Secondary Layer

The responsible of the second layer is to correct or handle the impact of the first layer or stochastic nature of renewable sources in the system. In this layer, two control methods are implemented to ensure the standard operation of the system.

### 5.2.2.1 Frequency Restoration

The frequency restoration is used to address the drawback of droop control, and it will take action while Gen#1 and Gen#2 are operating together. From 170s-to-340s and 395s-to-500s, as shown in Fig. 5.24, the frequency (E3: ping) is restored to a normal value while the Gen#2 was taking into account.

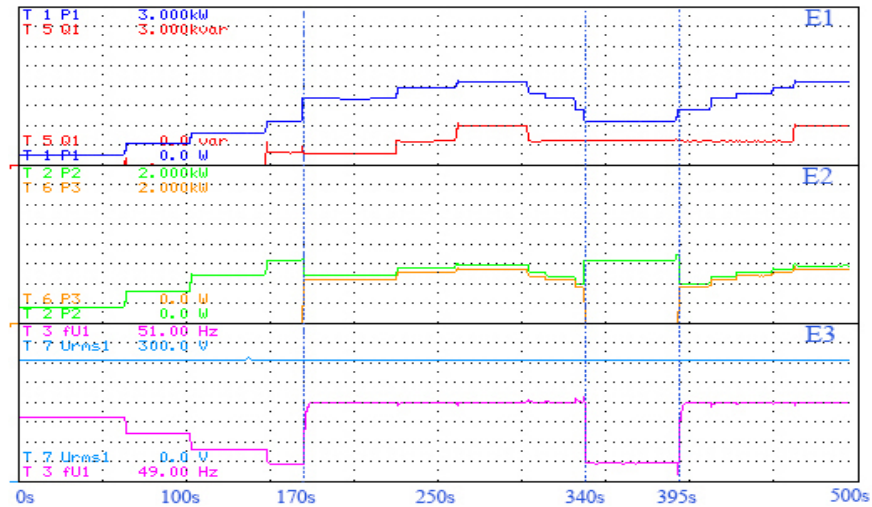


Fig. 5.24: Frequency restoration: (E1) Active and reactive power of demands; (E2) Active power of Gen#1(Green) and Gen#2(Orange); (E3) Ping (Frequency) and Cyan (Voltage)

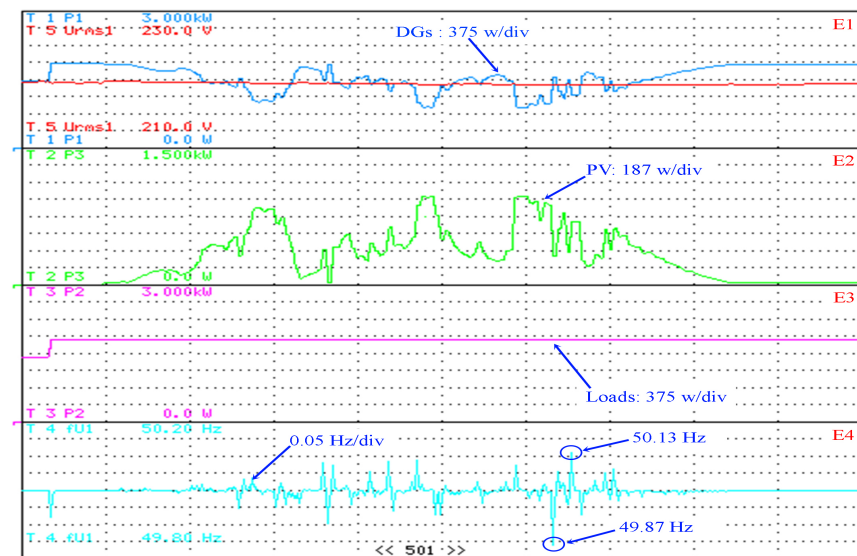


Fig. 5.25: Without BESS: (E1:cyan) Power of GEN#1 and Gen#2; (E2) Output power of PV; (E3) Total power demand; (E4) Grid's frequency

### 5.2.2.2 Frequency Deviation Mitigation

The battery energy storage system in this research is mainly used to smooth the PV power fluctuation. Figure 5.25 presents the system's behavior without BESS. E1 (cyan) is the power of GEN#1 plus GEN#2 and E1 (red-graph) is the grid's RMS voltage. E2 is the PV output power, E3 is the power demand, and E4 is the grid's frequency. It is obvious that without any energy storage system compensation, the power output of DGs and the system's frequency strongly fluctuate followed the variation of PV power output with the frequency deviation overshoot approximated 50.13 Hz.

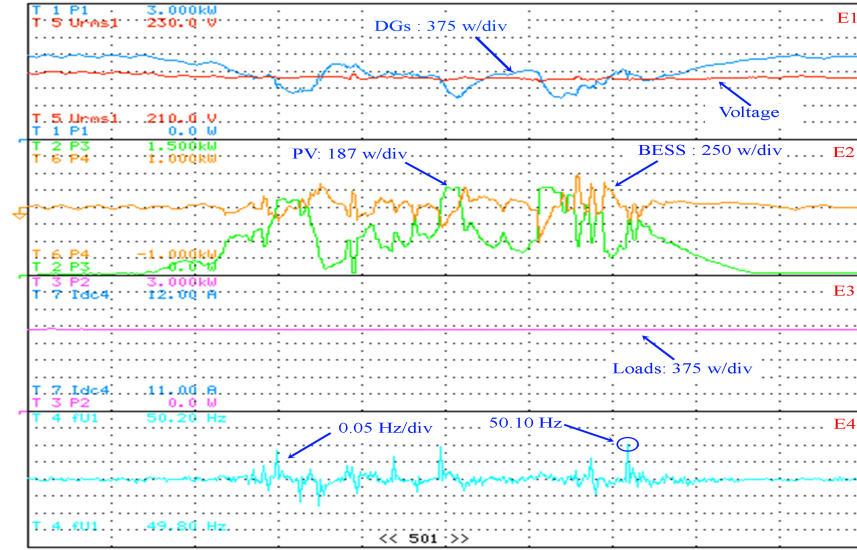


Fig. 5.26: LPF smoothing technique: (E1:cyan) power of GEN#1 and Gen#2; E2 (green-graph) output power of PV and E2 (orange-graph) output power of BESS; (E3) Total power demand; (E4) system frequency.

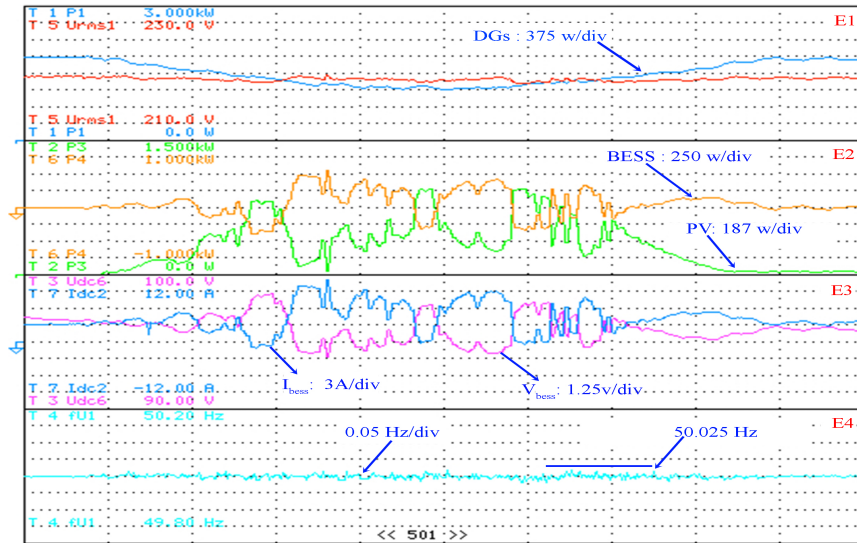


Fig. 5.27: Proposed smoothing technique: (E1:cyan) power of GEN#1 and Gen#2; E2 (green-graph) output power of PV and E2 (orange-graph) output power of BESS; E3 (pink-graph) BESS's voltage and E3 (blue-graph) BESS's current; (E4) system frequency.

The result of PV power smoothing based on LPF smoothing strategy is demonstrated in Fig. 5.26. In this figure, E1 (blue-graph) is the active power output of DGs, and E1 (red-graph) is the RMS voltage of the grid. E2 (green-graph) and E2 (orange-graph) are output power of PV and BESS, respectively. E3 (cyan-graph), E3 (ping-graph) are the DC voltage and current of BESS, and E4 is the system's frequency. By comparing it to Fig. 5.25 (without energy storage), the power output of the generator, and frequency are less oscillation with frequency deviation overshoot approximated 50.10 Hz.

Figure 5.27 is the result of PV power smoothing based on the proposed smoothing technique. As can be seen from this figure, the power oscillation of DGs (E1:blue-graph) is significantly reduced. Also, by observing to system's frequency in Fig. 5.27 (E4), Fig. 5.26 (E4) and Fig. 5.25 (E4), it is clear that the proposed smoothing method could suppress the frequency deviation more effectively than the LPF smoothing with the frequency deviation overshoot approximated 50.025 Hz.

### 5.2.3 Tertiary Layer

At the top layer of the hierarchical control, the state-of-art control scheme, and the cutting-edge-technology like MAS and IoT, are employed. Comparing to other agent development platforms such as JADE and Volttron, SPADE is more advanced in terms of agent management and borderless for development. Several case studies are conducted to investigate the MAS's performance.

#### 5.2.3.1 Multiagent System

##### ★ Generator Control

The strongly depends on the meteorological of renewable generation could result in the supply-demand imbalance when the microgrid operates in islanded mode. Such an imbalance may lead to system blackout. Consequently, the reserve generator is needed in that emergency case. The reserve generator represents the fossil-based generator such as diesel generator which has high production cost, and it is allowed to operate in critical condition only to maintain the stability of the system.

In this case, the Gen#2 works as a reserve generator. The DER agent controls the Gen#2 status and it determines whether Gen#2 needs to connect or disconnect. In Figure 5.28, element 3 (E3) represents the Gen#2. In case of power supply shortage, the DER agent will put the Gen#2 into operation as it can be seen during 25s-170s, 230s-300s, and 380s-500s. Otherwise, Gen#2 will be disabled (0-25s, 170s-230s, and 300s-380s) as it is obvious in Fig. 5.28.

##### ★ Load-Shedding

The load shedding is defined as a coordinated set of controls which results

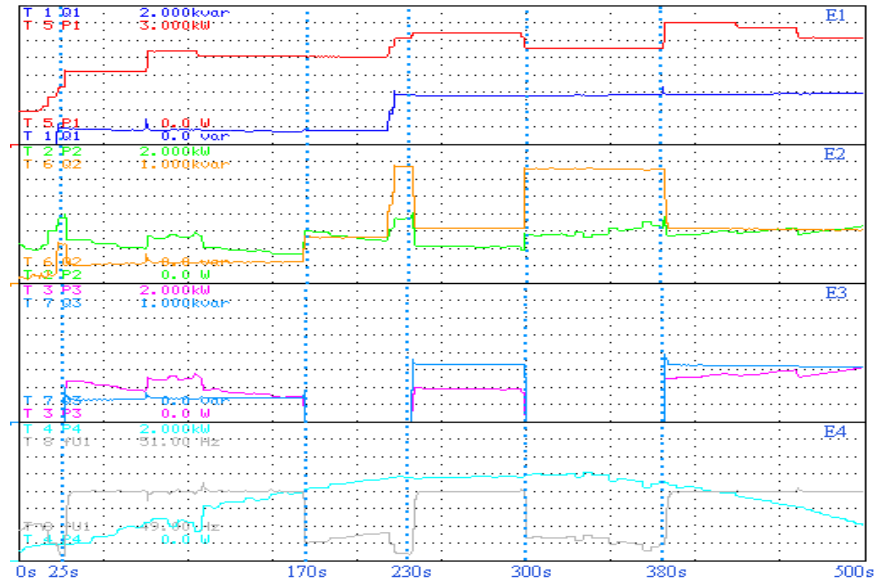


Fig. 5.28: Control reserve generator: (E1) Yellow (Critical load) and Red (Non-critical load); (E2) Power of Gen#1; (E3) Power of Gen#2; (E4) Cyan (PV) and Gray (f-Hz)

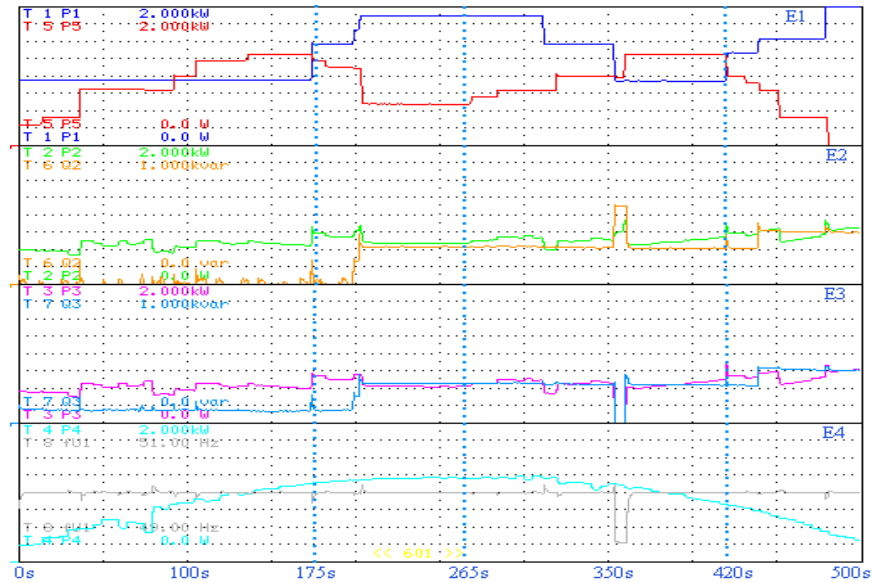


Fig. 5.29: Load-shedding: (E1) Blue (Critical load) and Red (Non-critical load); (E2) Power of Gen#1; (E3) Power of Gen#2; (E4) Cyan (PV) and Gray (f-Hz)

in decreasing of electric consumption. It will perform when the system faces the over-consumption. It means some non-critical loads are switched off. In this way, a system stable regime can be achieved. With the effectiveness of the secondary control (frequency restoration), the system's frequency will be controlled to operate at the normal value. Hence, performing load-shedding based on detection the value of frequency drop comparing to the threshold is hardly possible.

In this experiment, the LOAD agent will take responsibility for load-shedding. It will cut out the non-critical load based on surplus power consumption. In Figure 5.29,

the element1 (E1) represents the critical load's power (blue-graph) and non-critical load's power (red-graph). From 175s-to-265s and 420s-to-500s, the power supply is not fulfilled to the consumption, to prevent the system from collapse, the LOAD agent performs load shedding by cutting some non-critical load from the system. Consequently, the power of non-critical load is reduced during 175s-265s and 420s-500s (E1: red-graph).

### 5.2.3.2 Internet of Thing

Figure 5.30 shown the topology of web-monitoring based on IoT platform called ThingsBoard. The information from the system (e.g. active power, reactive power, voltage, and frequency) transferred to IoT platform via the CONTROL agent. With the integration of IoT, either operator or customer could monitor the system in real-time or near real-time as well as do network control remotely from anywhere via PC or Mobile-phone. Moreover, the system's historical data could be stored in data storage or cloud for on-line or off-line analysis.

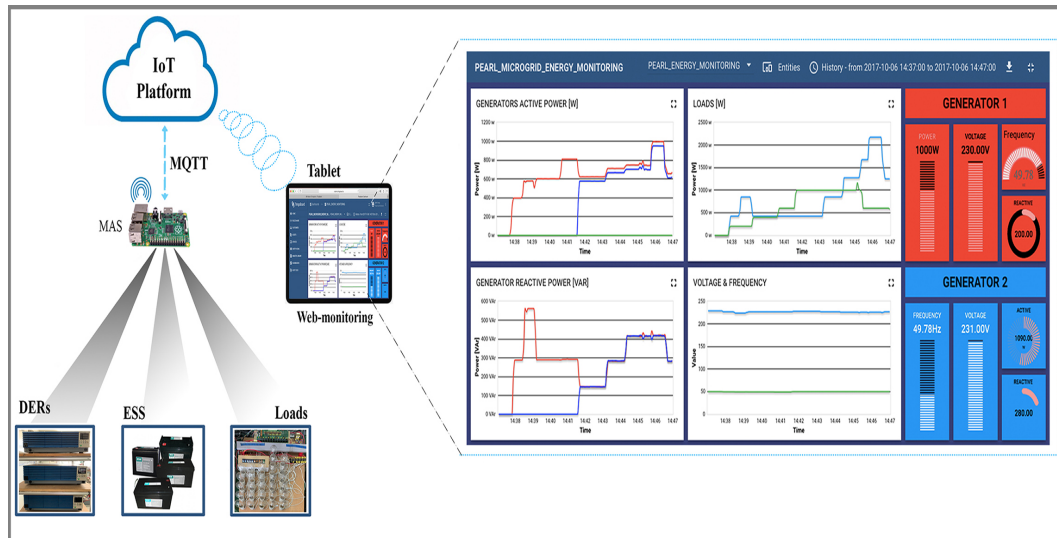


Fig. 5.30: Real-time web remote and monitoring

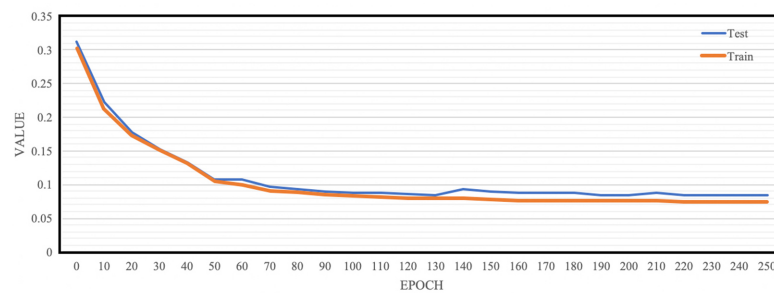
### 5.2.3.3 PV Power Prediction Based Artificial Neural Network

To ensure secure operation and economic integration of PV in the system, accurate forecasting of PV power is an important issue. In this research, the long-short term memory recurrent neural network (LSTM-RNN) and multilayer perceptron (MLP) are utilized to forecast the output power of PV systems. It is worth mentioning that the increasing number of layers and neurons could improve the accuracy of the model. However, it may increase the computation time and burden as well as the model over-fitted. As a result, the model must be designed by considering the computation constrain and accuracy. Through trial-and-error, the model of LSTM and MLP is obtained as provided in Table 5.3. The LSTM model consists of three layers such as one input

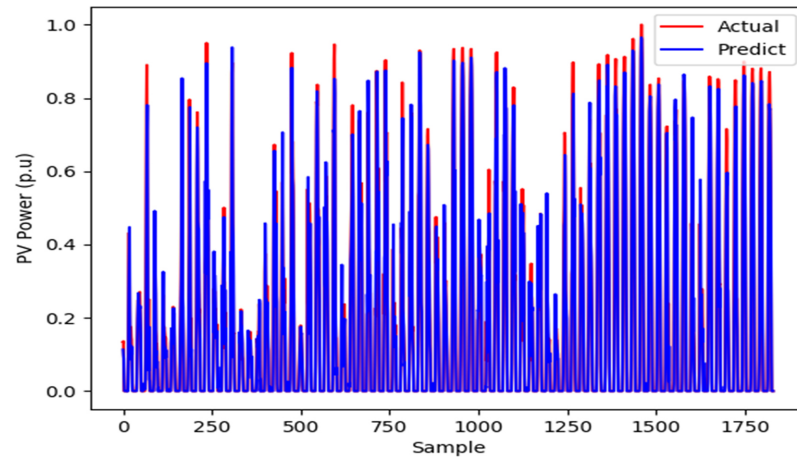
layer, one hidden layer with 200 neurons, and one output layer. The sigmoid and ADAM are utilized as the model's activation function and optimizer, respectively. Meanwhile, the MLP consists of six layers such as one input layer, four hidden layers and one output layer. The input layer contains 250 neurons. Each hidden layer composes of 500 neurons, and the output layer has 250 neurons. The ReLU and ADAM are utilized as the model's activation function and optimizer, respectively.

Table 5.3: LSTM and MLP Parameters

LSTM		MLP	
Parameter	Value	Parameter	Value
Number of hidden layer	1	Number of hidden layer	4
Number of hidden units	200	Number of neuron	250-500-500-500-250
Cost function	RMSE	Activation function	ReLU
Optimizer	ADAM	Optimizer	ADAM
Number of training epochs	250	Number of training epochs	250



(a) RMSE value of training and testing



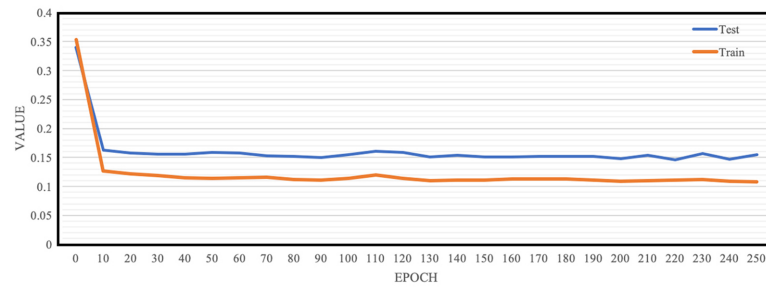
(b) Forecasted vs actual power

Fig. 5.31: PV power predicted based on LSTM

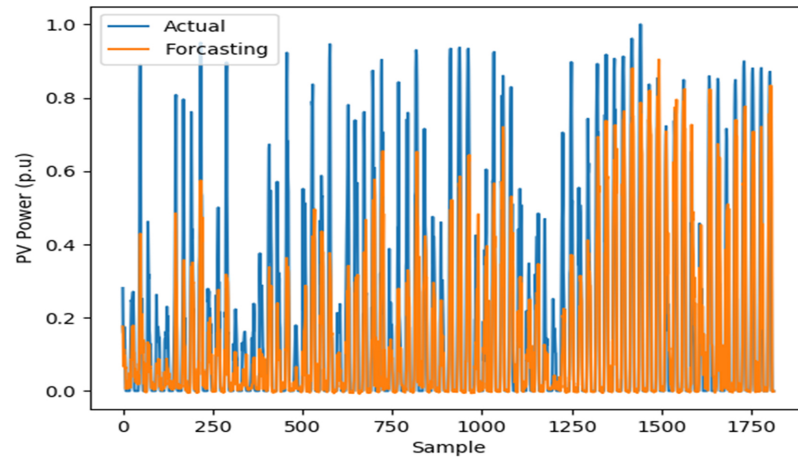
The dataset is divided into training and testing datasets. A total of 70% of the samples are used to train the PV power forecasting model, while the remaining samples are used for testing the model. The models were implemented using Python, Tensorflow library. The root-mean-square error (RMSE) is utilized to evaluate the performance



of the forecasting models. A smaller RMSE value indicates the predicted results are more accurate. Figure 5.31 shows the RMSE versus the Epoch (iteration) and the power forecast based on LSTM. The best validation performance is at epoch 250 with a value of RMSE=0.0744 and RMSE=0.0834 for training and testing, respectively. Figure 5.32 depicts the RMSE and power forecast based on MLP. Comparing these two artificial neural network architecture, it is obvious that the PV power prediction based on LSTM has far higher accuracy than MLP.



(a) RMSE value of training and testing



(b) Forecasted vs actual power

Fig. 5.32: PV power predicted based on MLP





## CONCLUSION AND FUTURE WORKS

### 6.1 Conclusion

The intermittent nature of the renewable sources is the main challenge issue of microgrid's control. Hence, this paper attempts to combine the several control together in the hierarchy structure. Following the IEC 62264 standard, the proposed control is classified into three layers based on the control functionality and speed. The major contribution of the proposed control are: (1) To realize the power-sharing of co-operation generators; (2) Handling the frequency deviation which results from primary control and the stochastic output of renewable sources; (3) Introducing the embedded MAS and the IoT technology to the microgrid. The real microgrid system has been set up to evaluate the controller performance in a real-time environment. The results prove the effectiveness of the hierarchical control to handle the various issues in the microgrid.

### 6.2 Future works

This research aims to solve the major issues of the microgrid and to bring it to the next level for future smart grid development through the implementation of distributed hierarchical control. The proposed control is firstly developed in Matlab/Simulink, and then verified with experimental. However, any research should always leave one with new knowledge and a desire to take that new knowledge to the next level. The techniques and contributions developed in this dissertation as described so far point to the following open research issues that can be studied in future:

- Implement the VSG control in DSP controller.
- Develop an artificial neural network framework that be able to run in embedded system like raspberry pi with aiding of neural computation stick.
- Implement the energy management system for the BESS based on the day-ahead prediction of PV output power.



- [1] N. Marwali, J. Jung, and A. Keyhani, "Control of distributed generation systems--- part ii: Load sharing control," *IEEE TRANSACTIONS ON POWER ELECTRONICS*, vol. 19, no. 6, pp. 1551--1561, 2004.
- [2] M. Shahidehpour and Y. Wang, "Communication and control in electric power systems: Applications of parallel and distributed processing," *IEEE Press Series on Power Engineering*, pp. 32--34, 2003.
- [3] S. Anand, B. Fernandes, and J. Guerrero, "Distributed control to ensure proportional load sharing and improve the voltage regulation in low voltage dc microgrid," *IEEE Transactions on Power Electronics*, vol. 28, no. 4, pp. 1900--1913, 2012.
- [4] V. Verma, G. Talpur *et al.*, "Decentralized master-slave operation of microgrid using current controlled distributed generation sources," *International Conference on Power Electronics, Drives and Energy Systems (PEDES)*, 2012.
- [5] G. Fanghong, W. Changyun, and S. Yong-Duan, "Distributed control and optimization technologies in smart grid systems," *CRC Press*, pp. 3--5, 2017.
- [6] "Final report on the august 14, 2003 blackout in the united states and canada: Causes and recommendations," *U.S.-Canada Power System Outage Task Force and Tech. Rep.*
- [7] M. Yazdanian and A. Mehrizi-Sani, "Distributed control techniques in microgrids," *IEEE Transactions on Smart Grid*, vol. 5, no. 6, 2014.
- [8] P. Christofides, R. Scattolini, and J. Liu, "Distributed model predictive control: A tutorial review and future research directions," *Computers and Chemical Engineering*, vol. 51, pp. 21--41, 2013.
- [9] F. Wang, "Agent-based control for networked traffic management systems," *IEEE Intelligent Systems*, vol. 20, no. 5, pp. 92--96, 2005.
- [10] D. Leng, K. Soontornatweesub, and S. Polmai, "Multi-agent system based real-time control for standalone microgrid," *International Seminar on Intelligent Technology and Its Applications (ISITIA)*, pp. 122--127, 2017.
- [11] D. Hatziargyriou, G. Anastasiadis, and G. Tsikalakis, "Environmental benefits from dg operation when network losses are taken into account," *IEEE Bucharest Power Tech Conference*, Dec 2009.

- [12] D. Schnitzer, D. Lounsbury, J. Carvallo *et al.*, "Microgrids for rural electrification: A critical review of best practices based on seven case studies," *United Nations Foundation*, February 2014.
- [13] M. Soshinskaya, W. Crijns-Graus, J. Guerrero, and J. Vasquez, "Microgrids: Experiences, barriers and success factors," *Renew Sust Energ Rev*, 2014.
- [14] A. Salam, A. Mohamed, and M. Hannan, "Technical challenges on microgrids," *ARPJ-Eng Appl Sci*, 2008.
- [15] W. Bower, D. Ton, R. Guttromson, S. Glover, J. Stamp, and D. Bhatnagar, "The advanced microgrid integration and interoperability," *Sandia National Laboratories*, 2014.
- [16] J. Joy, D. Jasmin, and V. John, "Challenges of smart grid," *IJAREEIE*, 2013.
- [17] A. George and K. Michael, "Measurement, and standards challenges for the smart grid," *Workshop on Technology*, Mar 2013.
- [18] C. Vineetha and C. Babu, "Smart grid challenges, issues and solutions," *IGBSG, Taipei*, 2014.
- [19] M. Stadler, G. Cardoso, S. Mashayekh, N. DeForest, and A. Agarwal, "Value streams in microgrids: A literature review," *Apply Energy*, 2016.
- [20] L. Che, M. Khodayar, and M. Shahidehpour, "Adaptive protection system for microgrids: Protection practices of a functional microgrid system," *IEEE Electrification Magazine*, 2014.
- [21] P. Basak, S. Chowdhury, S. Dey, and S. Chowdhury, "A literature review on integration of distributed energy resources in the perspective of control, protection and stability of microgrid," *Renewable and Sustainable Energy Reviews*, 2012.
- [22] A. Kumar and M. Azad, "Recent microgrid systems: A review," *IJAET*, 2015.
- [23] L. Darith and S. Polmai, "Virtual synchronous generator based on hybrid energystorage system for pv power fluctuation mitigation," *Applied Sciences*, 2019.
- [24] B. Guangqing, T. Hongtao, D. Kun, M. Ming, and W. Ningbo, "A novel photovoltaic virtual synchronous generator control technology without energy storage systems," *energies*, 2019.
- [25] Z. Shuai, Y. Sun, Z. Shen, W. Tian, C. Tu, and Y. Li, "Microgrid stability: Classification and a review," *Renewable and Sustainable Energy Reviews*, 2016.

- [26] M. Zamani, T. Sidhu, and A. Yazdani, "A protection strategy and microprocessor-based relay for low-voltage microgrids," *IEEE Transactions on Power Delivery*, 2011.
- [27] N. Schaefer, T. Degner, and A. Shustov, "Adaptive protection system for distribution networks with distributed energy resources," *DPSP, Manchester*, 2010.
- [28] H. Nikkhajoei and R. Lasseter, "Microgrid fault protection based on symmetrical and differential current components," *Commission PIERCE*, 2006.
- [29] S. Samantaray, G. Joos, and I. Kamwa, "Differential energy based microgrid protection against fault conditions," *ISGT, Washington DC*, 2012.
- [30] M. Khodayar, M. Barati, and M. Shahidehpour, "Integration of high reliability distribution system in microgrid operation," *IEEE Transactions on Power Systems*, 2012.
- [31] Z. Wang and J. Wang, "Self-healing resilient distribution systems based on sectionalization into microgrids," *IEEE Transactions on Power Systems*, 2015.
- [32] A. Khodaei, "Microgrid optimal scheduling with multi-period islanding constraints," *IEEE Transactions on Power Systems*, 2014.
- [33] A. Khodaei and M. Shahidehpour, "Microgrid-based co-optimization of generation and transmission planning in power systems," *IEEE Trans Power Syst*, 2013.
- [34] C. Papadimitriou, V. Kleftakis, and N. Hatziaargyriou, "A novel islanding detection method for microgrids based on variable impedance insertion," *Electric Power Systems Research*, 2015.
- [35] S. Ladislav, M. Roman, F. Leseck, and B. Zdenek, "Zero cross detection using phase locked loop," *IFAC-Paper OnLine*, vol. 49, no. 25, pp. 294–298, 2016.
- [36] K. Vikram and B. Vladimir, "Operation of a phase locked loop system under distorted utility conditions," *IEEE Transactions on Industry Applications*, vol. 33, no. 1, 1997.
- [37] S. Chung, "A phase tracking system for three phase utility interface inverters," *IEEE Transactions on Power Electronics*, vol. 15, no. 3, pp. 431–438, 2000.
- [38] A. Abubakar, D. Akoh *et al.*, "Development of phase lock loop system for synchronisation of a hybrid system with the grid," *Journal of Technological Development*, vol. 13, no. 1, 2016.
- [39] K. Åström and T. Hägglund, "Advanced pid control: Isa-the instrumentation, systems, and automation society," 2006.

- [40] R. Teodorescu, F. Blaabjerg, U. Borup, and M. Liserre, "A new control structure for grid-connected lcl pv inverters with zero steady-state error and selective harmonic compensation," *Applied Power Electronics Conference and Exposition*, vol. 1, pp. 580--586, 2004.
- [41] R. Teodorescu, F. Blaabjerg, M. Liserre, and P. Loh, "Proportional-resonant controllers and filters for grid-connected voltage-source converters," *IEEE Proceedings - Electric Power Applications*, vol. 153, pp. 750--762, 2006.
- [42] R. Teodorescu and F. Blaabjerg, "Flexible control of small wind turbines with grid failure detection operating in stand-alone and grid-connected mode," *IEEE Transactions on Power Electronics*, vol. 9, pp. 1323--1332, 2004.
- [43] F. Blaabjerg, R. Teodorescu, M. Liserre, and A. Timbus, "Overview of control and grid synchronization for distributed power generation systems," *IEEE Transactions on Industrial Electronics*, vol. 53, pp. 1398--1409, 2006.
- [44] T. Erika and D. Holmes, "Grid current regulation of a three-phase voltage source inverter with an lcl input filter," *IEEE Transactions on Power Electronics*, vol. 18, pp. 888--895, 2003.
- [45] S. Byeong-Mun, K. Youngroc, C. Hanju, and L. Hakju, "Current harmonic minimization of a grid-connected photovoltaic 500kw three-phase inverter using pr control," *Conversion Congress and Exposition*, pp. 1063--1068, 2011.
- [46] M. Castilla, J. Miret, J. Matas, L. Vicua, and J. Guerrero, "Linear current control scheme with series resonant harmonic compensator for single-phase grid-connected photovoltaic inverters," *IEEE Transactions on industrial electronics*, vol. 55, pp. 2724--2733, 2008.
- [47] M. Liserre, R. Teodorescu, and F. Blaabjerg, "Multiple harmonics control for three-phase grid converter systems with the use of pi-res current controller in a rotating frame," *IEEE Transactions on industrial electronics*, vol. 21, pp. 836--841, 2006.
- [48] J. Holland *et al.*, "Adaptation in natural and artificial systems: an introductory analysis with applications to biology, control, and artificial intelligence," *University of Michigan Press, Ann Arbor*, 1975.
- [49] J. Kennedy and R. Eberhart, "Particle swarm optimization," *Proceedings of IEEE International Conference on Neural Networks*, vol. 4, pp. 1942--1948, 1995.
- [50] P. Civicioglu, "Backtracking search optimization algorithm for numerical optimization problems," *Applied Mathematics and Computation*, vol. 219, 2013.

- [51] M. Wooldridge and N. R. Jennings, "Intelligent agents: Theory and practice," *The Knowledge Engineering Review*, vol. 10, no. 2, pp. 115--152, 1995.
- [52] A. FIPA standards, "<http://www.fipa.org>."
- [53] H. Cheng and B. Cheng, "Mobile-c: a mobile agent platform for mobile c-c++ agents," *Software---Practice and Experience*, vol. 36, no. 15, pp. 1711 -- 1733, Dec 2006.
- [54] P. Javier, G. Aranda, and M. Escriva, "Smart python multi-agent development environment," <https://pypi.python.org/pypi/SPADE>.
- [55] B. Akyol, J. Haack, B. Carpenter, S. Ciraci, M. Vlachopoulou, and C. Tews, "An agent execution platform for the electric power system," *Third International Workshop on Agent Technologies for Energy Systems Valencia*, 2012.
- [56] G. Pagani and M. Aiello, "Towards decentralization : A topological investigation of the medium and low voltage grids," *IEEE Transactions on Smart Grid*, vol. 2, pp. 538--547, Sep 2011.
- [57] J. Guerrero, J. Vásquez, J. Matas *et al.*, "Hierarchical control of droop-controlled ac and dc microgrids--a general approach toward standardization," *IEEE Transactions on Industrial Electronics*, vol. 58, pp. 158--172, Jan 2011.
- [58] A. Mehrizi-Sani and R. Iravani, "Potential-function based control of a microgrid in islanded and grid-connected models," *IEEE Transactions on Power Systems*, vol. 25, pp. 1883--1891, Nov 2010.
- [59] J. Guerrero, J. Vasquez, J. Matas *et al.*, "Hierarchical control of droop-controlled ac and dc microgrids --- a general approach toward standardization," *IEEE Trans. Ind. Electron*, vol. 58, no. 1, pp. 158--172, 2011.
- [60] L. Darith and P. Sompob, "Experiment on distributed cooperative control with multi-agent system for a single-phase microgrid," *International Conference on Electrical Engineering/Electronics, Computer, Telecommunications and Information Technology*, June 2015.
- [61] H. Hashim, Y. Xiangwu, and S. Abuzaid, "Mw-scale medium voltage cascaded h-bridge battery storage system based on virtual synchronous generators," *TENCON*, Nov 2017.
- [62] Q. Shafiee, J. Guerrero, and J. Vasquez, "Distributed secondary control for islanded microgrids---a novel approach," *IEEE Transactions on Power Electronics*, vol. 24, Feb 2014.

- [63] L. Hyung-Joo, C. Jin-Young, P. Gun-Soo *et al.*, "Renewable integration algorithm to compensate pv power using battery energy storage system," *International Youth Conference on Energy (IYCE)*, 2017.
- [64] R. Xinbo, W. Xuehua, P. Donghua *et al.*, "Control techniques for lcl-type grid-connected inverters," *Springer*, pp. 46–58, 2018.
- [65] K. Jalili and S. Bernet, "Design of lcl filters of active-front-end two-level voltage-source converters," *IEEE Transactions on Industrial Electronics*, vol. 56, no. 5, pp. 1674–1689, 2009.
- [66] M. Liserre, F. Blaabjerg, and S. Hansen, "Design and control of an lcl-filter-based three-phase active rectifier," *IEEE Transactions on Industry Applications*, vol. 41, no. 5, pp. 1674–1689, 2005.
- [67] IEEEStd.929, "Ieee recommended practice for utility interface of photovoltaic (pv) systems (2000)."
- [68] IEEEStd.1547, "Ieee standard for interconnecting distributed resources with electric power systems (2003)."

## APPENDICES





## DESIGN OF LCL FILTER

In grid-connected inverter, the PWM output voltage contains abundant of switching harmonic components, which results in the harmonic current injecting into the grid. Therefore, a filter is required to interface between the inverter bridge and the power grid. The LCL filter is usually employed since it has better ability of suppressing high frequency harmonics than the L filter. This section will focus on the design of the LCL filter.

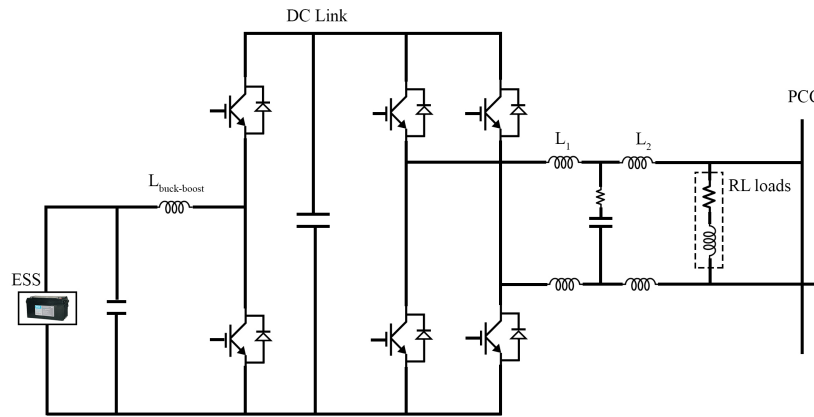


Fig. A.1: Single-phase full-bridge inverter with LCL filter

### A.1 Design of the Inverter-Side Inductor

From Fig. A.1, it can be observed that the current flowing through the filter inductor  $L_1$  and the switches are the same. Thus, the larger inductor current ripple will lead to large inductor and switching losses and high current stress of the switches. Therefore, the grid-side inductor should be properly sizing to limit the current ripple. According to the authors [64], the grid-side inverter can be determined as expressed below:

★ For Unipolar SPWM

$$L_{1\_min} = \frac{V_{in} T_{sw}}{8 \lambda_{c\_L1} I_1} \quad (A.1)$$

$$L_{1\_max} = \frac{\lambda v_{L1} V_c}{\omega_0 I_1} \approx \frac{\lambda v_{L1} V_g}{\omega_0 I_1} \quad (A.2)$$

Where  $V_{in}$  is the DC link voltage.  $I_1$  is rated RMS current vaue.  $T_{sw}$  is switching frequency.  $\omega_0$  is the fundamental angular frequency.  $V_g$  is the grid RMS voltage, and  $\lambda_{c\_L1}$  is ripple coefficient which practically set to 20-30%.

## A.2 Filter Capacitor Design

The filter capacitor will lead to reactive power. The larger the capacitance is, the higher the reactive power is introduced, and also the larger the current flows through inductor  $L_1$  and the power switches [65]. Hence, the conduction loss of the switches will increase. The maximum value of filter capacitor is expressed as:

$$C = \lambda_c \frac{P_0}{\omega_0 V_g^2} \quad (A.3)$$

where  $P_0$  is the rated active power output.  $\lambda_c$  is the ratio of the reactive power introduced by the filter capacitor to the rated output active power of the grid-connected inverter. In practice,  $\lambda_c$  is usually recommended to be about 5% [66].

## A.3 Grid-Side Inductor Design

The grid-side inductor  $L_2$  could be designed according to the harmonic restriction standards such as IEEE Std. 929-2000 and IEEE Std. 1547-2003 [67, 68]. Table A.1 lists the current harmonic restriction, including the limits on individual harmonics and the limit on the total harmonics distortion (THD) of the injected grid current. The minimum value of  $L_2$  can be obtained though Eq.A.4

$$L_2 = \frac{1}{L_1 C \omega_h^2 - 1} \cdot (L_1 + \frac{|V_{inv}(j\omega_h)|}{\omega_h \lambda_h I_1}) \quad (A.4)$$

where  $|V_{inv}(jxh)|$  is the RMS value of the inverter bridge output voltage,  $\frac{|V_{inv}(jxh)|}{V_{in}} = 28\%$ .  $I_1$  is the RMS value of the rated injected grid current, respectively.  $\omega_h$  is angular frequency at  $h$  order of the dominant harmonics which is equal to  $2 * \pi * 19950$ .  $\lambda_h$  is harmonic proportion,  $\lambda_h = 0.2\%$ .

Table A.1: Maximum harmonics limits of grid current

Harmonic order $h$ (odd harmonic)	$h < 11$	$11 \leq h < 17$	$17 \leq h < 23$	$23 \leq h < 35$	$35 \leq h$	TDH
Proportion to the rated grid-connected current (%)	4.0	2.0	1.5	0.6	0.3	5

Based on the formula described above, the calculated parameter of the LCL filter which used in this research is provided in Table A.2.

Table A.2: Inverter's parameters

Name	Symbol	Value	Name	Symbol	Value
Fundamental frequency	$f$	50 Hz	Output power	$P_0$	3 kW
Switching frequency	$f_s$	10 kHz	Inverter-side inductor	$L_1$	2 mH
DC link voltage	$V_{in}$	400 V	Filter capacitor	$C$	10 $\mu$ F
Grid's voltage	$V_{gRMS}$	220 V	Grid-side inductor	$L_2$	320 $\mu$ H



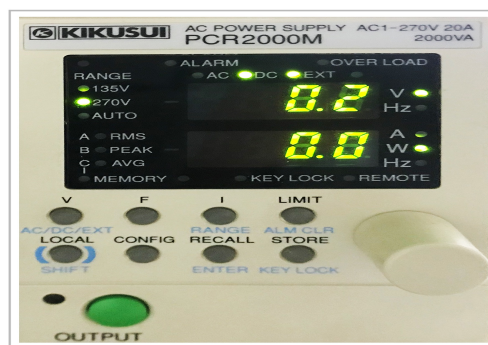
## OPERATION PROCEDURE

The section aims to provide the system operation as a reference for future usage. Some instructions are provided as the below:

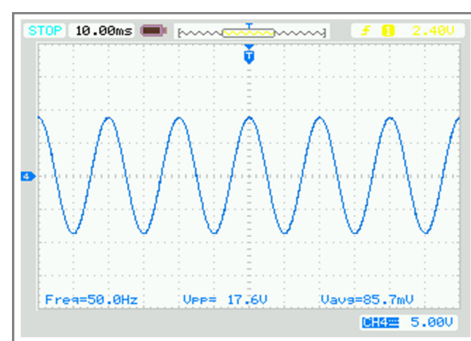
### B.1 Starting Distributed Generator

In this research, the programmable power supply, kikusui PCR 2000, is utilized to emulate the distributed generator. The control algorithm, modified droop control, is implemented in the DSP TI TMS320F28335 to control DG#1 and DG#2. The DG#1 works as the main generator to provide the synchronized voltage and frequency to other generators. Hence, the DG# must be started before starting other generator. The instructions on how to operate the DG#1 is provided as listed below:

- Step 1: Switched the output mode to DC + EXT as shown in Fig. B.1(a) by pressing SHIFT+V.
- Step 2: Debugged and started the code.
- Step 3: Checked the output control signal from the BNC connector to make sure the control signal is a sine wave with peak around 10V as depicted in Fig. B.1(b).
- Step 4: Pressed output button to start the DG.



(a) Switching output mode



(b) Control signal

Fig. B.1: System without energy storage system.

### B.2 Starting PV Simulator

In this research, the Kikusui PCR2000M is emulated the PV's characteristic. To operate the PV emulator, first, assuming that the DG#1 and PV power control algorithm are started. Then, the following step will take into account along with guideline in Fig. B.2.

- Step 1: Selected the COM port number of USB-Serial232.
- Step 2: Checked on the enable box.
- Step 3: Completed numbers 3 and 1 to interval and time scale text box, respectively.
- Step 4: Checked on Generated, clicked on Profile, and then clicked on the Browse button to choose the desired PV profile.
- Step 5: Clicked on the Relay button to turn on the CB. Once finished operation, clicked on the Relay button again to turn off the CB.
- Step 6: Clicked on the Start button to start injecting the power to the system.



Fig. B.2: PV emulator operation guideline

### B.3 Starting BESS

The BESS mainly use to suppress the frequency deviation which results from the intermittent nature of PV. Here, assuming that DG#1 is started and the PV emulator is ready to start. The operation of the BESS can be done by following the guideline in Fig. B.3 and the step below:

- Step 1: Debugged and started the BESS's control algorithm.
- Step 2: Turned on switch  $S_1$  and  $S_2$ .
- Step 3: Turned on the DC circuit breaker (DC\_CB) to start buck\_boost converter.
- Step 4: Checked the DC-Link voltage to make sure it properly boost to 400V.

- Step 5: Turned on the inverter control switch to enable the inverter control block.
- Step 6: Turned on the inverter switch to enable the bi-directional power flow of BESS..
- Step 7: Clicked the start button as shown in Fig B.4 to start the PV; at the same time, to transmit the PV output power and PV's ideal profile to BESS's controller.

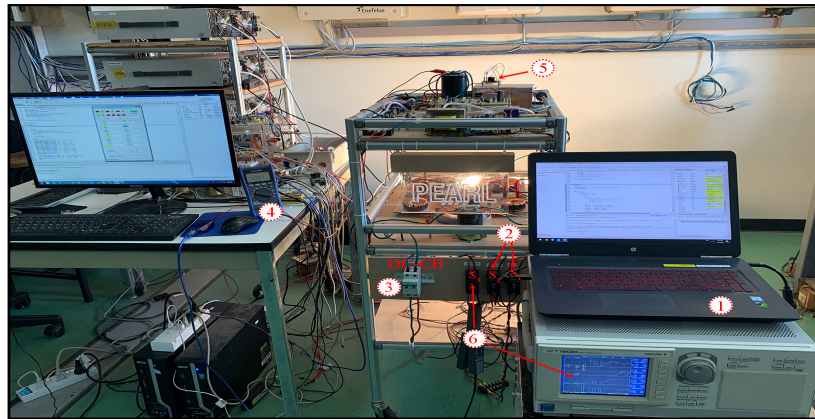


Fig. B.3: BESS operation guideline

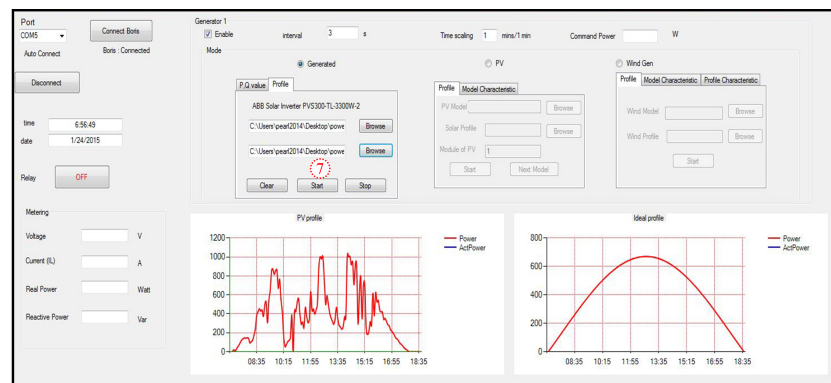


Fig. B.4: PV ideal profile

## B.4 Multiagent System Execution

The multi-agent system has been developed in Python using SPADE as the agent building platform. The SPADE's installation and agent execution are presented below:

### † SPADE Requirement

In the command window, type the following command:

- pip install rdflib
- pip install pyparsing==1.5.2

The SPADE platform can be downloaded at <https://github.com/javipalanca/spade/tree/2.3.2>.

Once the SPADE is downloaded, go to the downloaded SPADE's directory and type the following command to install and run SPADE platform.

- python setup.py install
- configure.py host.ip.address
- runspade.py

where *host.ip.address* is the host PC's ip4 address. After done execution the *runspade.py*, the SPADE platform will host on the *host.ip.address*. Then, the agent can be started and registered to the agent management system through using that IP address. Once the platform is successfully started, the WUI can be opened on the web as shown in Fig. B.5

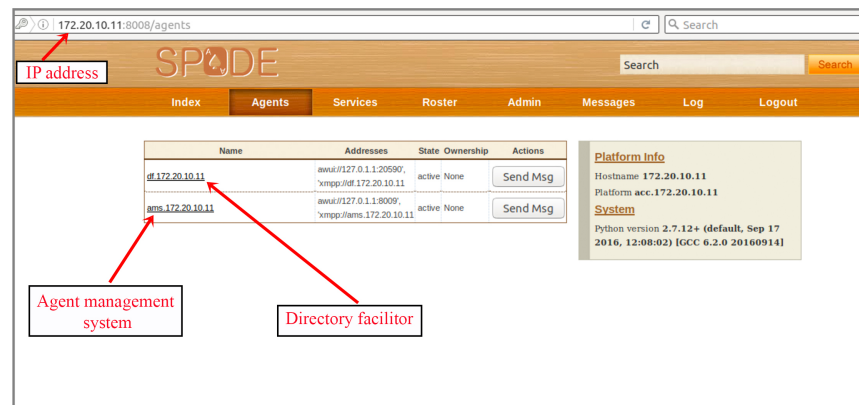


Fig. B.5: SPADE web user interface

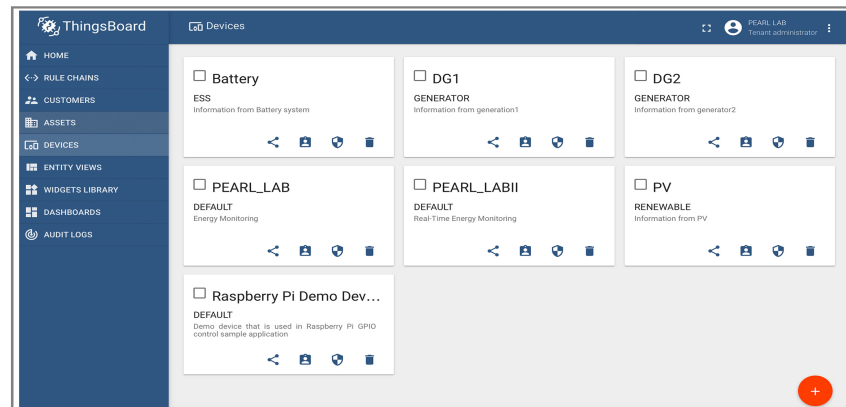


Fig. B.6: Web user interface of ThingsBoard

### † Internet of Things

The ThingsBoard IoT gateway is integrated into MAS. Once the agent starts, the information from the system is transmitted to the ThingsBoard platform. In this study, the ThingsBoard server runs as a demo server by registering an account on ThingsBoard's web page. However, the ThingsBoard server can be installed in any server PC as it provides as an

open-source. To access ThingBoard's wui, go to <https://demo.thingsboard.io/login> and sign in with the following information:

- User: `darith.leng@gmail.com`
- Password: `pi2017`

After sign-in successfully, the ThingsBoard's Wui will be shown as depicted in Fig.B.6. To view real-time dashboard, click on DASHBOARDS, then PEARL\_ENERGY\_MONITORING, and Open Dashboard.

### † Executed LSTM

The PV power prediction is developed using Python, Tensorflow. To execute the LSTM algorithm, there are some tools and libraries need to install first as listed below:

- Python version 3.5 or later.
- Ubuntu version 16.04 or later.
- TensorFlow version 1.5.
- Virtual environment version 16.4.3.

After completing the installation of the system requirement, the following steps are taken into account to execute the algorithm.

- Step 1: Activate the virtual environment by using a specific shell command:
  - Source `./venv/bin/activate`
 where **venv** is the installed directory of the virtual environment.
- Step2: Go to the algorithm directory and execute the command: `python3 LSTM.py` , as shown in Fig. B.7.

For further information on how to install Tensorflow and virtual environment, go to <https://www.tensorflow.org/install/pip>.

```

Last login: Thu Jul 16 21:10:26 on ttys000
Dariths-MacBook-Pro:~ darithleng$ source ./tf/bin/activate
(tf) Dariths-MacBook-Pro:~ darithleng$ cd /Users/darithleng/Desktop/LSTM/
(tf) Dariths-MacBook-Pro:LSTM darithleng$ python3 LSTM.py
(2695, 1)
[0.31450094]
tx: (2695, 5, 5) tex: (0, 5, 5) ty: (2695, 1) tey: (0, 1)
ShapeX: (1831, 5, 5)
ShapeY: (1831, 1)
2020-07-16 21:17:01.581364: I tensorflow/core/platform/cpu_feature_guard.cc:137]
Your CPU supports instructions that this TensorFlow binary was not compiled to
use: SSE4.2 AVX AVX2 FMA
i 0 , step_loss 0.092220575
RMSE_Train: 0.2891536
RMSE: 0.30075154
MSE: 0.090451494
i 10 , step_loss 0.043935
RMSE_Train: 0.20227753
RMSE: 0.21434914
MSE: 0.045945555
i 20 , step_loss 0.031382665
RMSE_Train: 0.17579536
RMSE: 0.18931824
MSE: 0.035841394
  
```

Fig. B.7: Shell command for executing the LSTM algorithm

## BIOGRAPHY

### Personal Information

Name	Darith Leng
Sex	Male
Nationality	Cambodian
Date of Birth	03 May, 1989
Place of Birth	Mongkolborey District, Bangteaymeanchey Province, Cambodia

### Education

#### Bachelor degree

Project	Grid Substation protection
Field of Study	Electrical and Energy
Duration	2008-2013
Department	Department Electrical Engineering
University	Institute of Technology of Cambodia

#### Master degree

Thesis	Study of a Multi-agent System for a Single-phase Microgrid
Field of Study	Computer Engineering
Duration	2013-2015
College	International College
University	King Mongkut's Institute of Technology Ladkrabang, Bangkok, Thailand

#### PhD degree

Thesis	Implementation of Distributed Hierarchical Control for a Standalone Single-Phase Microgrid
Field of Study	Electrical and Energy
Duration	2016-2020
Department	Electrical Engineering
University	King Mongkut's Institute of Technology Ladkrabang, Bangkok, Thailand

#### Researcher student



Research Topic	Virtual Synchronous Generator Based on Hybrid Energy Storage System for PV Power Fluctuation Mitigation
Field of Study	Power Electronic and Electrical Energy
Duration	July 2018-Feb 2019
Lab	Ise Laboratory
Department	Electrical Engineering
University	Osaka University, Osaka, Japan
<u>Research Interests</u>	Controlling Microgrid, Applying Multi-Agent System, and Optimization

## LIST OF PUBLICATIONS

Some parts of this work are published in the following articles.

1. Darith, L., Kittichot, S. and Sompob, P. "Multi-Agent System Based Real-Time Control for Standalone Microgrid" International Seminar on Intelligent Technology and Its Application (ISITIA 2017). Surabaya, INDONESIA, Aug 28-27, 2017.
2. Darith, L., Kittichot, S. and Sompob, P. "Experiment on Hierarchical Control Based Power Quality Enhancement for Standalone Microgrid" International Power Electronics Conference (IPEC 2018). Niigata, JAPAN, May 20-24, 2018.
3. Darith, L., Sompob, P. "Transient Respond Comparison Between Modified Droop Control and Virtual Synchronous Generator in Standalone Microgrid" International Conference on Engineering, Applied Sciences and Technology (ICEAST 2019). Luang Prabang, LAOS, July 2-5, 2019.
4. Darith, L., Sompob, P. "Virtual Synchronous Generator Based on Hybrid Energy Storage System for PV Power Fluctuation Mitigation" Applied Sciences, Vol 9, November 2019.